Resonance ionization spectroscopy and one-atom detection*

G. S. Hurst, M. G. Payne, S. D. Kramer, and J. P. Young

Oak Ridge National Laboratory, Oak Ridge, Tennessee 37830

Resonance ionization spectroscopy, RIS, is a multistep photon absorption process in which the final state is the ionization continuum of an atom. The RIS process can be saturated with available pulsed lasers, so that one electron can be removed from each atom of the selected type. This method was first applied to the determination of the absolute number of He(2^1S) excited states produced when pulsed beams of protons interacted with helium gas. Laser schemes for RIS are classified into five basic types; with these, nearly all of the elements can be detected with commercially available lasers. A periodic table is included showing schemes applicable to all of the elements except He, Ne, F, and Ar. A compact theory of the RIS process is presented which delineates the conditions under which rate equations apply. Questions on the effects of collisional line broadening, laser coherence time, and nonresonant multiphoton ionization processes are discussed. The initial demonstration of one-atom detection of Cs is described. By using laser beams to saturate the RIS process and by using proportional counters as single-electron detectors, one-atom detection is made possible. With RIS, one-atom detection is highly selective, has the ultimate in sensitivity, and has excellent space and time resolution. Furthermore, a modification of the technique in which single electrons (or single ions) are detected with a channel electron multiplier permits single-atom detection in a vacuum. Resonance ionization spectroscopy has application to *classical phenomena* such as the diffusion of free atoms, the chemical reaction of free atoms with a gas, the measurement of concentration fluctuations in a dilute vapor, and a variety of other atomic fluctuation phenomena. The authors describe how RIS can be used for *photophysics measurements* such as far wing collisional line broadening, measurements of photoionization cross sections for excited states, and collisional redistribution among excited states. *Modern applications* include the detection of single atoms in individual ionization tracks, such as those created by the binary fission of a parent atom, and the extension of this technique to the detection of stable or unstable daughter atoms in time coincidence with the decay of a parent atom. These methods are beig developed for use in low-level counting to determine, for example, the flux of solar neutrinos on the earth.

CONTENTS

I. Introduction 767
A. Energy pathways and resonance ionization spectroscopy 767
B. Concept of one-atom detection 768
C. Scope 769
II. Resonance Ionization Spectroscopy 769
A. Concept of RIS 769
B. RIS saturation by photoionization 771
C. RIS saturation by associative ionization 773
D. RIS schemes for the atoms 774
III. Theory of RIS and Related Processes 777
A. Introduction 777
B. Formulation of equations for the two-step RIS process 777
C. Effect of collisional line broadening on the two-step RIS process 780
D. Effect of laser coherence time on the two-step RIS process 784
E. Two-photon excitation 786
F. Background effects due to multiphoton ionization 788
IV. A Demonstration of One-Atom Detection 790
A. Sensitive detection of ionization 790
B. Experimental demonstration 791
C. Other laser experiments 793
V. Classical Applications 795
A. Photodissociation of molecules 795
B. Mutual diffusion of gases 798
C. Chemical reaction of free atoms 801
D. Statistical mechanics and atomic fluctuations 801
E. Measurement of the Fano factor 802
VI. Photophysics Applications 805
A. Previous use of RIS for study of excited states 805
B. Photophysics experiments with coaxial beams 806
C. New methods for measuring photoionization cross sections 807
D. Method for measurement of far wing line broadening 808
E. Studies of quenching phenomena 808
F. Studies of imprisonment of resonance radiation 809
VII. Modern Applications 809
A. One-atom detection in fission tracks 809
B. Detection of single daughter atoms 811
C. Solar neutrino measurements 813
D. Detection of exotic atoms 815
VIII. Conclusion 816
REFERENCES

*Research sponsored by the U.S. Department of Energy under contract W-7405-eng-26 with the Union Carbide Corporation.

I. INTRODUCTION

A. Energy pathways and resonance ionization spectroscopy

Some of the research which is reviewed in this article started with an effort to understand a very simple but striking effect of small concentrations of impurities on the total ionization created when a charged particle loses energy in a gas. In the context of radioactivity, the phenomenon is known as the Jesse effect. When even minute traces of impurities are admitted to helium gas, the total ionization due to the absorption of all of the energy of an alpha particle in the gas increases by nearly 50% (Jesse and Sadauskis, 1955). Niels Bohr (1915) pointed out that the total ionization observed in helium relative to air and hydrogen (Taylor, 1913) was too large and "difficult to explain unless the high value observed by Taylor possibly may be due to the presence

of a small amount of impurities in the helium used." In addition to its intrinsic interest as a curious phenomenon, the Jesse effect has its practical consequences. Traces of impurities make it difficult to obtain reliable data on the W values (mean energy expended per ion pair produced) for charged particles in gases. A recent review is the International Commission on Radiation Units and Measurements Report 31 (ICRU, 1978).

Ionization and emission spectroscopic studies have been directed toward the understanding of the interaction of radiation with matter since the discovery of x rays and of radioactivity before the turn of the century. Additional motivation for spectroscopic studies in noble gases and gas mixtures was created by the need to develop new gas lasers. A large body of careful work has been completed on the energy pathways involved as excited gases return to equilibrium. Some representative examples chosen to illustrate the fundamental cases where either high-energy electrons or protons are used to excite the pure noble gases are: *helium* (Bartell, Hurst, and Wagner, 1973), *neon* (Leichner, 1973; Leichner, Cook and Luerman, 1975), *argon* (Thonnard and Hurst, 1972), *krypton* (Leichner, 1973), and *xenon* (Keto, Gleason, and Walters, 1974; Leichner *et al.*, 1976).

An effort to understand the Jesse effect in noble gases motivated a comprehensive research program in which a pulsed 3-MV accelerator is used to study the energy pathways following charged-particle interactions with gases (Hurst *et al.*, 1974). The objectives of energy pathways research are to obtain (1) information on the spectrum of excited states produced by a charged particle in a noble gas, (2) the rate of decay of a selected excited state through various channels as a function of gas pressure, and (3) the modification of the decay channels due to the introduction of foreign species. These pathways studies have applications far beyond the understanding of the interaction of radiation with matter, to such varied topics as the development of gas lasers (Chen, Judish, and Payne, 1978) for isotope separation and to the development of sensitive methods for analysis of atmospheric constituents.

In the course of energy pathways research a need arose for a new kind of spectroscopic measurement. The main tool for investigating energy pathways had been time-resolved emission spectroscopy; such a method was used (Bartell, Hurst, and Wagner, 1973) to study proton excitation of helium gas. On the other hand, in a recent model of the pathways in helium (Payne, Klots, and Hurst, 1975), production and decay of the metastable He(2^1S) played the key role. Since metastable states do not radiate except when perturbed by collisions, it is difficult to obtain direct information on the abundance and their lifetimes by emission spectroscopy. Thus a new method, resonance ionization spectroscopy, was developed (Hurst *et al.*, 1975; Payne *et al.*, 1975) for the study of long-lived excited states using a laser photoionization technique. With resonance ionization spectroscopy (RIS) a laser is tuned to a resonance transition between the quantum-selected excited state and some intermediate (bound) state at higher energy. Photons in the same laser pulse photoionize the intermediate state; thus the amount of ionization versus photon wavelength shows a resonance structure. Absolute yields of selected excited states can be made whenever the photon fluence per pulse is large enough to saturate the ionization.

Actually, it has been clear since the 1913 work of Niels Bohr that the stepwise absorption of two photons could ionize an atom, and if the energy of each photon is less than the ionization potential of the atom, the process would require one resonance. Resonance ionization has received considerable attention in connection with isotope separation. See, for example, the Farrar and Smith (1968) and Smith (1974) bibliographies. Multistep ionization formed the basis of a French patent (Robieux and Auclair, 1965). Other patents were issued to Levy and Janes (1973) and to Nebenzahl and Leven (1973). Important uses were made of resonance ionization in the early 1970's by Stebbings and his colleagues (Stebbings *et al.*, 1973; Stebbings and Dunning, 1973; Dunning and Stebbings, 1974) at Rice University to create highly excited states in the noble gases for photoionization studies. Two-step selective photoionization of Rb atoms was reported by Ambartsumyan, Kalinin, and Letokhov (1971) and extended by Ambartsumyan and Letokhov (1972). Ambartsumyan *et al.* (1976) published a detailed paper on Rb.

The work on He(2^1S) (Hurst *et al.*, 1975; Payne *et al.*, 1975) was the first example of the use of saturated resonance ionization to make absolute measurements of the population of a quantum-selected species. It has been known since the discovery of x rays and of radioactivity that ionization could be measured in extremely sensitive as well as extremely accurate ways. However, traditional ionization measurements lack the selectivity (i.e., the spectroscopic features) of light absorption. By using a tunable laser as a source of light to produce ionization in two or more absorption steps, spectroscopic features are attached to ionization. We refer to the process as "resonance ionization" to distinguish it from the traditional nonselective ionization associated with x rays and radioactivity.

B. Concept of one-atom detection

The success of the first RIS experiment with helium established a firm basis for the belief that the same technique would allow single atoms to be detected. It was suggested in a patent filed in 1975 (Hurst, Payne, and Wagner, 1976) that a single atom in its ground state could be ionized with nearly 100% certainty with a pulsed dye laser. The claim was made that if the atom was in a proportional counter adjusted to detect one free electron, a single atom of the selected type could be detected. Furthermore, a proportional counter has the useful property that the average size of its pulses is directly proportional to the number of the free electrons which initiate it; therefore, if more than one atom is ionized, the height of the pulse measures the number of atoms which were in a defined volume at the particular time that a laser beam was pulsed through it. Fortunately, it turns out that with currently available lasers the RIS process can be used to selectively ionize almost

every kind of atom in its normal ground state. The first demonstration of one-atom detection was done with Cs (Hurst, Nayfeh, and Young, 1977a, 1977b).

Rutherford's unpublished lecture notes (courtesy of the University of Cambridge Library) contain the expression "the counting of atoms," but he meant that the energetic radiation product (e.g., an alpha particle) of the transmutation of a single atom could be detected. Here we have a much wider meaning of the expression "one-atom detection" (Hurst, 1978). Imagine a region of space whose volume can be reasonably large (e.g., 10 or even 100 cm^3). We can determine whether one atom—or how many atoms—of a selected type and in a selected quantum state is in the volume at the time of our choice. Furthermore, such measurements can be made in near vacuum or (under many conditions) at atmospheric pressure, so that if the volume contains enormously larger numbers of atoms or molecules of another type, these will not, in most cases, interfere with the detection of even one atom of the selected type. Since the detector has typically 1-μsec time resolution, it is possible to detect the small number of atoms which happen to be in the defined volume *at a particular time* as a consequence of mutual diffusion. Or, if an atom is injected into the detector at the time of some event such as the decay of a radioactive nucleus, it can be detected as an individual entity before it escapes from the detector. Time-resolved detection of a single selected atom that may be anywhere in a large volume in the presence of large concentrations of other atoms or molecules is nearly unique to RIS. For instance, this would be very difficult for a laser fluorescence technique because of the necessity of detecting photons from all points in the volume with high efficiency, while simultaneously discriminating scattered light.

Recently several other groups have announced the detection of single atoms, and one of the methods (Bekov, Letokhov, and Mishin, 1978) utilizes resonance ionization. That same group (Balykin *et al.*, 1977) had already developed a fluorescence method for neutral atomic beams. Independently, but nearly simultaneously, Greenless *et al.* (1977) developed a beam method in which time resolution for particular atoms can be recovered by time correlation of the fluorescence. Another group (Gelbwachs, Klein, and Wessel, 1977) claimed one-atom detection. These and other fluorescence methods are discussed in more detail in Sec. IV.

The RIS technique applies to the specific detection of "free" atoms—that is, atoms of a given type which move about in a near vacuum or a gaseous atmosphere. Atoms which are attached to surfaces or are bound in a molecule can also be detected with the technique described here if they can be liberated by some external event. And, of course, the atoms which leave a surface spontaneously can also be detected as free atoms. In one class of applications of the methods, atoms are dissociated from molecules or from surfaces at a known time and then detected after various short time delays. Another family of applications depends on the sudden appearance of a daughter atom due to the decay of a single radioactive parent. The decay of the parent can give a radiation signal which is used to activate the detector of the single daughter atom.

C. Scope

A brief rate equation theory of RIS and a discussion of the first use of RIS to determine the absolute population of a quantum-selected excited species are presented in Sec. II. Also in Sec. II a description is given of the importance of such measurements in the broader subject of the kinetics behavior of transient species. A wide range of RIS schemes and further details on the laser requirements for saturating the RIS process for nearly every element in the Periodic Table are also treated. In Sec. III a theoretical discussion is given of some processes which are of key importance in using RIS for ultrasensitive measurements. The two-step RIS process is treated in detail, and two-photon excitation is discussed both as a useful way to excite high-lying states and as a possible multiphoton background problem. Collisional line broadening is discussed because of its importance in determining the selectivity of the method. Off-resonance multiphoton ionization is discussed as a possible background effect. Section IV deals with the actual demonstration of one-atom detection. Classical applications of both RIS and one-atom detection with examples such as molecular dissociation, diffusion and reaction of atoms, statistical mechanics, and fluctuation phenomena are discussed in Sec. V. In Sec. VI we describe how RIS can be used for photophysics applications such as line broadening and photoionization cross sections. Some modern physics applications of one-atom detection are emphasized in Sec. VII. These include the detection of single atoms in fission particle tracks and the more general detection of daughter atoms in space and time coincidence with the decay of parent atoms. Finally, a description of the recently planned use of one-atom detection for solar neutrino measurements, as well as some comments on similar rare-event detection, is presented.

II. RESONANCE IONIZATION SPECTROSCOPY

A. Concept of RIS

Some basic features of the RIS process, in particular the conditions required for its saturation, can be described by considering an elementary case. Even though the saturated RIS process was first used to measure an excited-state population, our presentation is simplified to consider, first, a population of atoms in their ground state. Thus, by saturation of the RIS process, we mean that each atom of a quantum-selected species which was in its ground state before it was subjected to the photon field of a pulsed laser will be converted to a positive ion and a free electron during the short duration of the laser pulse.

In Fig. 1 we show schematically what is involved in the most elementary of all RIS processes. A pulsed laser beam produces photons of just the correct energy, $\hbar\omega$, to excite an atom initially in its ground state, 1, to an excited level, 2. Another photon at the same energy can photoionize state 2, but, of course, not state 1. During the laser pulse the population of state 2 grows at the expense of state 1. Typically, after about 10^{-9} sec the rate of stimulated emission from the excited state will just equal its rate of production. Thus

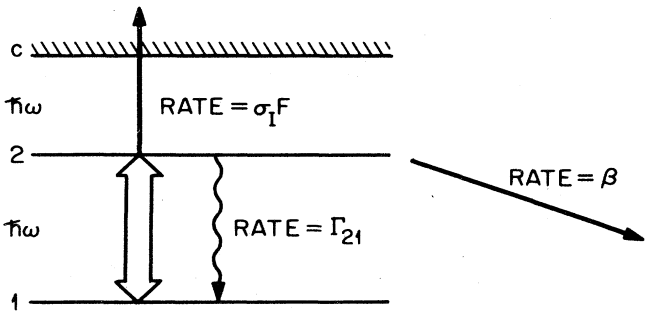

FIG. 1. Schematic for the RIS process in which the final state is reached by *photoionization*. An atom in ground state (1) can be ionized by first exciting to another bound state (2), making ionization a resonance process. Symbols are explained in the text.

an equilibrium persists as long as the laser intensity is kept sufficiently high during a pulse. Such an equilibrium is actually a quasisteady state because photons of the same wavelength can slowly photoionize the intermediate state. If the *photon fluence* (photons per unit of beam area) is large enough, a necessary condition for saturation of the RIS process has been met. If, in addition, the rate of photoionization, which depends on the *photon flux* (photons per cm^2 per second), is larger than the rate β at which the intermediate state is destroyed by possible competing processes (i.e., processes which convert the intermediate state to a species that can no longer be photoionized), then another necessary condition has been satisfied. When both the flux condition and the fluence condition are satisfied, in which case each selected state is converted to one electron plus one positive ion, the RIS process is said to be saturated. Furthermore, the process is so selective that only those excited states of the chosen type are ionized. We shall show later in this section that the selective two-step process can be generalized immediately to include a variety of multistep processes so that nearly all of the known elements can at the present time be subjected to the RIS process.

In order to show quantitatively the necessary and sufficient conditions for saturating the RIS process, we use a rate equation formulation and leave the justification of rate equations for Sec. III. The concept of a saturated RIS process could have been originated since the work of Einstein; however, the light source necessary to saturate the RIS process was not available prior to about 1970. Let $\sigma_a(\nu)$ be the cross section for photon absorption (from state 1 to state 2), let $\sigma_s(\nu)$ be the stimulated emission cross section, and let $\sigma_I(\nu_0)$ be the cross section for photoionization of state 2 at the central frequency ν_0. A laser beam is characterized by letting

$I(\nu)d\nu$ = the number of photons per cm^2 per second and in the frequency interval ν and $\nu+d\nu$,

where, for simplicity, a Gaussian line shape is used; i.e.,

$$I(\nu)=\frac{F}{\sqrt{2\pi}\Delta\nu^2}\exp-\left[\frac{(\nu-\nu_0)^2}{2\Delta\nu^2}\right]. \tag{2.1}$$

In Eq. (2.1), F is the photon flux and $\Delta\nu$ is the laser linewidth, i.e., $I(\nu)$ drops to $e^{-1/2}$ of its maximum when $|\nu-\nu_0|=\Delta\nu$.

The rate of change of levels 1 and 2 are then given by

$$\frac{dn_1}{dt}=-n_1\int d\nu\,\sigma_a(\nu)I(\nu)+\Gamma_{21}n_2+n_2\int d\nu\,\sigma_s(\nu)I(\nu), \tag{2.2a}$$

$$\frac{dn_2}{dt}=n_1\int d\nu\,\sigma_a(\nu)I(\nu)-n_2\int d\nu\,\sigma_s(\nu)I(\nu)-\Gamma_{21}n_2-\beta n_2-\sigma_1 F n_2, \tag{2.2b}$$

while the rate of ionization is given by

$$\frac{dn_I}{dt}=\sigma_I F n_2. \tag{2.2c}$$

Using Einstein's detailed balancing arguments and taking advantage of the fact that both $\sigma_a(\nu)$ and $\sigma_s(\nu)$ are narrow compared to $\Delta\nu$,

$$\int d\nu\,\sigma_a(\nu)I(\nu)=\frac{g_2}{g_1}\frac{\lambda_0^2\Gamma_{21}F}{8\sqrt{2}\pi^{3/2}\Delta\nu}\equiv\bar{\sigma}_a F=\frac{g_2}{g_1}\bar{\sigma}_s F, \tag{2.3a}$$

$$\int d\nu\,\sigma_s(\nu)I(\nu)=\bar{\sigma}_s F, \tag{2.3b}$$

where the g's are the statistical weights of the levels and where the $\bar{\sigma}_s$'s are the average cross sections for the phototransitions. It is useful to note that with broadband lasers one generally has $\bar{\sigma}_s\simeq\lambda_0^2\Gamma/8\pi\Delta\nu_{1/2}$, where Γ is the spontaneous transition rate and $\Delta\nu_{1/2}$ is the full width at half-maximum (FWHM) of the laser. With these relations, Eqs. (2.2a) and (2.2b) simplify and can be solved to obtain n_I if we assume a square pulse of width T_L:

$$n_2=\frac{\bar{\sigma}_a F n_1(0)}{b-a}(e^{-at}-e^{-bt}), \tag{2.4}$$

$$n_1=(\sigma_I F)\frac{\bar{\sigma}_a F n_1(0)}{b-a}\left|\frac{1}{a}\left(1-e^{-at}\right)-\frac{1}{b}\left(1-e^{-bt}\right)\right|, \tag{2.5}$$

where $n_1(0)$ is the initial ground-state population and

$$a=\frac{x_2}{2}-\sqrt{\left(\frac{x_2}{2}\right)^2-x_1^2},\quad b=\frac{x_2}{2}+\sqrt{\left(\frac{x_2}{2}\right)^2-x_1^2},$$

with

$$x_1^2=\bar{\sigma}_a F(\beta+\sigma_I F),\quad x_2=\Gamma_{21}+\beta+(\bar{\sigma}_a+\bar{\sigma}_s+\sigma_I)F.$$

Now it will generally be true that if a laser is tuned near line center and if its linewidth is not excessive, both $\bar{\sigma}_a$ and $\bar{\sigma}_s$ are much larger than σ_I. With one condition on the flux, i.e.,

$$\sigma_I F\gg\beta, \tag{2.6}$$

$x_2\gg x_1$, and $b\gg a$. Equation (2.4) then simplifies, with $\Gamma_{21}\ll(\bar{\sigma}_a+\bar{\sigma}_s)F$,

$$n_2=\frac{g_2}{g_1+g_2}n_1(0)e^{-at}, \tag{2.7}$$

where we have also restricted the time such that e^{-bt} can be neglected. Thus, with the flux condition [Eq. (2.6)], we have the simple quasiequilibrium picture; when states 1 and 2 are strongly coupled with the laser field, the sum of their populations [i.e., $n_1(0)$] decays at the rate e^{-at} where $a=[g_2/(g_1+g_2)]\sigma_I F$. Finally, if

$$\frac{g_2}{g_1+g_2}\phi\sigma_I\gg 1, \tag{2.8}$$

where ϕ is the fluence and is equal to FT_L for a square pulse, then $n_I = n_1(0)$ (i.e., complete ionization). Expression (2.8) is the fluence condition.

To saturate the RIS process, a flux condition [Eq. (2.6)] and a fluence condition [Eq. (2.8)] must hold. Usually the flux condition is not difficult to meet unless the intermediate state used in the RIS process is rapidly quenched. The fluence condition may or may not be difficult to obtain, depending on the mode of ionizing the intermediate state and the availability of suitable lasers.

B. RIS saturation by photoionization

The purpose of this section is to show how the flux condition and the fluence condition required for saturation of the RIS process translate to laser requirement in context with the first experiment in which these conditions were met. In Sec. I we briefly reviewed the motivation for the RIS experiment to obtain the absolute population of a long-lived excited state in helium, [i.e., He(2^1S)]. Verification of the abundance, as well as the lifetime, of this metastable state was regarded as a crucial test of an energy pathways model proposed to explain time-resolved spectroscopic studies and total ionization studies of helium gas excited by beams of charged particles. Since, at some gas pressures, the lifetime of He(2^1S) is longer than the width of a laser pulse, the study of a metastable state, using RIS techniques, proceeds just as described above for atoms in the ground state.

The pathways model for helium, while consistent with a large body of experimental and theoretical information, needed to be examined with an independent method which went to the heart of the question of the population and lifetimes of metastable states. For these reasons, a new photoionization method (RIS) was developed (Hurst *et al.*, 1975) so that all of the long-lived metastable states of a given set of quantum numbers would be converted to ionization. When quantum-selected states are selectively photoionized to saturation, it is straightforward to measure the population of the states by measuring the number of ion pairs produced.

The concept of the experiment is shown in Fig. 2. A Van de Graaff accelerator produces proton pulses which ionize and excite the target gas at moderate pressure. An ionization pulse is produced immediately in response to the total energy absorbed in the gas cell. But excited states are also created, and we wish to know the absolute population of the He(2^1S) state as a function of time for a particular He pressure. Suppose the proton pulse leaves behind a group of excited states as shown schematically in Fig. 3. Each one of these can be selected out and excited to an intermediate state by the application of a laser pulse that provides a large flux of photons at the appropriate wavelength. When the flux condition and the fluence condition are satisfied, each selected excited state is converted to one electron plus one positive ion and the RIS process is saturated. If a laser pulse is fired into the ionization cell, a secondary ionization pulse is produced and the magnitude of the secondary pulse gives the absolute number of He(2^1S) states which were in the volume swept by the laser pulse at the time it was fired. Each encounter between the proton pulse and the delayed laser pulse is recorded on a transient recorder.

A commercial (Phase-R Company) laser provided (1) a beam of reasonable quality over a 10-mm diameter, (2) an energy per pulse of about 0.7 J at 5015 Å, (3) a photon spectrum of about 30 Å FWHM, and (4) a pulse width of about 300 nsec. Figure 4 shows a typical recording of the signals at 0.6 Torr He. With −50 V applied to the field plates spaced 20 cm apart, the positive ion signals were collected in about 8 μsec, in agreement with ion mobility and diffusion data. It was shown that below 10^8 ion pairs the pulse heights are linearly related to the number of ion pairs. A simple ratio of pulse heights gives the number of quantum-selected atoms per ion pair. Figure 5 shows the ratio of peak heights plotted against energy per pulse at 5015 Å. The fact that an increase of a factor of 3 in energy per pulse increases the ratio by ~20% suggests that the ionization is close to saturation at the 0.4 J/cm^2 (i.e., 80% ionization) level.

We can now examine the He(2^1S) data at low pressure with respect to the rate equation theory formulated for the processes schematized in Fig. 1. At low pressure, using a laser with 30-Å linewidth to promote He(2^1S

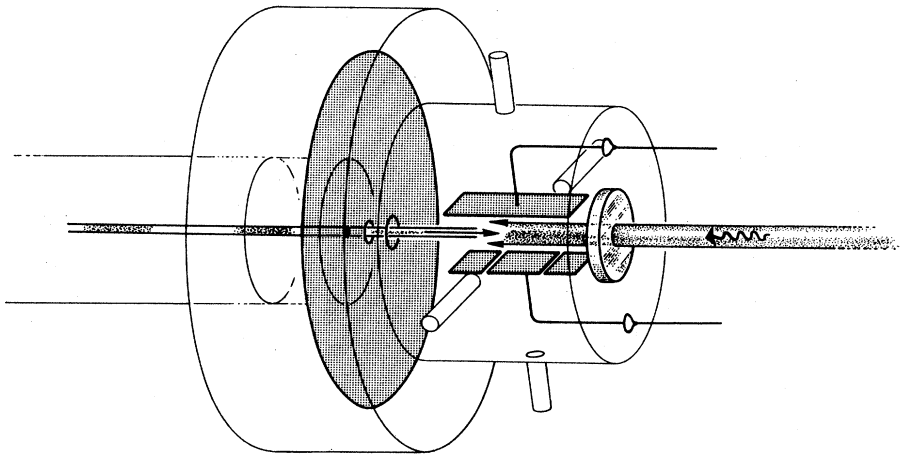

FIG. 2. Schematic of the RIS experiment on He(2^1S). A pulsed beam of protons excites a gas in a parallel-plate ionization chamber. After a short time delay, a laser pulse sweeps out quantum-selected excited states by the two-step ionization process. When saturation is achieved, the number of excited states which were in the region swept by the laser beam is just the number of electrons or positive ions created by the laser.

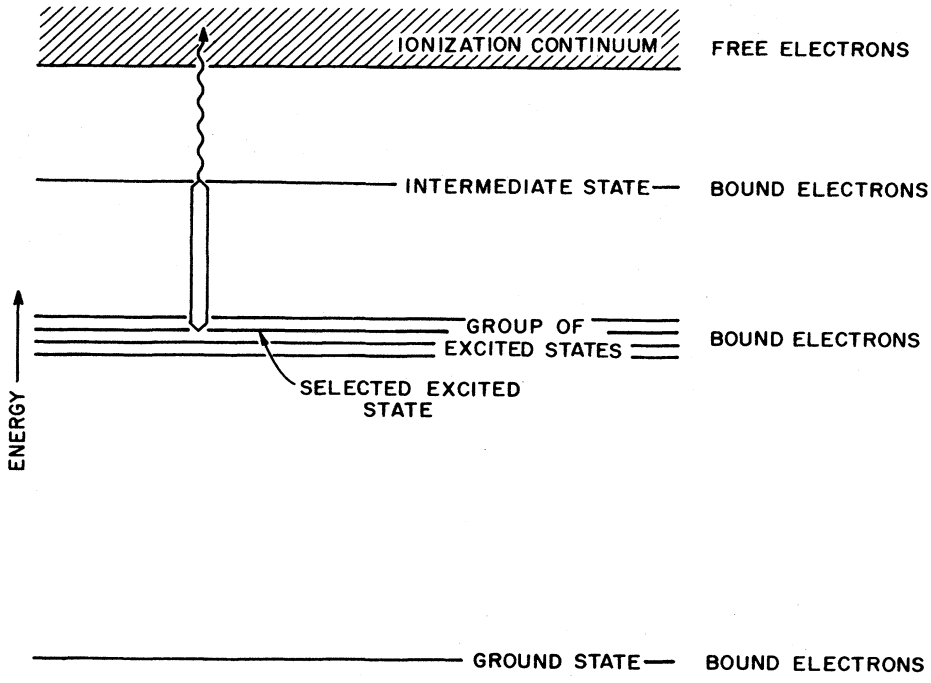

FIG. 3. Resonance ionization spectroscopy (RIS) was first put to use to measure the population of excited states in a gas. As a consequence of proton interaction with helium, a group of excited states was created. Excited states are selectively promoted to an intermediate state in the RIS process. When an intermediate state is chosen so that a second photon at the same wavelength can ionize it, a single laser tuned to the correct wavelength can be used to make an absolute measurement of the selected excited state. To achieve saturation, a condition in which one free electron is removed from each excited state, typically requires lasers that can deliver greater than 0.1 J of photons per cm^2 of beam area.

$\rightarrow 3^1P$) at 5015 Å gives $\bar{\sigma}_a \approx 10^{-15}$ cm^2 and $\bar{\sigma}_s \approx 3\times10^{-16}$ cm^2, compared with $\sigma_I = 1.1\times10^{-17}$ cm^2 at 5015 Å (Dunning and Stebbings, 1974). With these, $x_1 = 1\times10^{-16}$ F and $x_2 = 1.3\times10^{-15}F$. A convenient way to calculate F is to note that the number of photons in a 1-J pulse is $5.0\times10^{14}\lambda$, where λ is the wavelength in Å. Thus at 1 J/cm^2, the fluence is 2.5×10^{18} photons cm^{-2} at 5000 Å. For a pulse width (taken to be a square pulse) of 0.25-μsec duration, $F = 10^{25}$ photons $cm^{-2}sec^{-1}$, $x_1 = 10^9$ sec^{-1}, $x_2 = b = 1.3\times10^{10}$ sec^{-1}, and $a = 7\times10^7$ sec^{-1}; indeed $b \gg a$. Quasiequilibrium persists after about 3×10^{-10} sec, and the flux condition is satisfied: $\sigma_I F = 4\times10^7$ sec^{-1} while $\beta = 3\times10^5$ sec^{-1} (due to the radiation-trapped transition $1s3p \rightarrow 1s^2$). The fluence condition is also met since Eq. (2.8) gives $14 \gg 1$. These agree with the saturation of the signal in Fig. 5.

From the work of Alkhazov (1968) on electron excitation, Bartell, Hurst, and Wagner (1973) estimated that about 1 μsec after proton excitation the He(2^1S) population per direct ion pair is 0.27 at 0.6 Torr. This is in reasonable agreement with Fig. 5. At times greater than 1 μsec the He(2^1S) population includes not only its

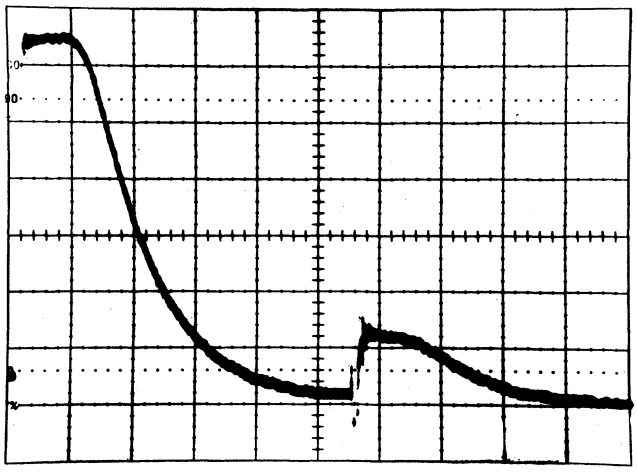

FIG. 4. An oscilloscope trace of the positive ionization current as a function of time. The large pulse is direct ionization created by protons; the smaller pulse is created by the laser tuned to 5015 Å and delayed 22 μsec.

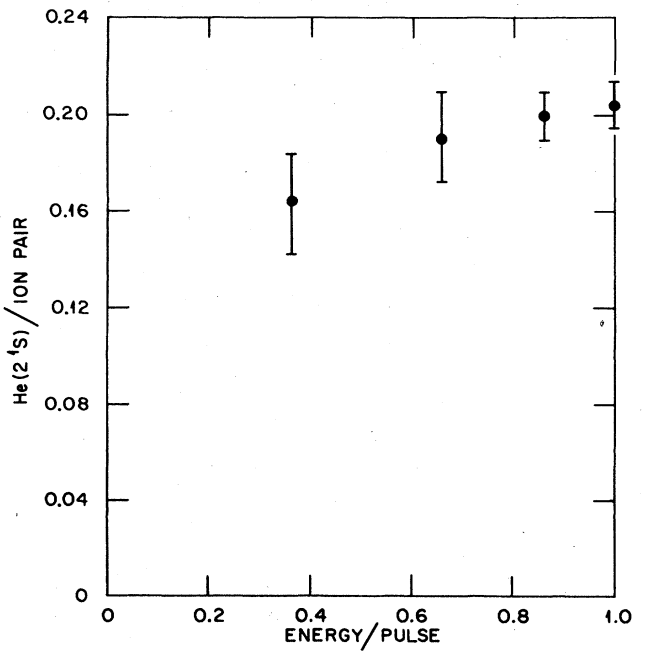

FIG. 5. The number of He(2^1S) states per ion pair as a function of the laser energy per pulse (700 mJ–1 on energy scale).

directly excited population but also much of the original populations of He(2^1P), He(3^1S), and He(3^1P) which—because of radiation trapping—cascade preferentially to He(2^1S). Cascade effects were included, of course, in estimating the 27%, as was the effect of energetic electrons escaping to the walls of the cell. In summary, the determination of an excited-state population by using the RIS method was consistent not only with a simple rate theory of the RIS process itself but also with a body of literature on the expected population of He(2^1S).

C. RIS saturation by associative ionization

Saturation of the ionization was also accomplished by single-photon absorption followed by collisions with ground-state atoms. This technique requires less laser energy per pulse than does the two-step photoionization. This version of the RIS technique was applied to kinetic studies of He(2^1S) over a wide range of helium pressures (Payne *et al.*, 1975) and to the determination of the He(2^1S) population under conditions where the primary electrons were stopped in the gas. Thus the resonance ionization (i.e., the excited-state populations) could be compared directly with the Jesse effect.

For helium, the states lying above the 3^3P can be converted to ionization by an associative process (known as the Hornbeck–Molnar reaction). The intermediate state He(3^1P) is converted to ionization with a two-body cross section of about 3×10^{-16} cm^2 (Wellenstein and Robertson, 1972a) and to He(3^1D) with a cross section of about 30×10^{-16} cm^2 (Wellenstein and Robertson, 1972b; He(3^1D) is associatively ionized with a cross section of about 20×10^{-16} cm^2. Effectively, the He(3^1P) is converted to $(He)_2^+$ at a rate of about $10^7\,P$, where P is the helium pressure in Torr and the rate is in inverse seconds. However, a competing process is collisional conversion of 3^1P to 3^1S (with $\sigma=4.5\times10^{-16}$ cm^2) which is not associatively ionized but, instead, radiates (3×10^7 sec^{-1}) to 2^1P. Return of He(2^1P) to He(2^1S) occurs at the rate of $1.9\times10^6+6.4\times10^4P$, completing a cycle (Bartell, Hurst, and Wagner, 1973; Payne, Klots, and Hurst, 1975). During the cycle there is a loss from the He(2^1P) state due to resonance radiation transport to the wall at a rate of 0.9×10^6 sec^{-1} and due to excimer formation at a rate of $90\,P^2$. These losses are not important over a wide range of pressure since the chance that an atom promoted to the He(3^1P) intermediate state will enter the return part of the cycle (where the losses occur) is small. As the pressure increases, associative ionization dominates over photoionization; at 15 Torr, photoionization contributes only a few percent at an energy of about 1 J/pulse (with a 300-nsec pulse).

Saturation of the ionization of He(2^1S) as a consequence of the laser pulse (0.7 J at 5015 Å) was checked by attenuating the beam by a factor of 3 and observing that $R(t)$, the ratio of the second to the first peak height, was unchanged within experimental error. Whenever associative ionization occurs at a rapid rate (i.e., higher pressure), a very modest energy (i.e., 0.1 J) per pulse is required to saturate the ionization, even when the spectrum is wide (30 Å FWHM). In fact, with a narrow-band laser very low photon fluence is required for saturation, because each intermediate state excited with the laser is rapidly converted to ionization by collision.

Measurements were carried out under saturation conditions for a large number of delay times at each of the several pressures. The decay curve for 100 Torr is shown in Fig. 6. At times greater than 2 μsec following excitation, it was found from RIS measurements that the He(2^1S) population decays exponentially with a decay constant given by $\beta=220\,P+1.4\,P^2$. At low pressures this rate agrees well with Phelps (1955), and at pressures above 100 Torr it is nearly the same as that of the 601-Å, collision-induced emission of He(2^1S) (Bartell, Hurst, and Wagner, 1973; Payne, Klots, and Hurst, 1975). Furthermore, the absolute population of the He(2^1S) as a function of gas pressure was also used to prove that two-body conversion of 2^1P to 2^1S does indeed occur (Payne *et al.*, 1975). This is the most conclusive evidence thus far that the major source of the Jesse effect in He is due to the He(2^1S) state.

This work was the first in which the RIS process was saturated by exciting an atom to a state which could be ionized in a collisional process (associative ionization). The paper (Payne *et al.*, 1975) also discussed the concept of ionizing Rydberg states by many types of collisions. For n about 25, saturated ionization can be achieved by field ionization as well, provided the buffer gas pressure is not too large—say 50 Torr.

Thus it was shown that the RIS technique can be extended to situations where the final step is collision induced. Associative ionization is one collisional mechanism; Penning ionization of an impurity and charge transfer to electronegative impurities may provide other useful mechanisms. Utilization of these collision processes in resonance ionization spectroscopy can be very important because it makes possible the use of lasers having rather modest energy per pulse and hence lasers having better performance in terms of repetition rate, pulse width, and spectral line shapes.

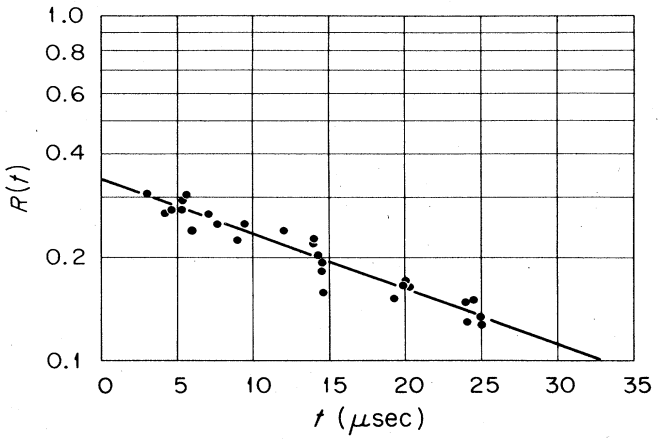

FIG. 6. The absolute population of He(2^1S) states per direct ion pair as a function of time, $R(t)$, after 2-MeV proton excitation of He at 100 Torr.

D. RIS schemes for the atoms

A wide variety of laser schemes can be used to carry out a resonance ionization process, and many of these are easily saturated (Hurst *et al.*, 1979a). Because of the attraction of using the RIS process for the detection of single atoms in their ground state, we shall, unless otherwise specified, assume that the atom is initially in the ground state. It is convenient to adopt a notation, suggested by nuclear physics, to describe the RIS process. Thus we proceed as follows:

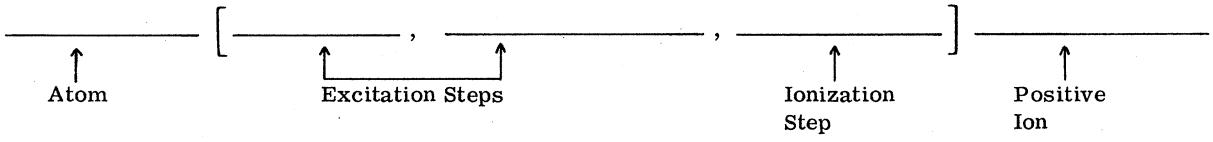

Some examples will make this notation clear. Thus,

(a) $Cs[\omega_1, \omega_1 e^-]Cs^+$ (Hurst, Nayfeh, and Young, 1977a; 1977b) means that Cs can be excited by a photon of frequency ω_1, following which the atom can be ionized with another photon of the same frequency, producing a free electron e^- and a positive ion Cs^+. On the other hand,

(b) $Y[\omega_1, \omega_2, \omega_3, Ee^-]Y^+$ (Bekov *et al.*, 1978)

indicates that a Y atom in its ground state absorbs photons in three steps, creating a Rydberg state which is ionized with an electric field E. A two-photon excitation process was recently reported as the first step for resonance ionization of H:

(c) $H[\omega_1\omega_2, \omega_1 e^-]H^+$ (Bjorklund *et al.*, 1978).

A similar example of two-photon excitation was suggested for Xe:

(d) $Xe[\omega_1\omega_1, \omega_2 e^-]Xe^+$ (Bushaw and Whitaker, 1976).

Note that we use the notation $\omega_1\omega_1$ to designate a two-photon resonance and reserve the notation $2\omega_1$ for a single photon which is generated by frequency doubling. In example (d) a two-photon allowed transition is driven at a single frequency ω_1 to a level which is photoionized by a photon of a different frequency ω_2. Generalizations of these examples are illustrated in Fig. 7.

Each of the basic photoionization schemes can be modified so that photons are not involved in the final step. For instance, in Fig. 8 we illustrate the case where two-step excitation creates a Rydberg state which can be ionized using an electric field E, or by various collisional processes. In the figure, $A[\omega_1, \omega_2, Ae^-]A_2^+$ represents a process where associative ionization with a like atom is the final step, while $A[\omega_1, \omega_2, Be^-]AB^+$ implies that associative ionization occurs with a buffer gas atom. Furthermore, a buffer gas atom can play a catalyst role in the process $A[\omega_1, \omega_2, Be^-]A^+$. Molecular additives M can cause Penning ionization, $A[\omega_1, \omega_2, Me^-]M^+$, from an excited state; or if M has a positive electron affinity, chemi-ionization, $A[\omega_1, \omega_2, MM^-]A^+$, can occur.

Table I summarizes some of the RIS processes known to date along with parameters of the lasers used. When saturation of the process was of particular interest, it is so designated.

We can now address the question of which laser scheme is appropriate for a given element of the Per-

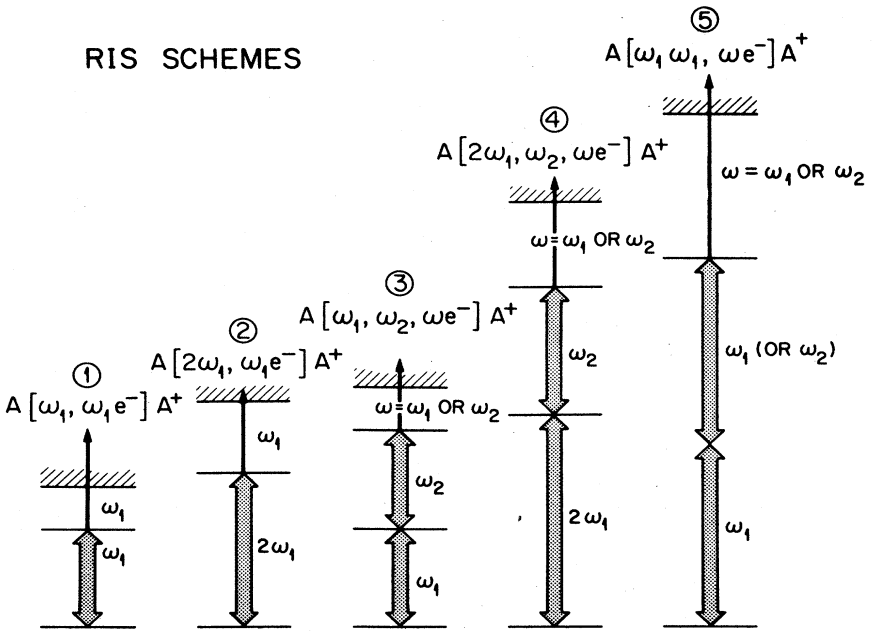

FIG. 7. Classification of RIS schemes for sensitive detection of the elements. With these five schemes, all of the elements except He, F, Ne, and possibly Ar can be detected.

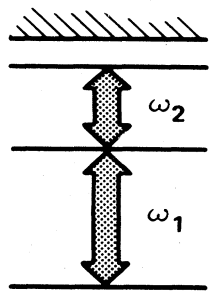

FIG. 8. Ionization of Rydberg states by processes that do not require photons. Rydberg states prepared, for example, by an ω_1, ω_2 process can be ionized with electric fields and by various kinds of collision processes (see text).

iodic Table. Spacing of the energy levels in each atom determines which scheme can be used because available lasers are restricted in their wavelength ranges. The properties in a given atom which determine to first order the kind of laser required are (1) the energy level of the first excited state, (2) the quantal character of the accessible lower-lying levels (i.e., whether one-photon or two-photon allowed), and (3) the magnitude of the ionization potential of the atom. These facts—as well as the other specifications of available pulsed lasers such as the peak power, energy per pulse, pulse duration, and beam quality—were taken into account in arriving at the suggested schemes. The five basic schemes of Fig. 7, ordered roughly according to complexity, are adequate for nearly all of the elements. A possible scheme for each of the elements (except He, F, Ne, and Ar) of the Periodic Table is given in Fig. 9. The key for interpreting the data is included in the figure; it includes the chemical symbol, first ionization potential, first excited state, and second excited state where needed. The simplest RIS scheme, taken from Fig. 7, which can be used to detect the element is circled in the center of each block. Where optical levels are not known, a possible scheme is sometimes given with a question mark. The criteria used in deriving the simplest RIS scheme follow. It is assumed

TABLE I. Table of some RIS experiments.

Process		
$H[\omega_1\omega_2, \omega_1 e^-]H^+$	Nd:Yag pumped dye laser system; $\lambda_1 = 2660$ Å, $\lambda_2 =$ ca 2240 Å; saturated a small volume.	Bjorklund *et al.* (1978)
$He(2^1, {}^3S)[\omega_1, \omega_1 e^-]He^+$	Nitrogen pumped dye laser at various wavelengths to produce 3^1P, 4^1P, 5^1P, 3^3P, 4^3P, and 5^3P atoms	Dunning and Stebbings (1974)
$He(2^1S)[\omega_1, \omega_1 e^-]He^+$	Coaxial flashlamp dye laser; $\lambda_1 = 5015$ Å, 1 J in 300 nsec; saturated a large volume.	Hurst *et al.* (1975)
$He(2^1S)[\omega_1, He e^-](He)_2^+$	Coaxial flashlamp dye laser; $\lambda_1 = 5015$ Å, less than 100 mJ in 300 nsec; saturated a large volume.	Payne *et al.* (1975)
$Li[\omega_1, \omega_2, \omega e^-]Li^+$	Coaxial flashlamp dye lasers; $\lambda_1 = 6709$ Å, $\lambda_2 = 6105$ Å; saturated a large volume.	Kramer *et al.* (1979)
$Na[\omega_1, \omega_2, \omega e^-]Na^+$ $Na[\omega_1, \omega_2, Ee^-]Na^+$	Coaxial flashlamp dye lasers; $\lambda_1 = 5896$ Å, $\lambda_2 = 5683$ Å, $\lambda_1 = 5890$ Å, $\lambda_2 = 4196$ Å	Mayo and Lucatorto (1978) Bekhov, Letokhov, and Mishin (1978)
$Mg[\omega_1, \omega_2 e^-]Mg^+$	Nd: glass pumped dye laser; $\lambda_1 = 2853$ Å, $\lambda_2 = 2900$ to 4000 Å; absorption spectroscopy, ionization not recorded.	Bradley *et al.* (1973)
$K[\omega_1, \omega_1 e^-]K^+$	Nitrogen pumped dye laser; $\lambda_1 = 4047$ Å	Calcott *et al.* (1979)
$Ca(^3P_2)[\omega_1, \omega_2 e^-]Ca^+$	Argon ion pumped dye laser (cw); $\lambda_1 = 6162$ Å, $\lambda_2 = 4880$ Å and other autoionization peaks	Brinkmann *et al.* (1974)
$Rb[\omega_1, \omega_2 e^-]Rb^+$	Ruby laser, dye laser system; $\lambda_1 = 7948$ Å, $\lambda_2 = 3471$ Å	Ambartsumyan, Kalinin, and Letokhov (1971); Ambartsumyan and Letokhov (1972)
$Rb[\omega_1, \omega_2 e^-]Rb^+$	Ruby pumped dye laser system; $\lambda_1 = 4126$ Å, $\lambda_2 = 6943$ Å; saturated a small volume.	Ambartsumyan *et al.* (1976)
$Xe[\omega_1\omega_1, \omega_1 e^-]Xe^+$	Nitrogen pumped dye laser; $\lambda_1 = 2525$ Å; (ionization not recorded).	Bushaw and Whitaker (1976)
$Cs[\omega_1, \omega_1 e^-]Cs^+$	Linear flashlamp dye laser; $\lambda_1 = 4555$ Å or 4593 Å; saturated a small volume; demonstrated one-atom detection	Hurst, Nayfeh, and Young (1977a; 1977b)
$Cs[\omega_1, \omega_1 e^-]Cs^+$	Coaxial flashlamp dye laser; $\lambda_1 = 4555$ Å; saturated large volume; absolute measurement of number of photodissociated atoms.	Grossman *et al.* (1977a; 1977b)
$Cs[\omega_1, \omega_1 e^-]Cs^+$	Coaxial flashlamp dye laser; $\lambda_1 = 4555$ Å or 4593 Å saturated large volume; measured Cs atoms from ^{252}Cf fission	Kramer *et al.* (1978)
$Y[\omega_1, \omega_2, \omega_3, Ee]Y^+$	Nitrogen pumped dye laser system; $\lambda_1 = 5556$ Å, $\lambda_2 = 6800$ Å, $\lambda_3 = 5950$–5770 Å	Bekov *et al.* (1978)

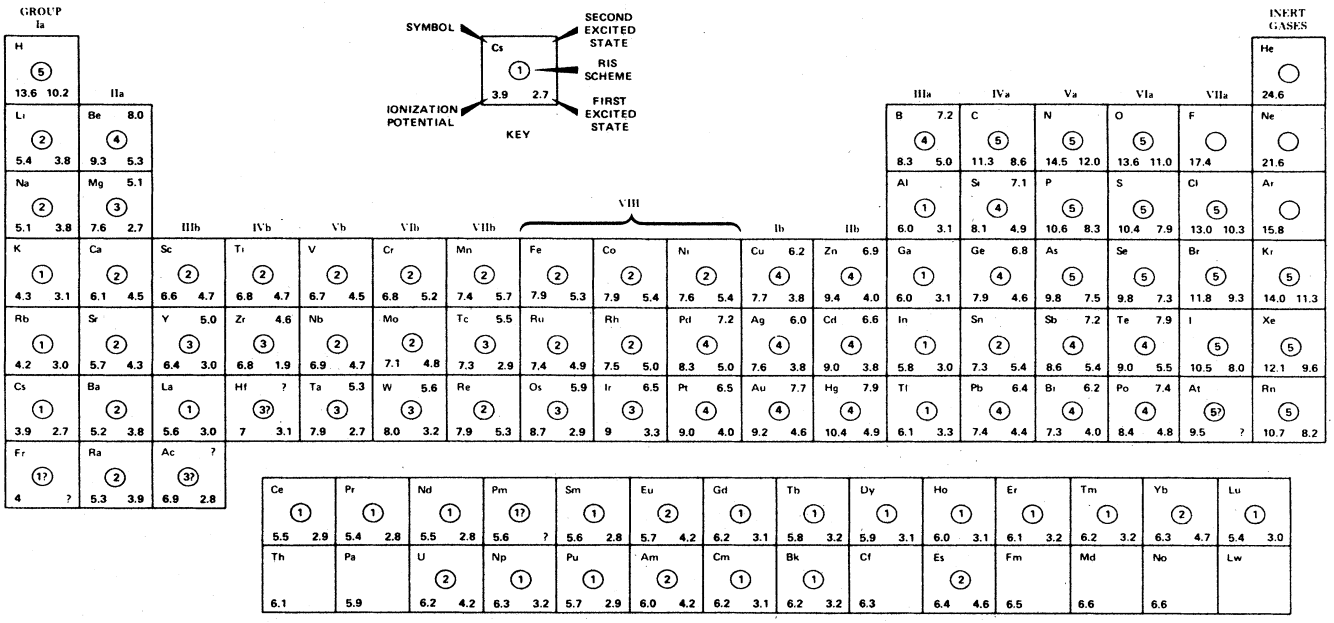

FIG. 9. Resonance ionization spectroscopy schemes for the elements. For elements H through Ac: ionization potentials (I.P.) and energy levels (E.L.), respectively, see Moore (1948) and Martin, Zalubas, and Hagen (1978); Th, Pa, Am, Bk, Cf, Es, Fm, Md, and No: Sugar (1974)—I.P.; U: Hertel (1967)—I.P., Carlson *et al.* (1976)—E.L.; Np: Lawrence Livermore Laboratory (1977)—I.P., Fred *et al.* (1977)—E.L.; Pu: Smith and Hertel (1969)—I.P., Richards and Ridgeley (1965)—E.L.; Am: Fred and Tomkins (1957)—E.L.; Cm: Smith (1971)—I.P., Worden and Conway (1976)—E.L.; Bk: Conway *et al.* (1977)—E.L.; Es: Worden *et al.* (1974)—E.L.

that the fundamental range of tunable dye lasers, which will have sufficient power to saturate photoionization, is 3800–7500 Å (3.25–1.65 eV). It is further assumed that dye lasers can be doubled over the range of 2170–3600 Å (5.71–3.44 eV). The higher the scheme designation, the more complex the process. Schemes 1 and 2 are the most simple: they require one laser, but in scheme 2 a portion of the output must be doubled. In schemes 1 and 2, time coincidence is guaranteed. In schemes 3 and 4, it is possible that two lasers may be used; this adds an additional requirement that time and space coincidence must be controlled. Scheme 5 utilizes two-photon transitions to states for which single-photon transitions are not allowed, and this further complicates the process. For the applications involving scheme 5, the ground-state–first excited-state transition may involve photons obtained by doubling, redoubling, and mixing a fundamental wavelength. Use of an ultraviolet excimer laser could also be advantageous in this scheme. Using known energy levels, 23 elements can be detected by scheme 1; 25 elements by scheme 2; and 39 elements can be detected by two-laser schemes 3, 4, and 5. Four elements are presently out of the range of RIS schemes. Many of these ionization schemes can be slightly altered so that Rydberg states are excited. These states can be ionized in a variety of ways without photons (see Fig. 8 for examples); thus the energy-per-pulse requirement for saturation of RIS can be greatly reduced.

In general, the quantitative evaluation of a particular RIS process requires a knowledge of dipole matrix elements for all transitions between each discrete level and lower levels. These quantities are poorly known for many atoms. In addition, under pressurized conditions various collision cross sections are also needed. In most cases the need for this information can be eliminated by using dye lasers with narrow linewidths (e.g., 0.01 Å), power densities $\approx 10^4$ W/cm^2, and 5- to 10-nsec pulse widths. The narrow linewidth and low power densities permit saturation of all discrete-discrete transitions in a time which is short compared with the pulse width. Short pulse widths make spontaneous emission negligible and, combined with relatively low pressure, minimize the effects of inelastic collisions. An additional bonus is that moderate power densities, narrow linewidth for the laser, and the low pressure lead to a highly selective resonance process. Thus we are often left with a situation where the major unknown is the photoionization cross section of the highest resonant level.

Experimental information on photoionization cross sections for excited states is still sparse. Until recently, all data of this type came from the application of detailed balancing to studies of radiative recombination in plasmas. Studies have been reported by Mohler (1933) for the $6p\,^2P$ states of Cs and by Rothe (1969, 1971) for the $3p\,^2P$ states of Na and the $2p\,^2P$ states of Li. More recently, with atomic beam and flashlamps, Nygaard (1975) measured the $6p\,^2P_{1/2,3/2}$ states of Cs, and Stebbings *et al.* (1973) and Dunning and Stebbings (1974), using a pulsed dye laser, studied a number of excited states in He. Cell experiments have also been carried out to yield rough estimates for a few excited states in Cs and Rb.

A variety of theoretical methods have been used to calculate photoionization cross sections for excited states. Burgess and Seaton (1960) have used the quantum defect method. Parametric potential methods have

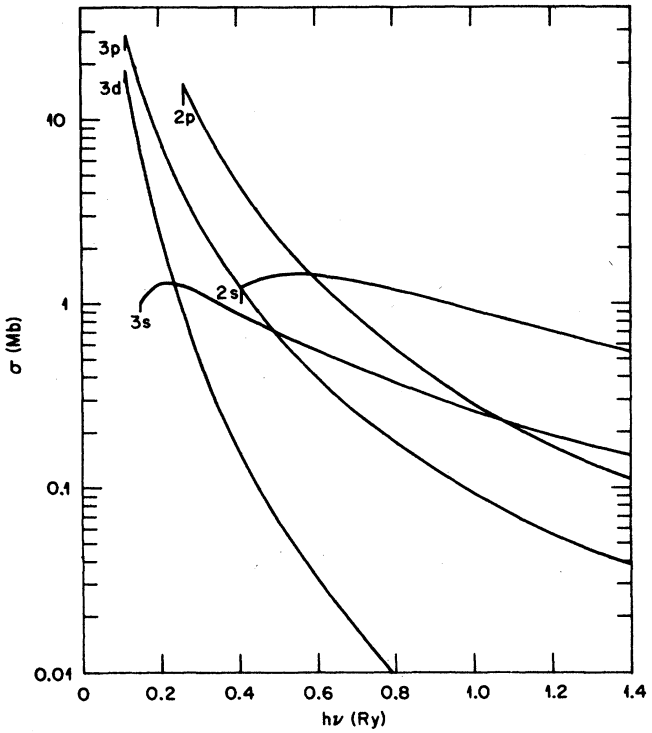

FIG. 10. Cross sections for the photoionization of various excited states of Li as a function of photon energy in Rydbergs. These results were provided by S. T. Manson (private communication).

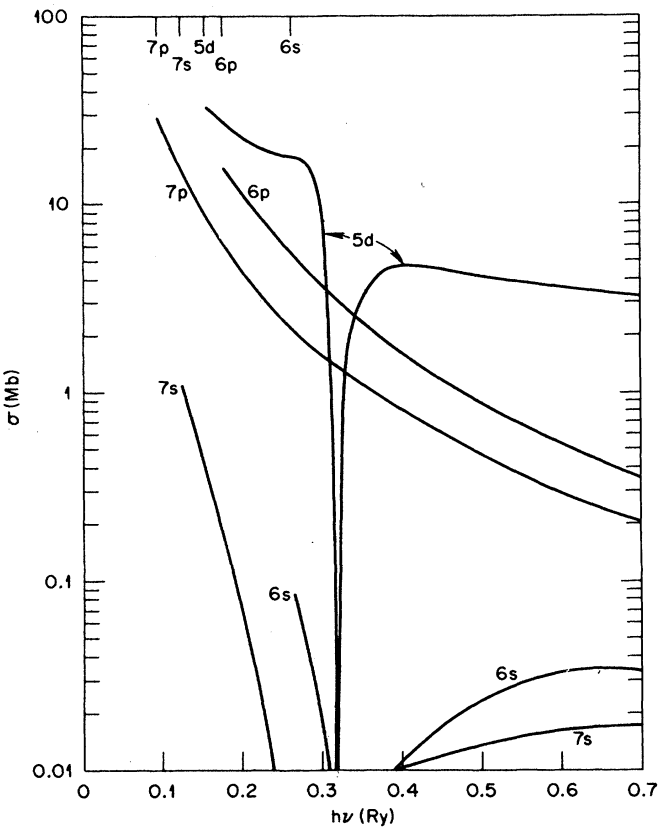

FIG. 11. Cross sections for the photoionization of various excited states of Cs as a function of photon energy in Rydbergs. The results were provided by S. T. Manson (private communication).

been used by Aymar, Luc-Koenig, and Farnoux (1976), as well as by Weisheit (1972). Finally, Msegane and Manson (1975) have made extensive use of variations on the HSF (Hartree–Slater–Fock) method. Figures 10 and 11 summarize some recent results for Li and Cs, respectively.

III. THEORY OF RIS AND RELATED PROCESSES

A. Introduction

The purpose of this section is to provide a brief theoretical discussion on a variety of effects related to the interaction of laser fields with atoms in order to evaluate the RIS technique as a tool for making a large variety of ultrasensitive and unambiguous physical measurements. We use the simplest physical models and the most elementary mathematics which enable one to understand the effect under discussion.

Some of the questions that we shall try to answer are: (1) What are the laser requirements for RIS when various excitation and ionization schemes are used? (2) Under what conditions of pressure, laser bandwidth, and laser power density can one describe the atom–field interaction problem in terms of rate equations as opposed to a full density matrix treatment of the problem? (3) What restrictions are imposed on RIS by background effects due to multiphoton ionization of any buffer gas or impurity that might be present, and to what extent can this be avoided by the proper choice of lasers for a carefully thought out RIS scheme? (4) To what extent is selectivity lost by pressure-broadening effects and how can this be avoided by choosing a proper detection method? Since we anticipate readers who are not presently engaged in laser physics, it is hoped that this treatment can serve not only to answer questions (1)–(4), but also as a springboard to literature which treats many of the topics in more detail.

B. Formulation of equations for the two-step RIS process

The two-step RIS scheme is the simplest of all methods for the selective detection of atoms by a saturated ionization process and has been the most widely used method (Hurst *et al.*, 1975; Payne *et al.*, 1975; Hurst, Nayfeh, and Young, 1977a, 1977b; Grossman *et al.*, 1977a, 1977b; Nayfeh *et al.*, 1977). In this process, one uses a single laser tuned to resonance between the ground state of the selected atom and an excited state lying more than halfway to the ionizing continuum (Fig. 12). Thus a second photon from the same laser can ionize the atom; and at sufficiently high photon flux and photon fluence, each of the selected atoms can be ionized. We believe that it is appropriate that this scheme be treated theoretically with enough generality so that questions about line shape, conditions for saturation, and the applicability of rate equations can be answered in some detail. Many of these questions can be answered in terms of a simple model in which the atom

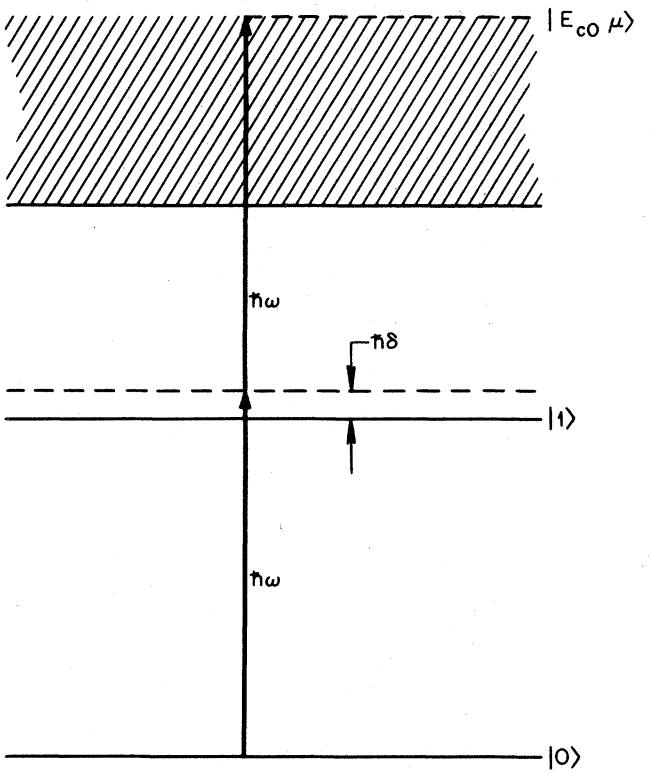

FIG. 12. Energy level diagram for the two-discrete state plus continuum model used in discussing two-step ionization. The laser used for the RIS process produces photons of energy $\hbar\omega$ which is off resonance for the discrete-discrete transition by $\hbar\delta=\hbar(\omega-\omega_1+\omega_0)$. The continuum energy is $E_{c0}=\hbar\omega_0+2\hbar\omega$.

has only two discrete states of importance and an ionizing continuum. We shall see that the two-state + continuum model is tractible mathematically and that even though hyperfine structure, fine structure, collisional redistribution among magnetic sublevels, and other effects may keep the model from applying in detail to many atoms at the relatively high power levels required for saturated ionization, it still suggests general guidelines for when rate equations would apply; and the rate equations can incorporate the neglected effects. Further, in dealing with far wing line-broadening effects, the model is appropriate, provided the two discrete levels are interpreted properly. Estimates of conditions for saturation under different conditions of pressure, laser coherence time, and laser state of polarization are also given correctly within factors of 2 or 3.

We assume that the laser is tuned very near to resonance (see Fig. 12) between state $|0\rangle$ and state $|1\rangle$ and that with the power levels being used, only the states $|0\rangle$, $|1\rangle$, and the continuum states $|E_c,\mu\rangle$ have any appreciable amplitude for being populated. Thus solutions of the time-dependent Schrödinger equation are approximately of the form of a linear combination of the two discrete state vectors $|0\rangle$ and $|1\rangle$ and the continuum states $|E_c,\mu\rangle$. In $|E_c,\mu\rangle$ the parameter μ is an angular momentum quantum number and E_c is the energy of the continuum state. The coefficients of these state vectors are then the probability amplitudes for being in the respective states at the time in question

$$|\psi(t)\rangle=a_0(t)e^{-i\omega_0 t}|0\rangle+a_1(t)e^{-i\omega_1 t}|1\rangle+\sum_{\mu}\int dE_c e^{-i\omega_c t}C(E_c,\mu,t)|E_c,\mu\rangle\,, \tag{3.1}$$

where, if $\hat{H}_0$ is the Hamiltonian of a simple isolated atom of our dilute gas (or vapor) in the absence of the laser field: $\hat{H}_0|0\rangle=\hbar\omega_0|0\rangle$, $\hat{H}_0|1\rangle=\hbar\omega_1|1\rangle$, $\hat{H}_0|E_c,\mu\rangle=\hbar\omega_c|E_c,\mu\rangle$, $\langle 0|0\rangle=1$, $\langle 1|1\rangle=1$, $\langle 0|1\rangle=0$, $\langle i|E_c,\mu\rangle=0$ $(i=0,1)$, $\langle E_c,\mu|E_c',\mu'\rangle=\delta_{\mu,\mu'}\delta(E_c-E_c')$. The total Hamiltonian is ($\hat{P}=-e\sum_i \mathbf{r}_i$ is the electronic dipole operator)

$$\hat{H}=\hat{H}_0-\hat{P}\cdot\mathbf{E}(t)+\hat{V}_c(t)\,, \tag{3.2}$$

where $-\hat{P}\cdot\mathbf{E}(t)$ is the field–atom interaction term and $\hat{V}_c(t)$ is a stochastic perturbation due to collisions of the atom with the molecules of a buffer gas. The $-\hat{P}\cdot\mathbf{E}(t)$ form of the laser field–atom interaction term has been shown by Power and Zinau (1959) to be correct to all orders in the vicinity of a dipole-allowed transition, provided that the wavelength of the light is very large compared with the size of the atom. We shall treat the laser field classically since it is well known that such a treatment gives identical results to nonrelativistic quantum electrodynamics in a large number of limiting cases. Among the situations where a classical treatment of the laser field is correct are

(1) weak light interacting with atoms near an absorption resonance,

(2) when the laser field is a coherent field (correct here at all power levels),

(3) very intense light where the number of photons of a particular $\mathbf{k}$ and ω in a cube of size λ^3 is large (i.e., the correspondence principle limit where Maxwell's equations apply).

For generality, we take $\mathbf{E}(t)$ to be of the form

$$\mathbf{E}(t)=\mathbf{k}\sum_i E_{i0}(t)\cos[\omega t+\eta_i(t)]\,, \tag{3.3}$$

where the $\mathbf{E}_{i0}(t)$ are such that $\mathbf{E}(t)$ represents a pulse of short duration compared with the radiative lifetime of $|1\rangle$. Thus the light is linearly polarized in the z direction, but $\mathbf{E}(t)$ may be due to many sources in the most general situation. The various terms in $\mathbf{E}(t)$ can, for a laser, represent different cavity modes [with $\eta_i(t)$ containing a part $\Delta\omega_i t$ for the different mode frequencies]; or for an incoherent source, the different terms could represent contributions to $\mathbf{E}(t)$ due to different excited atoms with $\eta_i(t)$ having a stochastic part due to time of excitation, position of the source atom, and line-broadening effects. In general, $E_{i0}(t)$ will also be stochastic. Thus, except for the limiting case of a single-mode laser emitting transform-limited-linewidth pulses, there are many $E_{i0}(t)$; and both $E_{i0}(t)$ and $\eta_i(t)$ are stochastic so that no repeatability [in the detailed time history of $\mathbf{E}(t)$] can be expected. It is easy to show that a sum of trigonometric terms such as that in Eq. (3.3) can be written as

$$\mathbf{E}(t)=\mathbf{k}E_0(t)\cos[\omega t+\eta(t)]\,, \tag{3.4}$$

where $E_0(t)$ and $\eta(t)$ are related in a rather complicated

way to the individual $E_{i0}(t)$ and $\eta_i(t)$. In Eq. (3.4) we expect that $E_0(t)$ and $\eta(t)$ are both strongly stochastic for a laser of much broader bandwidth than is expected for pulses with Fourier-limited bandwidths. The laser line shape is determined by $E^2(\omega)$, where $E(\omega)$ is the Fourier transform of $\mathbf{E}(t)$. By the convolution theorem we have

$$E^2(\omega) \propto \mathcal{F}_\tau[\overline{\mathbf{E}(t)\cdot\mathbf{E}(t+\tau)}]\,, \tag{3.5}$$

where $\overline{\mathbf{E}(t)\cdot\mathbf{E}(t+\tau)}$ is the average of $\mathbf{E}(t)\cdot\mathbf{E}(t+\tau)$ over t and $\mathcal{F}_\tau(F)$ indicates the Fourier transform of the function in parentheses with respect to τ, i.e.,

$$\mathcal{F}_\tau(F) = \int_{-\infty}^{\infty} e^{i\omega\tau}F(\tau)\,d\tau\,. \tag{3.6}$$

Typically, $E^2(\omega)$ may reproduce reasonably well from pulse to pulse, but the detailed time dependence of $\mathbf{E}(t)$ will not. The detailed fluctuations in $E_0(t)$ and $\eta(t)$ do not reproduce, but the relative frequency of which one gets a particular $E_0(t)$ and $\eta(t)$, as well as the way fluctuations in these quantities decay, is reproducible. This is suggestive of ergodic behavior in which the time average over any time which is very large compared with the field coherence time can be replaced by an ensemble average over the phase space of the source or equivalently over the stochastic variables η_i and E_i. Thus, if $\langle\ \rangle$ represents the ensemble average,

$$E^2(\omega) \propto \mathcal{F}_\tau[\langle\mathbf{E}(t)\cdot\mathbf{E}(t+\tau)\rangle]\,. \tag{3.7}$$

The quantity $\langle\mathbf{E}(t)\cdot\mathbf{E}(t+\tau)\rangle$ is the lowest-order field autocorrelation function. If in Eq. (3.4) $\eta(t)$ is constant and $E_0(t)$ is a reproducible, smoothly varying function of time, the linewidth is determined by the extent in time of $E_0(t)$. If the pulse length is τ_L, then the bandwidth follows as $\Delta\omega_L \approx 1/\tau_L$. Such laser pulses are said to have transform-limited bandwidths.

We shall devote much of our space here to cases where the laser field has a transform-limited bandwidth so that higher-order autocorrelation functions of the field are simply products of the lowest-order autocorrelation function, *or* to cases where the power density is sufficiently low and the bandwidth large enough so that another simplification occurs which requires only a knowledge of the laser line shape to describe the RIS process. With high-power, broad-band lasers—which can charge a_0 and a_1 in times short compared with the coherence time of the laser—a detailed treatment requires knowledge of all higher-order field autocorrelation functions. Approximate theories have been developed for this region and references can be found in deMeijere and Eberly (1978). A brief discussion of excitation with powerful broad-band lasers will be given later in this section.

We shall use Eqs. (3.3)–(3.6) in characterizing the laser throughout the present section. A detailed discussion of laser coherence effects has been given by Glauber (1963); for an elementary discussion of coherence, see Loudon (1973).

We now substitute Eqs. (3.1) and (3.2) into the time-dependent Schrödinger equation and use the orthogonality of $|0\rangle$, $|1\rangle$, and $|E_c,\mu\rangle$ in order to obtain

$$\begin{aligned}
i\frac{da_0}{dt} &= u_{00}(t)a_0 + 2\omega_R e^{-i(\omega_1-\omega_0)t}a_1(t)\cos[\omega t+\eta(t)]\,g(t)\,,\\
i\frac{da_1}{dt} &= u_{11}(t)a_1 + 2\omega_R^* e^{i(\omega_1-\omega_0)t}a_0(t)\cos[\omega t+\eta(t)]\,g(t) + \sum_\mu \int dE_c C(E_c,\mu,t)\left\langle 1\left|\frac{P_z\varepsilon_0}{2\hbar}\right|E_c,\mu\right\rangle e^{i(\omega_1-\omega_0)t}2g(t)\cos(\omega t)\,,\\
i\frac{dC}{dt}(E_c,t) &= 2e^{-i(\omega_1-\omega_c)t}\left\langle E_c,\mu\left|\frac{P_z}{2\hbar}\right|1\right\rangle a_1\varepsilon_0 g(t)\cos(\omega t)\,,
\end{aligned} \tag{3.8}$$

where $\omega_R = \langle 0|\hat{P}_z\varepsilon_0/2\hbar|1\rangle$, $\varepsilon_0^2 = \langle E_0^2(t)\rangle|_{t=0}$, $g(t) = E_0(t)/\varepsilon_0$, $\hbar u_{00} = \langle 0|\hat{V}_c(t)|0\rangle$, $\hbar u_{11} = \langle 1|\hat{V}_c(t)|1\rangle$, and we have assumed that $\hat{V}_c$ has no off-diagonal matrix elements while P_z has only off-diagonal elements. Collisional shifts on continuum states have been neglected, as have free–free transitions which would largely modify the energy spectrum of the photoelectrons if the bound-free matrix elements vary slowly with ω_c in the region near $\omega_c = \omega_{c0} \equiv \omega_0 + 2\hbar\omega$. In the above, ω_R is usually called the Rabi flopping frequency because of the role it plays when a very-narrow-bandwidth cw laser is tuned to exact resonance for one-photon absorption. In the latter situation the probability of remaining in the lower state for times small compared with the upper states' radiative lifetime is $|a_0|^2 = \cos^2(|\omega_R|t)$. Thus the population "flops" between the states $|0\rangle$ and $|1\rangle$ provided that $|\omega_R|T \gg 1$ (T = lifetime of $|1\rangle$).

We break the cosine function in Eq. (3.8) into complex exponentials according to $\cos x = \frac{1}{2}(e^{ix}+e^{-ix})$ and find that one part combines with the other complex exponential to give a slowly oscillating term, while the other term oscillates very rapidly. Perturbation theory can be used to determine the relative importance of the two terms at low power, and it is found that the slowly oscillating term gives a much larger contribution to a_1 and $C(E_c,\mu,t)$. In fact, retaining the rapidly oscillating term is inconsistent with the assumption of being near resonance with $|1\rangle$ so that no other excited states are important.

Thus we make what is ordinarily called the rotating wave approximation and keep only the most resonant (i.e., slowly oscillating) term. Letting $\alpha(E_c,\mu) = \langle 1|P_z/2\hbar|E_c,\mu\rangle$, $\delta = \omega_0 - \omega_1 + \omega$, and eliminating $C(E_c,t)$,

$$\begin{aligned}
i\frac{da_0}{dt} &= u_{00}(t)a_0 + \omega_R g(t)e^{+i\delta t}e^{+i\eta(t)}a_1\,,\\
i\frac{da_1}{dt} &= u_{11}(t)a_1 + \omega_R^* g(t)e^{-i\delta t}e^{-i\eta(t)}a_0\\
&\quad - i\sum_\mu \int dE_c\varepsilon_0^2|\alpha(E_c,\mu)|^2 g(t)\\
&\quad \times \int_{-\infty}^{t} dt' g(t')a_1(t')e^{i(\omega_c-\omega_1-\omega)(t'-t)}\,.
\end{aligned} \tag{3.9}$$

If $\alpha(E_c, \mu)$ is slowly varying in the region of E_c near $E_{c0} = \hbar\omega_{c0} = \hbar(\omega_0 + 2\omega)$, we can simplify Eq. (3.9) considerably (Choi and Payne, 1977). The condition that must be satisfied is that there must exist a Δ such that $|\Delta|$ is much larger than $|\omega_R|$, the laser bandwidth Δ_L, and the ionization rate of state $|1\rangle$. The quantity $|\Delta|$ must also be small enough so that $\alpha(E_c, \mu)$ can be regarded as constant for E_c in the interval $E_{c0} - |\Delta| \leq E_c \leq E_{c0} + |\Delta|$. For laser bandwidths $<10^{12}$/sec and laser power densities $<10^{10}$ W/cm^2, such a Δ almost always exists unless ω_{c0} is near an autoionizing resonance. When such a Δ exists, one breaks the integral over E_c into a region $E_{c0} - \Delta \leq E_c \leq E_{c0} + \Delta$, within which $\alpha(E_c, \mu)$ is replaced by $\alpha(E_{c0}, \mu)$ and a second integral over the rest of the continuum. With our assumptions, the integral over the interval about E_{c0} leads to a good approximation to a Dirac delta function in time; and the other part contains a rapidly oscillating function of time (for all E_c being integrated over) which enables one to evaluate the time integral by successive integration by parts. We obtain

$$
\begin{aligned}
i\frac{da_0}{dt} &= u_{00}(t)a_0 + \omega_R g(t) e^{i\delta t} e^{i\eta(t)} a_1 , \\
i\frac{da_1}{dt} &= u_{11}(t)a_1 + \omega_R^* g(t) e^{-i\delta t} e^{-i\eta(t)} a_0 \\
&\quad - g^2(t)(\Delta_0 + i\Gamma)a_1 , \\
\Gamma &= \hbar\Pi \sum_\mu |\alpha(E_{c0}, \mu)|^2 \varepsilon_0^2 ,
\end{aligned}
\tag{3.10}
$$

and

$$
\Delta_0 = P\int \frac{dE_c \sum_\mu |\alpha(E_c, \mu)|^2 \varepsilon_0^2}{\omega_c - \omega_0 - 2\omega} ,
$$

where P denotes principal value. It is important to note that Γ enters in as a damping term in the equation for da_1/dt. The term 2Γ represents a rate of photoionization out of $|1\rangle$, and it is consequently related to the photoionization cross section and to the peak photon flux. The term Δ_0 is a dynamic Stark shift in $|1\rangle$ due to coupling to the continuum states, and it is inconsistent to keep it without also incorporating such shifts in $|0\rangle$ and $|1\rangle$ due to off-resonance discrete states. Typically, the inclusion of such shifts is not important in two-photon ionization for power densities less than 10^8 W/cm^2 (Choi and Payne, 1977) unless the transition in question is weak. This is a consequence of the shifts' being small compared with the reciprocal pulse length until the laser power beomes rather high.

In preparation for dealing with the stochastic properties of $u_{00}(t)$, $u_{11}(t)$, $g(t)$, and $\eta(t)$, we now convert to a density matrix form of Eqs. (3.10). Letting $A_1 = a_1 \exp[i\delta t + i\eta(t)]$, $Z_1 = |A_1|^2 - |a_0|^2$, $Z_2 = 2\,\mathrm{Re}(a_0^* A_1)$, $Z_3 = 2\,\mathrm{Im}(a_0^* A_1)$, and $Z_4 = |A_1|^2$, we use Eqs. (3.10) in order to find differential equations for Z_i:

$$
\begin{aligned}
\frac{dZ_1}{dt} &= -2\Gamma Z_4 g^2 - 2\omega_R g Z_3 , \\
\frac{dZ_2}{dt} &= \left(u_{11} - u_{00} - \delta - \frac{d\eta}{dt}\right) Z_3 - g^2 \Gamma Z_2 , \\
\frac{dZ_3}{dt} &= -\left(u_{11} - u_{00} - \delta - \frac{d\eta}{dt}\right) Z_2 + 2\omega_R g Z_1 - \Gamma g^2 Z_3 , \\
\frac{dZ_4}{dt} &= -2\Gamma Z_4 g^2 - \omega_R g Z_3 .
\end{aligned}
\tag{3.11}
$$

Obviously, Z_4 is the probability of the atom's being in state $|1\rangle$ at time t, Z_1 is the probability of being $|1\rangle$ minus the probability of being in $|0\rangle$, and Z_2 and Z_3 are related to the time-dependent expectation value of P_z (i.e., to $\langle\psi(t)|\hat{P}_z|\psi(t)\rangle$). If photoionization were absent, the first three equations would be sufficient, and we would have $Z_1^2 + Z_2^2 + Z_3^2 = 1$ as a consequence of unitarity [i.e., $Z_1^2 + Z_2^2 + Z_3^2 = (|a_0|^2 + |a_1|^2)^2$ where $|a_0|^2 + |a_1|^2 = 1$]. In the presence of photoionization we have

$$
Z_1^2 + Z_2^2 + Z_3^2 = \left[1 - 2\int_{-\infty}^{t} \Gamma g^2(t') Z_4(t')\, dt\right]^2 , \tag{3.12}
$$

and the probability of ionization for the particular laser pulse with the particular time history of u_{00}, u_{11}, E_0, and η is

$$
P_I = 2\int_{-\infty}^{\infty} \Gamma g^2(t') Z_4(t')\, dt' . \tag{3.13}
$$

In order to get some understanding of the effects of collisions and laser coherence, we shall now consider separately the following situations:

1. The laser has a transform-limited bandwidth, but collisions may be important. ($\eta = $ const, fluctuations in g are unimportant, but collisional line-broadening effects are included through u_{00} and u_{11}.)
2. Collisional line-broadening effects are absent ($u_{00} = u_{11} = 0$), but the coherence time of the laser is short compared with the pulse length of the laser; consequently the laser bandwidth is far larger than its transform-limited value. Thus fluctuations in η and g must be accounted for.

Cases 1 and 2 will be considered in order.

C. Effect of collisional line broadening on the two-step RIS process

Before getting into the actual derivation, we note that typically $|\langle 0|P_z|1\rangle| \approx e a_B$, where a_B is the Bohr radius. Thus, since the average power density near $t = 0$ is $I \approx C\varepsilon_0^2/8\pi$ and $\omega_R \approx e a_B \varepsilon_0/2\hbar$, we find that with I in W/cm^2 typical values of ω_R are $|\omega_R| \approx 10^8\sqrt{I}$, where $|\omega_R|$ is the Rabi frequency in radians/sec. Correspondingly, if the photoionization cross section of $|1\rangle$ at frequencies near ω is $\sim 10^{-18}$ cm^2, we have for the photoionization rate constant $\Gamma \approx 3I$, where Γ has units of sec^{-1}. With buffer gas pressures <100 Torr, the time between collisions that introduce appreciable phase shifts is $\gtrsim 10^{-10}$ sec, while the duration of these collisions is $\leq 10^{-12}$ sec. The estimate of $|\omega_R| \approx 10^8\sqrt{I}$ represents a fairly strong transition, and values $\approx 10^7\sqrt{I}$ are not rare. Thus, if $I \lesssim 10^6$ W/cm^2, we see from Eqs. (3.11) that the laser field produces very little change in the Z_i during a single collision.

Except for the largest power densities being considered, we can choose a time τ which is large compared with the duration of a collision but sufficiently small so that $|\omega_R|\tau \ll 1$ and $\Gamma\tau \ll 1$. During the period of time $t \to t + \tau$ the Z_i evolve according to $dZ_2/dt = (u_{11} - u_{00} - \delta)Z_3$, $dZ_3/dt = -(u_{11} - u_{00} - \delta)Z_2$, with Z_1 and Z_4 being constant. Letting $W = Z_2 + iZ_3$,

$$
W(t+\tau) = W(t)\exp\left(-i\int_t^{t+\tau} [u_{11}(t') - u_{00}(t') - \delta]\, dt'\right) . \tag{3.14}
$$

We have allowed for the fact that during a single collision we can have $\int dt'(u_{11}-u_{00}) \gg 1$, and thereby a large phase change is introduced. Equations (3.11) and (3.14) apply to a single atom, subject to a particular time history of $u_{11}(t)-u_{00}(t)$. Typically, in an ionization study, there will be many atoms in the laser beam, and $u_{11}-u_{00}$ will have a different time history for different atoms. We want to arrive at equations which give a prediction of the average behavior of the atom. To describe the average behavior, we replace Eqs. (3.11) by a set averaged over a large number of atoms seeing the same laser pulse, but with different u_{11} and u_{00}:

$$\begin{aligned}
\frac{d\bar{Z}_1}{dt} &= -2\Gamma\bar{Z}_4 g^2 - 2\omega_R g\bar{Z}_3 ,\\
\frac{d\bar{Z}_2}{dt} &= -g^2\Gamma\bar{Z}_2 - \delta\bar{Z}_3 + \overline{\left(\frac{dZ_2}{dt}\right)}_{\text{coll}} ,\\
\frac{d\bar{Z}_3}{dt} &= \delta\bar{Z}_2 - \Gamma\bar{Z}_3 g^2 + 2\omega_R g\bar{Z}_1 + \overline{\left(\frac{dZ_3}{dt}\right)}_{\text{coll}} ,\\
\frac{d\bar{Z}_4}{dt} &= -2\Gamma\bar{Z}_4 g^2 - \omega_R g\bar{Z}_3 ,
\end{aligned} \tag{3.15}$$

where we include the average of the terms involving $u_{11}-u_{00}$ by way of $\overline{(dZ_2/dt)}_{\text{coll}}$ and $\overline{(dZ_3/dt)}_{\text{coll}}$. We have also restricted δ so that $|\delta|\tau \ll 1$. Thus the results apply very near line center (i.e., $|\delta| \lesssim 10^{11}$). To get the average rates of change of $\bar{Z}_2$ and $\bar{Z}_3$, we use Eqs. (3.14) with $\delta = 0$:

$$\overline{\left(\frac{dW}{dt}\right)}_{\text{coll}} = \frac{\overline{W(t+\tau)-W(t)}}{\tau} \simeq \overline{W(t)}\ \overline{[\exp(-i\phi)-1]} , \tag{3.16}$$

where

$$\phi = \int_t^{t+\tau} [u_{11}(t')-u_{00}(t')]\,dt'$$

and we have broken the average of $W[\exp(-i\phi)-1]$ into a product of averages by assuming that $W(t)$ depends only on collisions occurring before the time interval in question and that at relatively low pressures the time history of collisions in $t \leq t' \leq t+\tau$ is totally uncorrelated with what has occurred before. We have reduced the effect of collision in the region near line center to calculating $\overline{e^{-i\phi}}$ for $t \to t+\tau$. Let

$$P(\phi,t,t')d\phi = \text{probability of a net change in } \phi \text{ in the range } \phi \to \phi+d\phi \text{ for the time } t \to t' . \tag{3.17}$$

Letting $\gamma(\nu)d\nu$ = probability per unit time of a collision which gives a phase change $\nu \to \nu+d\nu$, we get

$$\frac{\partial P}{\partial t'}(\phi,t,t') = \int_{-\infty}^{\infty} \gamma(\nu)\,d\nu\,[P(\phi-\nu,t,t')-P(\phi,t,t')] . \tag{3.18}$$

Obviously,

$$\overline{e^{-i\phi}} = \int_{-\infty}^{\infty} d\phi\, P(\phi,t,t+\tau)e^{-i\phi} . \tag{3.19}$$

Multiplying Eq. (3.18) by $e^{-i\phi(t')}$ and integrating over ϕ, we obtain an equation that can be trivially solved to give

$$\begin{aligned}
\overline{e^{-i\phi}} &= \exp\left[\tau\int_{-\infty}^{\infty}\gamma(\nu)d\nu(e^{i\nu}-1)\right] ,\\
&\equiv \exp[\tau(-\Gamma_c+i\Delta_c)] ,
\end{aligned} \tag{3.20}$$

where Γ_c is a positive number, and

$$\Gamma_c = \int_{-\infty}^{\infty}\gamma(\nu)(1-\cos\nu)\,d\nu ,$$

$$\Delta_c = \int_{-\infty}^{\infty}\gamma(\nu)\sin\nu\,d\nu .$$

If collisions are sufficiently infrequent so that $\Gamma_c\tau \ll 1$ and $\Delta_c\tau \ll 1$, we get from Eqs. (3.15)–(3.20):

$$\begin{aligned}
\frac{d\bar{Z}_1}{dt} &= -2\Gamma\bar{Z}_4 g^2 - 2\omega_R g\bar{Z}_3 ,\\
\frac{d\bar{Z}_2}{dt} &= -(\delta+\Delta_c)\bar{Z}_3 - (g^2\Gamma+\Gamma_c)\bar{Z}_2 ,\\
\frac{d\bar{Z}_3}{dt} &= (\delta+\Delta_c)\bar{Z}_2 - (g^2\Gamma+\Gamma_c)\bar{Z}_3 + 2\omega_R g\bar{Z}_1 ,\\
\frac{d\bar{Z}_4}{dt} &= -2\Gamma g^2\bar{Z}_4 - \omega_R g\bar{Z}_3 .
\end{aligned} \tag{3.21}$$

In the absence of photoionization (i.e., $\Gamma = 0$), Eqs. (3.21) reduce to the Bloch equations, which were originally developed in connection with nuclear magnetic resonance, but which have been widely used in quantum electronics. A little thought about the assumption required to obtain Eqs. (3.21) tells one a great deal about the region of validity of the Bloch equations. For the ionization probability we get

$$\bar{P}_I = 2\Gamma\int_{-\infty}^{\infty} g^2(t')\bar{Z}_4(t')\,dt' . \tag{3.22}$$

We see that with these assumptions the effect of collisions is to cause an additional damping of the off-diagonal elements of the density matrix. The limit which leads to the validity of rate equations occurs if $|\omega_R| \ll \Gamma_c$ and $|\Delta| <$ (duration of collision)$^{-1}$. For instance, if the pressure of the buffer gas is large ($\gtrsim 100$ Torr), Γ_c can approach 10^{10}–10^{11}/sec. Therefore, if $I < 10^4$ W/cm^2, we have $|\omega_R| < 10^9$–10^{10} sec^{-1}, and $\bar{Z}_1$ and $\bar{Z}_4$ change very little in a time $1/\Gamma_c$. Letting $\bar{W} = \bar{Z}_2 + i\bar{Z}_3$, Eqs. (3.21) lead to

$$\begin{aligned}
\bar{W}(t) &= 2i\omega_R\int_{-\infty}^{t} g(t')\bar{Z}_1(t') \\
&\qquad \times \exp\left|-[\Gamma g^2+\Gamma_c-i(\delta+\Delta_c)](t-t')\right| dt' \\
&\approx \frac{2i\omega_R g(t)\bar{Z}_1(t)}{\Gamma+\Gamma_c-i(\delta+\Delta_c)} ,
\end{aligned} \tag{3.23}$$

where we have used the fact that $\bar{Z}_1(t)$ varies very little in a time interval $5/\Gamma_c$, while nearly all of the contribution to the integral comes from $t-5/\Gamma_c \leq t' \leq t$. In this approximation, both $\bar{Z}_2$ and $\bar{Z}_3$ are proportional to $\bar{Z}_1$ so that the off-diagonal elements of the density matrix can be eliminated. Noting that $\bar{Z}_1 = \rho_{11}-\rho_{00}$, $Z_4 = \rho_{11}$, we obtain

$$\begin{aligned}
\frac{d\rho_{00}}{dt} &= \frac{2|\omega_R|^2 g^2\Gamma_c}{\Gamma_c^2+(\delta+\Delta_c)^2}(\rho_{11}-\rho_{00}) ,\\
\frac{d\rho_{11}}{dt} &= -2\Gamma\rho_{11}g^2 - \frac{2|\omega_R|^2 g^2\Gamma_c}{\Gamma_c^2+(\delta+\Delta_c)^2}(\rho_{11}-\rho_{00}) .
\end{aligned} \tag{3.24}$$

Equations (3.24) are a set of rate equations equivalent to those that would be written intuitively for an atom which has an absorption and stimulated emission cross section such that ($\mathcal{F}$ = photon flux)

$$\mathcal{F}\sigma_a(\delta) = \sigma_s(\delta)\mathcal{F} = \frac{2|\omega_R|^2 g^2 \Gamma_c}{\Gamma_c^2 + (\delta + \Delta_c)^2}, \tag{3.25a}$$

and

$$\mathcal{F}\sigma_I = 2\Gamma g^2, \tag{3.25b}$$

where σ_I is the photoionization cross section. Equation (3.25b) substantiates the interpretation of Γ that was given earlier. The degeneracy factors do not enter here as they did in the rate equation discussion of the He(2^1S) detection experiment because collisional effects which would change m_z have been neglected.

In summary, rate equations are valid in the presence of pressure-broadening effects and with narrow-band lasers, provided $\Gamma_c \gg |\omega_R|$. In other words, the validity of rate equations with narrow-band plane polarized light requires that collisional dephasing cause the atom to lose memory of how it was excited in a time that is small compared with the time required for a further stimulated emission or absorption to become probable. Rate equations do not apply if $|\omega_R| \gtrsim \Gamma_c$, and the width of the absorption line becomes dominated by power broadening. However, we shall see later that for most transitions, even power densities $<10^4$ W/cm^2 are sufficient to level (i.e., make the upper and lower populations equal) the upper and lower populations in a time short compared with the pulse length. The use of high power levels (i.e., $|\omega_R| \gtrsim \Gamma_c$) is usually unnecessary if a separate more powerful laser which is tuned far from resonance is used for the ionization step.

Consider the simple model of broadening by a van der Waals interaction in order to estimate the order of magnitude of Γ_c. If $K_6 = C_6/h$, where the van der Waals interaction difference potential is $\Delta V(R) = C_6/R^6$, we find for a single collision at impact parameter b:

$$\nu = \text{phase change} = K_6 \int_{-\infty}^{\infty} \frac{dt}{[b^2 + v^2 t^2]^3},$$

$$= \frac{3\Pi}{16}\frac{K_6}{v b^5}. \tag{3.26}$$

Thus the average rate of collisions which give $\nu \to \nu + d\nu$ is the same as the rate of collisions in the correct $b \to b + db$ range and

$$\gamma(\nu) = 2\Pi\, \overline{b(\nu, v)\frac{db}{d\nu}(\nu, v) v N}, \tag{3.27}$$

where $b(\nu, v)$ is the impact parameter which gives a phase change ν when the relative velocity is v and N is the concentration of buffer gas molecules. The bar denotes the average over relative velocities. We get from Eqs. (3.20), (3.26), and (3.27)

$$\Gamma_c \simeq 17(K_6)^{2/5}(\bar{v})^{3/5} N,$$

$$\Delta_c \simeq -3(K_6)^{2/5}(\bar{v})^{3/5} N. \tag{3.28}$$

Typically, $K_6 \simeq 10^{-30}$ cm^6/sec, $v \simeq 10^5$/sec, $N \simeq 3\times 10^{16} P$ (P in Torr). Thus $\Gamma_c \simeq 5\times 10^8 P$. When $P > 100$ Torr, we can have $\Gamma_c \simeq 10^{11}$/sec. The van der Waals form of the difference potential is usually inadequate to describe Γ_c and Δ_c (Hindmarsh, 1974) in detail, as is the assumption of straight-line orbits. However, the estimate of the order of magnitude of Γ_c and Δ_c is reasonable. At line center the model predicts $\sigma_a(0)F = \sigma_s(0)F = |\omega_R|^2/\Gamma_c \approx 10^{16} I/\Gamma_c$; or when $\Gamma_c \simeq 10^{11}$, we get $\sigma_a(0)F \simeq 10^5 I$ so that $I \simeq 10^4$ W/cm^2 will saturate many discrete–discrete transitions if a narrow-band laser is used in the presence of a buffer gas with $P \simeq 100$ Torr. At $I = 10^4$ W/cm^2, rate equations apply with a modified Γ even if a second laser with $I' \lesssim 10^8$ W/cm^2 is present which can ionize $|1\rangle$, providing that the second laser is well out of resonance for any discrete–discrete process beginning from $|0\rangle$. The 10^8 W/cm^2 restriction on I' is due to the importance of keeping dynamic Stark shifts in $|0\rangle$ and $|1\rangle$ small compared with the pressure-broadened linewidth so that they can be neglected. Such shifts arise due to the off-resonance laser field coupling $|0\rangle$ and $|1\rangle$ to other levels to which they have dipole-allowed transitions. These shifts leave a two-discrete state picture intact but introduce power-dependent shifts in δ. We emphasize again that leveling of the upper and lower populations can be achieved with narrow-bandwidth lasers in the region of laser power where rate equations apply providing that $\Gamma_c \tau_L \gg 1$. At higher power, the simplicity of rate equations is lost and a more complex theory is required. However, at line center, the upper and lower level populations will still (on the average) become equal. When such a laser is tuned away from line center, the core of the line will have a width $\gtrsim 2|\omega_R|$, since this is the reciprocal of the time over which the laser can change the Z_{ij}. Resonance ionization spectroscopy can still be used but with less selectivity. When the laser power is such that $|\omega_R| \gg \Gamma_c$ and two or more sequential discrete-discrete steps are used in the RIS scheme, a subtle effect occurs in which power-dependent shifts in the atomic levels play an important role (Moody and Lambropoulos, 1977). This effect will be discussed further later in this section.

In the preceding discussion of line-broadening effects we have assumed $\delta T_c \ll 1$, where T_c is the collision duration at an impact parameter where the total phase change is 1 radian. When $\delta T_c \gg 1$, the line shape becomes sensitive to the details of what happens during single collisions, and we enter the so-called quasistatic region (Hindmarsh, 1974) of the absorption line shape. In this region absorption is a very rare event since it requires collisions in which δ becomes equal to $u_{11} - u_{00}$ at some intranuclear separation. At such a separation the energy levels of the quasimolecule are separated by exactly the correct amount for resonant absorption. Even though the resonance condition may only be satisfied for a time $\approx 10^{-12}$ sec, this mechanism still dominates the far wing absorption in almost all cases where $u_{11} - u_{00} - \delta$ becomes zero at some R for the δ in question. In contrast to the $\delta T_c \ll 1$ case, where it is important to deal very carefully with the stochastics of phase changes which accumulate over many collisions, and their interplay with excitation which also occurs continuously for a time interval which spans several collisions, we have here a situation in which excitation only occurs during collisions. The attention focuses on the details of what happens during a rather rare single collision, with many collisions which do not satisfy $u_{11} - u_{00} = \delta$ (but do introduce phase changes which destroy memory) occurring in between. We therefore need rates of absorption and stimulated emission due to collisions

in which $u_{11}-u_{00}-\delta$ becomes zero, because even at lower pressures the times between such collisions are random, and quantum interference effects between collisions average out so that rate equations which focus on transitions during individual collisions apply in general. The required rate is calculated by returning to Eq. (3.10) and neglecting Δ_0, Γ, and $\eta(t)$ while assuming that $|a_0|\approx 1$. We get during a single collision

$$a_0 \simeq \exp\left[-i\int_{-\infty}^{t} u_{00}(t')\,dt'\right], \tag{3.29a}$$

$$|a_1|^2 = |\omega_R|^2 g^2(t_0)\left|\int_{-\infty}^{t}\exp(-i\delta t')\exp\left[i\int_{-\infty}^{t'}[u_{11}(t'')-u_{00}(t'')]\,dt''\right]dt'\right|^2, \tag{3.29b}$$

where t_0 is the time at which the distance of closest approach occurs for the collision. If we assume that the integrand oscillates rapidly, causing strong cancellation except for times close to $\delta-u_{11}(t_c)+u_{00}(t_c)=0$, we obtain for $|a_1|^2$ (averaged over a small range of impact parameters to wash out interference between the two crossings)

$$\overline{|a_1|^2} = \text{probability of absorption during a collision with a particular relative velocity and impact parameter} = \frac{4\pi|\omega_R|^2 g^2(t_0)}{\left|\frac{d}{dt}(u_{11}-u_{00})\right|_{t=t_c}}. \tag{3.30}$$

We have approximated $\delta = u_{11}(t)+u_{00}(t)$ by a linear function of time near each of the two t_c. Thus we are also assuming that $d(u_{11}-u_{00})/dt|_{t_c}\neq 0$, so that Eq. (3.30) would not hold near a satellite (Hindmarsh, 1974). Near a satellite, emission is enhanced due to the resonance's lasting for a longer time period. We assume, as has been found to be the case with some spectral lines (Hindmarsh, 1974), that $u_{11}-u_{00}$ is of the van der Waals type until δ becomes so large that we are many Ångstrom units in wavelength from line center. Then $u_{11}-u_{00}=K/(b^2+v^2t^2)^3$, where v is relative velocity and b is impact parameter. Evaluating $d(u_{11}-u_{00})/dt|_{t=t_c}$ and calculating a rate constant R for absorption, we get

$$R=\overline{Nv\sigma}, \tag{3.31a}$$

where

$$\sigma = 2\pi\int_0^{(K/\delta)^{1/6}}\overline{b|a_1|^2}\,db, \qquad = \frac{4\pi^2}{3v}|\omega_R|^2 g^2(t_0)K^{1/2}\delta^{-3/2}. \tag{3.31b}$$

Thus,

$$R=\tfrac{4}{3}\pi^2 N|\omega_R|^2 g^2(t_0)K^{1/2}\delta^{-3/2}. \tag{3.32}$$

To get some idea about how large R is at different points away from line center, we take $N=3.2\times10^{16}\,P$, $\omega_R\simeq 10^7\sqrt{I}$, $K\simeq 10^{-30}$ cm^6/sec, λ_0 = line center wavelength = 5000 Å. Thus, with I in W/cm^2, P in Torr, and with $P\simeq 100$ Torr, we have $R\approx 6.4I/\Delta\lambda^{3/2}$, with $\Delta\lambda$ the displacement from line center in Ångstrom units. With $I=10^8$ W/cm^2 and $\Delta\lambda\simeq 10$ Å, we have $R\simeq 2.03\times10^7$/sec. The rate constant for absorption is equal to the rate constant for stimulated emission so that the populations of the upper and lower levels for short-pulse-length lasers satisfy

$$\frac{d\rho_{00}}{dt}=R(\rho_{11}-\rho_{00}),$$

$$\frac{d\rho_{11}}{dt}=-R(\rho_{11}-\rho_{00})-2\Gamma g^2\rho_{11}. \tag{3.33}$$

Thus near line center we can use a Lorentzian line for R as in Eqs. (3.29), but on the far wing, where $\delta-u_{11}+u_{00}$ becomes equal to zero, we use an R similar to Eq. (3.32). At very high power levels, Eqs. (3.29) may fail because of saturation effects. This usually occurs for $\omega_R\gtrsim 10^{12}$/sec, and in this case a Landau–Zener solution of Eqs. (3.10) leads to a better estimate of R, providing δ is sufficiently large for the approximation to apply.

It is important to note that once

$$\int_{-\infty}^{\infty}\Gamma g^2 dt > 5$$

every atom which reaches the excited state is ionized. At line center all atoms get to the excited state, but due to saturation of the discrete–discrete transition this may also have been true at a power level approximately 1000 lower. On the far wing, however, the number getting excited has continued to grow so that the ionization signal is perhaps approximately 100 to 1000 times larger relative to line center than would be observed if the upper-state population were monitored following excitation with a weak laser. The rather impressive far wing line broadening of a Cs line by a dye laser with various power levels is shown in Fig. 13. At a later point in this section we discuss RIS schemes that avoid this lack of selectivity.

Resonance ionization spectroscopy also has applications to low-pressure situations where pressure-broadening effects are unimportant. These applications can be either cell experiments or experiments on atomic beams. If we neglect Doppler effects, which can be very important at low power levels, and assume $\omega_R\tau\gg 1$, where τ is the laser pulse length, the probability of ionization becomes (Choi and Payne, 1977)

$$P_I = 1-\exp\left[-\int_{-\infty}^{\infty}\Gamma g^2(t)\left(1-\frac{|\delta|}{\sqrt{\delta^2+4\omega_R^2 g^2(t)}}\right)dt\right]. \tag{3.34}$$

Equation (3.34) is derived for $|\delta|\tau>10$, but when $\omega_R\tau\gg 10$ it also holds for smaller $|\delta|$ as well. Equation (3.34) also depends on $\omega_R\gg\Gamma$ and upon the laser band-

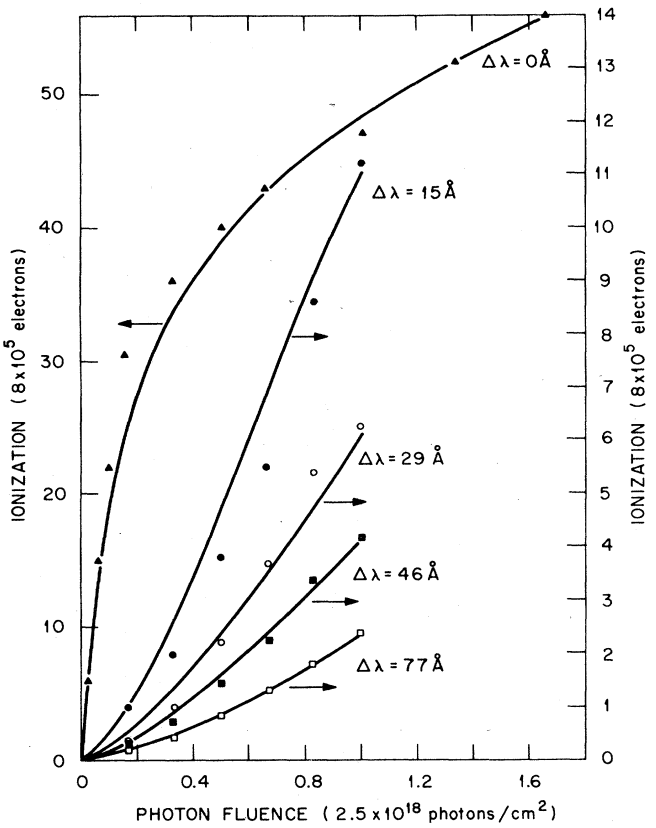

FIG. 13. Two-photon ionization signal as a function of power and detuning from the 4593 Å line of Cs. The Cs line is broadened by 760 Torr of Ar.

width being transform limited. That is, if $\Delta\omega_L$ is the laser bandwidth,

$$\Delta\omega_L\tau \approx 1 .$$

With such narrow-band lasers and with ω_R and $|\delta| \gg 1/\tau$, several types of adiabatic perturbation theory lead to Eq. (3.34). If $\Gamma\tau$ is not too large compared with unity, the FWHM of P_I is about $2|\omega_R|$ (i.e., the width is due to power broadening). When $\Gamma\tau \gg 1$, the width can be much larger than $|\omega_R|$ and is given roughly by $2|\omega_R|\sqrt{\Gamma\tau}$.

D. Effect of laser coherence time on the two-step RIS process

The main effects of laser coherence time for two-photon ionization near a one-photon resonance have to do with the excitation process itself. This is because the resonance situation usually involves a rapid leveling (on the time average at least) of the upper- and lower-state populations with ionization proceeding at a far slower rate out of the upper level. For this reason we use Eqs. (3.11) with $u_{11} = u_{00} = 0 = \Gamma$ in order to investigate the effects of laser coherence time on excitation. In this approximation Z_4 decouples and

$$\begin{aligned} \frac{dZ_1}{dt} &= -2\omega_R g Z_3 , \\ \frac{dZ_2}{dt} &= -\left(\delta + \frac{d\eta}{dt}\right) Z_3 , \\ \frac{dZ_3}{dt} &= \left(\delta + \frac{d\eta}{dt}\right) Z_2 + 2\omega_R g Z_1 . \end{aligned} \tag{3.35}$$

In this case g and $d\eta/dt$ have stochastic properties which must be dealt with.

Letting $W = Z_2 + iZ_3$, we obtain W (and hence Z_3) as an integral of Z_1. When the integral for Z_3 in terms of Z_1 is substituted back into the first of Eqs. (3.35), we obtain after some manipulation

$$Z_1 = -1 + \alpha^2 \int_{-\infty}^{t} Z_1(t') K(t, t')\, dt' , \tag{3.36}$$

where

$$K(t, t') = -\int_{t'}^{t} dt'' g(t') g(t'') \cos[q(t') - q(t'')] ,$$

$q(t) = \delta t + \eta(t)$, and $\alpha = 2\omega_R$. As described before, these equations represent the response of the atom to a particular time history of $g(t)$ and $\eta(t)$. Perturbation theory yields

$$Z_1 = -1 - \alpha^2 \int_{-\infty}^{t} K(t, t_2)\, dt_2 + \alpha^4 \int_{-\infty}^{t} dt_2 \int_{-\infty}^{t_2} dt_3 K(t, t_2) K(t_2, t_3) - \alpha^6 \int_{-\infty}^{t} dt_2 \int_{-\infty}^{t_2} dt_3 \int_{-\infty}^{t_3} dt_4 K(t, t_2) K(t_2, t_3) K(t_3, t_4) + \cdots . \tag{3.37}$$

The ensemble-averaged Z_1 involves $\langle K(t, t_2)\rangle$, $\langle K(t, t_2) K(t_2, t_3)\rangle$, $\langle K(t, t_2) K(t_2, t_3) K(t_3, t_4)\rangle$, etc. That is, in the most general case, $\bar{Z}_1$ depends on laser field autocorrelation functions of all orders. However, if $\alpha \ll \Gamma_L$, the laser field can only change $\bar{Z}_1$ over times that are long compared with the field autocorrelation time, and most of the contribution to the integral in Eq. (3.36) comes from times very near $t' = t$ (i.e., within $5/\Gamma_L$ or so). In this situation one can accurately use $\langle Z_1(t') K(t, t')\rangle \simeq \bar{Z}_1(t') \langle K(t, t')\rangle$. We get

$$\bar{Z}_1 \cong -1 + \alpha^2 \int_{-\infty}^{t} \bar{Z}_1(t') \langle K(t, t')\, dt'\rangle . \tag{3.38}$$

Equation (3.38) is strictly speaking only an expansion in (α/Γ_L), but it is often used in more general situations where this parameter α/Γ_L is not small (van Kampen, 1975). The problem with Eq. (3.38) is that a perturbation expansion shows that it is only exact if higher-order field autocorrelation functions factor into a product of first field autocorrelation functions. That is, $\langle K(t, t_2) K(t_2, t_3)\rangle \approx \langle K(t, t_2)\rangle \langle K(t_2, t_3)\rangle$, etc. This type of an assumption is only exact for a coherent field. Similar approximations have been used by a number of workers (Mallow, 1975; Carmichael and Walls, 1975; Eberly, 1976; Kimble and Mandel, 1977) in dealing with a variety of atom–laser field problems. In situations where $\bar{Z}_1 \to 0$ (i.e., the upper- and lower-level populations are leveled) is achieved in a small fraction of the laser pulse duration while $\alpha/\Gamma_L \ll 1$, this approximation probably also works very well for $\alpha/\Gamma_L > 1$ in predicting the increased linewidth due to power-broadening effects.

The rate equation limit will now be shown to correspond to $\alpha/\Gamma_L \ll 1$. We choose a model for the light field in which the source is a group of gas phase atoms excited at random times and each producing a classical E field which decays exponentially in the time following excitation. The emission of this light source is pressure broadened due to collisions with a buffer gas. With

this model, one can derive field autocorrelation functions of all orders. We find

$$\langle K(t,t')\rangle = -\int_{t'}^{t} dt''\langle g^2(t')\rangle \times \exp[-\Gamma_L(t''-t')]\cos[\delta(t''-t')]\,. \quad (3.39)$$

The line shape of the light field based on such a model is Lorentzian. To derive the rate equations, we differentiate Eq. (3.38):

$$\frac{d\bar{Z}_1}{dt} = \alpha^2 \int_{-\infty}^{t} \bar{Z}_1(t')\frac{\partial}{\partial t}\langle K(t,t')\rangle dt'\,. \quad (3.40)$$

In the integral, contributions come only from times $t - 5/\Gamma_L \leq t' \leq t$; and over this region, $\bar{Z}_1(t')$ is nearly constant since α is too small to change $\bar{Z}_1$ appreciably in such a small time period. Thus,

$$\frac{d\bar{Z}_1}{dt} \simeq -\alpha^2\bar{Z}_1 K(t,-\infty)\,,$$

$$\simeq -\frac{\alpha^2\Gamma_L\langle g^2(t)\rangle}{\Gamma_L^2+\delta^2}\bar{Z}_1\,. \quad (3.41)$$

Since $\bar{Z}_1 = \rho_{11} - \rho_{00}$ and $\rho_{00} + \rho_{11} = 1$, we can convert Eq. (3.41) into two rate equations for ρ_{00} and ρ_{11}.

In order to give a better picture of the situation where $\Gamma_L\Upsilon_L \gg 1$ and $\alpha/\Gamma_L \gg 1$, we follow other work and assume the validity of Eqs. (3.38) and (3.39). These equations are easily shown to be equivalent to the following Bloch equations:

$$d\bar{Z}_1/dt = -\alpha h(t)\bar{Z}_3\,,$$

$$d\bar{Z}_3/dt = \alpha h(t)\bar{Z}_1 - \Gamma_L\bar{Z}_3 + \delta\bar{Z}_2\,,$$

$$d\bar{Z}_2/dt = -\Gamma_L\bar{Z}_2 - \delta\bar{Z}_3\,,$$

where $h(t) = [\langle g^2(t)\rangle]^{1/2}$. It follows that

$$\frac{d}{dt}[\bar{Z}_1^2 + \bar{Z}_2^2 + \bar{Z}_3^2] = -2\Gamma_L[\bar{Z}_2^2 + \bar{Z}_3^2]\,,$$

which provides rigorous information about the decay of $\bar{Z}_2$ and $\bar{Z}_3$. The similarity between these equations and the Bloch equations derived for pressure-broadening effects is obvious. The features of solutions to the above equations can be illustrated by taking $h(t) = 0$ for $t < 0$ and $h(t) = 1$ for $t \geq 0$. Using $\alpha/\Gamma_L \gg 1$, we find

$$\bar{Z}_1 \cong -\frac{\delta^2}{\delta^2+\alpha^2}\exp\left[-\frac{\Gamma_L\alpha^2 t}{\delta^2+\alpha^2}\right] - \frac{\alpha^2}{\delta^2+\alpha^2}\exp\left[-\Gamma_L t\left(1-\frac{\frac{1}{2}\alpha^2}{\delta^2+\alpha^2}\right)\right]\cos[\sqrt{\delta^2+\alpha^2}\,t]\,.$$

Now, $\rho_{11} = (1+\bar{Z}_1)/2$, and if $\Gamma_L t \gg 1$, we see that ρ_{11} is substantial for $|\delta| < \alpha$ even at times as short as α^{-1}. For $|\delta| > \alpha$, the populations are nearly leveled in a time T_s given by

$$T_s \simeq 2[1+\delta^2/\alpha^2]\Gamma_L^{-1}\,.$$

When T_s is shorter than either the laser pulse length or the lifetime against spontaneous emission, saturation can occur over a δ region which is large compared with α. The role of power broadening is clear, even though this model of the pulse shape is not very realistic. Obviously a similar discussion would apply to pressure broadening with Γ_L replaced by Γ_c. The extended region over which saturation occurs will also reflect itself in the RIS linewidth. In particular, if Γ were large enough to produce ionization in the laser pulse (i.e., $\Gamma\Upsilon_L \simeq 1$), the width would be $\sim \alpha\sqrt{\Upsilon_L\Gamma_L}$, where Υ_L is the time at which the square pulse is terminated. Despite the more complex appearance of the solution to the Bloch equations, as compared with Eq. (3.41), conclusions about saturation and the linewidth for an RIS signal are extremely similar. That is, a linewidth based on blindly using Eq. (3.41) at the higher power levels also gives an RIS linewidth $\sim\alpha\sqrt{\Gamma_L\Upsilon_L}$.

A generalization of (3.41) to include a more general laser line shape and photoionization, but still requiring $\alpha/\Gamma_L \ll 1$, is

$$\frac{dN_0}{dt} = \int d\nu\, I(\nu,t)\sigma(\nu)(N_1 - N_0)\,,$$

$$\frac{dN_1}{dt} = -\int d\nu\, I(\nu,t)\sigma(\nu)(N_1 - N_0) - \mathcal{F}(t)\sigma_I N_1\,, \quad (3.42)$$

where $N_0 = N_T\rho_{00}$ = number of atoms in the lower discrete state, N_T = total number of the selected atoms in the beam, $N_1 = N_T\rho_{11}$ = number of atoms in the upper excited state; $I(\nu,t)$ = number of photons per unit frequency interval per second per cm^2 in the beam at time t; $\sigma(\nu)$ = cross section for absorbing a photon of fequency ν or for stimulating emission at frequency ν if the atom is in the upper state; $\mathcal{F}(t)$ = photon flux = $\int I(\nu,t)\,d\nu$. With no pressure broadening and with short pulses, $\sigma(\nu)$ is very sharply peaked at the resonance and $\int I(\nu,t)\sigma(\nu)\,d\nu = I_\delta(t)\int\sigma(\nu)\,d\nu$, where by $I_\delta(t)$ we mean the number of photons per unit frequency per cm^2 per second at the resonant wavelength when the laser line center is tuned δ angular frequency units away. From Eq. (3.41) we see that a laser with a bandwidth $\sim 10^{10}$/sec permits a leveling of the populations in $\sim 10^{-9}$ sec with a peak power density of 10^3 W/cm^2. Thus, in the absence of line-broadening effects, very modest power densities (consistent with rate equations) level the populations very quickly.

In conclusion, when the bandwidth of the laser is large compared with $|\omega_R|$, rate equations apply and the rate of excitation is proportional to the value of $I(\nu,t)$ evaluated at the resonant frequency. This characteristic points out an important practical consideration when using powerful broadband lasers for the discrete–discrete step. When the laser is sufficiently powerful to saturate the ionization, it is usually many times more powerful than what is required for saturating the discrete–discrete step. Thus, even if the laser is tuned relatively far from resonance, photons on the wing of the line could still saturate a discrete–discrete transition, leading to total ionization of the selected atoms. Consequently, when high selectivity is required and background effects might be important, the most effective RIS scheme is one where relatively low-power, relatively narrow-bandwidth lasers are used to saturate one or more discrete–discrete transitions, and a long-wavelength laser such as a Nd:Yag is used for the final (ionization) step. Short pulse length (i.e., $\sim 10^{-8}$ sec) is also desirable (despite the accompanying higher peak power requirements) because it reduces the possibility of inelastic collisions out of excited states as well as

confusion due to spontaneous emission. Our considerations on far wing line broadening further reinforce the argument for using narrow-bandwidth dye lasers with modest peak power for the discrete–discrete transitions. We shall see below that the need for long wavelengths at all high fluxes is compatible with a need to keep multiphoton ionization to a minimum.

E. Two-photon excitation

When one-photon excitation can be achieved with photons of energy $\lesssim 5.6$ eV, the use of one or more relatively weak dye lasers to saturate discrete–discrete transitions and a strong laser with $\lambda \gtrsim 6000$ Å for ionization provides a convenient vehicle for RIS with commercially available laser systems. However, sufficiently powerful tunable sources are not available for $\lambda < 2170$ Å. Consequently, if one is to use RIS on atoms which have their lowest excited states at energies >5.6 eV, it is necessary to use a more complicated scheme, such as two-photon excitation, to reach the lower excited states. We shall now present an elementary discussion of two-photon excitation with pulsed lasers in order that the laser requirements and the problems associated with this method can be evaluated.

To get a rough idea about the two-photon process, consider the case in which a laser beam interacts with an atom initially in the ground state $|0\rangle$. The atom has a dipole-allowed transition to a state $|1\rangle$, but the laser's angular frequency is off resonance so that $\hbar\omega = E_1 - E_0 + \hbar\Delta$. If the laser linewidth is very small compared with Δ, then this level will not be populated after the laser pulse is gone. In fact, from the energy time uncertainty principle the atom can only spend a time $\sim 1/\Delta$ in this level and, consequently, the amplitude for being in the level must adiabatically follow the laser field. If ω is much closer to resonance between $|0\rangle$ and $|1\rangle$ than with any other dipole-allowed transition from the ground state, and if $2\hbar\omega \cong E_2 - E_0$ for a state $|2\rangle$ which has dipole-allowed transitions to $|1\rangle$, we expect that a good approximation to the state vector of the system initially in state $|0\rangle$ is (see Fig. 14)

$$|\psi(t)\rangle = a_0 e^{-i\omega_0 t}|0\rangle + a_1 e^{-i\omega_1 t}|1\rangle + a_2 e^{-i\omega_2 t}|2\rangle , \qquad (3.43)$$

where differential equations for a_0, a_1, and a_2 are to be found by using Eqs. (3.43) and the orthogonality properties of $|0\rangle$, $|1\rangle$, and $|2\rangle$ in the time-dependent Schrödinger equation. We have $\hat{H}|\psi\rangle = i\hbar\partial|\psi\rangle/\partial t$ with $\hat{H}$ given by Eq. (3.2) with $\hat{V}_c(t) = 0$. Then

$$\begin{aligned} i(da_0/dt) &= -2\omega_R(0,1)g(t)a_1 \exp[-i(\omega_1-\omega_0)t]\cos[\omega t+\eta(t)] , \\ i(da_1/dt) &= -2\omega_R^*(0,1)g(t)a_0 \exp[i(\omega_1-\omega_0)t]\cos[\omega t+\eta(t)] , \\ &\quad -2\omega_R(1,2)g(t)a_2 \exp[-i(\omega_2-\omega_1)t]\cos[\omega t+\eta(t)] , \\ i(da_2/dt) &= -2\omega_R^*(1,2)g(t)a_1 \exp[i(\omega_2-\omega_1)t]\cos[\omega t+\eta(t)] , \end{aligned} \qquad (3.44)$$

where $\omega_R(0,1) = \langle 0|P_z|1\rangle\varepsilon_0/2\hbar$; $\omega_R(1,2) = \langle 1|P_z|2\rangle\varepsilon_0/2\hbar$; $g(t) = E_0(t)/\varepsilon_0$; $\varepsilon_0^2 = \langle E_0^2(t)\rangle_{t=0}$; and, as before, Eq. (3.4) has been used for the laser field. The possibility of ionizing the population of $|2\rangle$ has been neglected. We break the cosine function up into its complex exponential parts and notice that $|da_0/dt| < 2|\omega_R(0,1)|$, $|da_2/dt| < 2|\omega_R(1,2)|$. Thus, if $|\omega_1 - \omega_0 - \omega|$ and $|\omega_1 - \omega_0 + \omega|$ are both much larger than $|d\ln g/dt|$, $|\omega_R(0,1)|$, and $|\omega_R(1,2)|$, the equation for da_1/dt can be simplified by integrating both sides with respect to t. The right-hand side of the integral (a rapidly oscillating complex exponential times a slowly varying function of time) can be asymptotically evaluated by integration by parts. Thus,

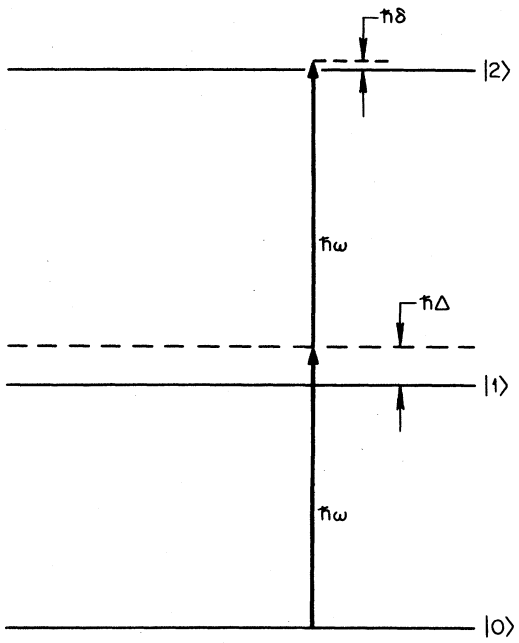

FIG. 14. Energy level diagram used in discussing the two-photon absorption promoting the atom from state $|0\rangle$ to state $|2\rangle$. The laser pulse has photons at line center of energy $\hbar\omega$. The photons are off resonance for the transition between $|0\rangle$ and $|1\rangle$ by $\hbar\Delta$ and for the two-photon excitation by the much smaller amount $\hbar\delta$.

$$\begin{aligned} a_1(t) &= \omega_R^*(0,1)g(t)a_0(t) \\ &\quad \times\left[\frac{\exp[i(\omega_1-\omega_0+\omega)t]e^{i\eta}}{\omega_1-\omega_0+\omega} + \frac{\exp[i(\omega_1-\omega_0-\omega)t]e^{i\eta}}{\omega_1-\omega_0-\omega}\right] \\ &\quad + \omega_R(1,2)g(t)a_2(t) \\ &\quad \times\left[\frac{\exp[i(\omega-\omega_2+\omega_1)t]e^{i\eta}}{\omega-\omega_2+\omega_1} + \frac{\exp[i(\omega_1-\omega_2-\omega)t]e^{-i\eta}}{\omega_1-\omega_2-\omega}\right]. \end{aligned} \qquad (3.45)$$

Equation (3.45) represents the adiabatic following relation between a_1 and the laser field that we mentioned earlier. Using Eq. (3.45), we can eliminate a_1 in the other equations and, on keeping only the most resonant terms in analogy with the rotating wave approximation,

$$\begin{aligned} i(da_0/dt) &= D_0 g^2 a_0 - \Omega(0,2)g^2 e^{+i\delta t}e^{2i\eta}a_2 , \\ i(da_2/dt) &= D_2 g^2 a_2 - \Omega^*(0,2)g^2 e^{-i\delta t}e^{-2i\eta}a_0 , \end{aligned} \qquad (3.46)$$

where

$$\begin{aligned} \Omega(0,2) &= \omega_R(0,1)\omega_R(1,2)/\omega-\omega_2+\omega_1 , \\ \delta &= -\omega_2+\omega_0+2\omega , \\ D_0 &= -|\omega_R(0,1)|^2\left[\frac{1}{\omega_1-\omega_0+\omega}+\frac{1}{\omega_1-\omega_0-\omega}\right] , \end{aligned}$$

$$D_2 = -|\omega_R(1,2)|^2\left[\frac{1}{\omega-\omega_2+\omega_1}+\frac{1}{\omega_1-\omega_2-\omega}\right].$$

In analogy with the transformation that we made earlier on Eqs. (3.10), we let $A_2 = a_2\exp[i\delta t + 2i\eta]$, $Z_1 = |A_2|^2 - |a_0|^2$, $Z_2 = 2\,\mathrm{Re}(a_0^* A_2)$, $Z_3 = 2\,\mathrm{Im}(a_0^* A_2)$, and find

$$\begin{aligned}\frac{dZ_1}{dt} &= -2\Omega(0,2)g^2 Z_3\,,\\ \frac{dZ_2}{dt} &= \left[(D_2-D_0)g^2-\delta-2\frac{d\eta}{dt}\right]Z_3\,,\\ \frac{dZ_3}{dt} &= -\left[(D_2-D_0)g^2-\delta-2\frac{d\eta}{dt}\right]Z_2+2\Omega(0,2)g^2 Z_1\,.\end{aligned} \tag{3.47}$$

$Z_1^2+Z_2^2+Z_3^2=1$ follows from Eqs. (3.47). Clearly, ionization could be included in these equations by incorporating the coupling of a continuum to $|2\rangle$ and eliminating it to leave a damping term and level shift. Also, perturbation due to collisions could be incorporated with fewer complications.

In cases where there is no state $|1\rangle$ which is much closer to a one-photon resonance than all others, one must include all states $|i\rangle$ which have the property $\langle 0|P_z|i\rangle\neq 0$ and $\langle i|P_z|2\rangle\neq 0$. All of the states $|i\rangle$ (including continuum states) can be eliminated, and Eqs. (3.46) are obtained once again except $\Omega(0,2) = \mathrm{S}_i\omega_R(0,i)\omega_R(i,2)/(\omega-\omega_2+\omega_1)$. D_0 and D_2 also become sums of terms, one for each state $|i\rangle$. In the far off one-photon resonance case, one can estimate orders of magnitude for $\Omega(0,2)$, D_0, and D_2 by putting in a common $\omega-\omega_2+\omega_i$ for all i. For example,

$$\begin{aligned}\Omega(0,2) &\approx \frac{1}{\omega-\omega_2+\overline{\omega}_i}\,\mathrm{S}_i\langle 0|P_z|i\rangle\langle i|P_z|2\rangle\frac{\mathcal{E}_0^2}{4\hbar^2}\\ &\approx \frac{\langle 0|P_z^2|2\rangle\mathcal{E}_0^2}{4\hbar^2}(\omega-\omega_2+\overline{\omega}_i)^{-1}\,,\\ &\approx \frac{10e^2a_B^2\mathcal{E}_0^2}{4\hbar^2(\omega-\omega_2+\overline{\omega}_i)}\approx 10I\ (\mathrm{W/cm^2})\,.\end{aligned} \tag{3.48}$$

In the above we have taken $|\omega-\omega_2+\overline{\omega}_i|\simeq 10^{16}/\mathrm{sec}$, $\langle 0|P_z^2|2\rangle\simeq 10e^2a_B^2$. The terms D_0 and D_2 are of the same order of magnitude but are generally larger than $|\Omega(0,2)|$ in absolute value. These terms D_0 and D_2 are also commonly referred to as ac Stark shifts, and they can play an extremely important role in determining the line shape for two-photon transitions when a powerful narrow-band laser is used. This is due to the fact that the two-photon Rabi frequency $\Omega(0,2)$ is smaller or of the same order of magnitude as the ac Stark shift.

The effect of laser coherence time for two-photon excitation is similar to that for one-photon excitation. Let Γ_L be the laser bandwidth. We see from Eqs. (3.47) that $|dZ_1/dt|<2|\Omega(0,2)|$; so that if $\Gamma_L\gg|\Omega(0,2)|$, we can choose a time τ_0 which is very large compared with $1/\Gamma_L$ but so small that Z_1 does not change appreciably for t in the interval $t_0\leq t\leq t_0+\tau_0$. Steps similar to those which led to Eq. (3.40) give for $\Delta=0$

$$\frac{dZ_1}{dt}\approx -4|\Omega(0,2)|^2\langle g^4(t)\rangle Z_1/\Gamma_L\,. \tag{3.49}$$

The decay constant in Eq. (3.49) is only roughly correct since it depends on the details of the laser phase and amplitude fluctuations. Thus $\Gamma_L\gg|\Omega(0,2)|$ assures the validity of rate equations. Typically, rates for two-photon absorption and stimulated emission are $R\simeq 100I^2/\Gamma_L\simeq 2\times10^{-10}I^2/\Delta\lambda_L$. With a power density $I\simeq 3\times10^8$ W/cm^2 we have $R\simeq 2\times10^7/\Delta\lambda_L$. With a laser linewidth $\Delta\lambda_L\simeq 0.01$ Å we get $R\simeq 2\times10^9$/sec. We note that rather high power densities and fairly narrow linewidths are required if one is to saturate the ionization signal when the RIS process begins with two-photon excitation. A laser pulse of length $\simeq 10^{-8}$ sec, energy per pulse $\simeq 0.03$ J, and a beam waist $\gamma_L\simeq 0.05$ cm will usually produce the intensity required for saturation if the linewidth satisifies $\Delta\lambda_L\lesssim 0.01$ Å (i.e., $\Delta\omega_L\simeq 10^{10}$ sec^{-1}). Dye lasers pumped by the second or third harmonic of a Nd:Yag laser serve as powerful tools for RIS processes which begin in this way (Bjorklund *et al.*, 1978).

We shall discuss multiphoton ionization as a source of background to RIS later in this section. Such a background is expected to be severe when high power and short wavelengths are required simultaneously. For instance, if one wanted to detect very small quantities of Xe, a two-photon excitation process with high power densities around $\lambda\approx 2500$ Å would be required. With 3×10^8 W/cm^2 at $\lambda\simeq 2500$ Å, only small concentrations of atoms or molecules with ionization potentials $\lesssim 10$ eV could be tolerated before a considerable background would be produced due to nonresonant two-photon ionization. If single-atom detection of Xe were desired, the buffer gas might have to be restricted to Ne or He with only small concentrations of other gases allowed.

Before closing this section we should mention that if perturbations due to collisions had been incorporated in Eqs. (3.47), the same type of analysis which led to Eqs. (3.24) for the one-photon excitation case would lead to similar equations here. That is, if $\Gamma_c\gg|\Omega(0,2)|$, we would obtain for a transform-limited-bandwidth laser

$$\begin{aligned}\frac{d\rho_{00}}{dt} &= \frac{2|\Omega(0,2)|^2g^4\Gamma_c}{\Gamma_c^2+(\Delta+\Delta_c)^2}(\rho_{22}-\rho_{00})\,,\\ \frac{d\rho_{22}}{dt} &= -2\Gamma\rho_{22}g^2-\frac{2|\Omega(0,2)|^2g^4\Gamma_c}{\Gamma_c^2+(\Delta+\Delta_c)^2}(\rho_{22}-\rho_{00})\,.\end{aligned} \tag{3.50}$$

At line center the rate constant for two-photon absorption is then $R\approx 2|\Omega(0,2)|^2g^4/\Gamma_c$, or $R\simeq 200\,I^2(t)/2\times10^8 P\approx 10^{-6}I^2/P$, where P is pressure in Torr.

The use of transform-limited-bandwidth lasers at sufficiently high power levels presents interesting new effects for RIS which begin with a two-photon transition. Here the ac Stark shifts are time dependent and are usually larger than the two-photon Rabi frequency $\Omega(0,2)$. Thus interesting crossing effects occur on one side of the unperturbed resonance, and this results in an asymmetric line shape (Choi and Payne, 1977). A further effect occurs when three-photon ionization uses two one-photon resonances with the first transition being driven by a much more powerful laser. In the latter case a linear ac Stark shift splits the atomic levels so that optimum RIS signal occurs when the second laser is detuned by $\pm|\omega_R|$ (ω_R is the Rabi frequency for the first transition) from the second resonance. The latter effect has been studied experimentally by Moody and Lambropoulos (1977) and by Hagan *et al.* (1978). In us-

ing RIS as a detection scheme in which two or more discrete–discrete transitions are involved, the power level should be no higher than necessary, and the situation of widely different Rabi frequencies for the transitions should be avoided. In cases where high-precision spectroscopy is not required, simplifications are achieved by using a bandwidth which is several times larger than either the ac Stark shifts or the two-photon Rabi frequencies, which are kept small by using the minimum power which will level the populations. In the latter case, rate equations apply and saturation can still be achieved. For three-photon resonances, ac Stark shifts are large compared with the corresponding Rabi frequencies. Such higher-order resonances will probably never be useful as the first step for RIS because of the high power requirements and the difficulties of assessing the effects of the power shifts and the added broadening due to a large rate of ionization which, in most cases, results from high power densities.

Two-photon excitation has already proven itself as a powerful spectroscopic tool. This is largely a consequence of the fact that when counter-propagating beams of very narrow bandwidth are used, the dominant process (if the power level is not too high and the laser satisfies $2\omega = \omega_2 - \omega_0$) is to absorb one photon from each of the counter-propagating beams. In doing so, an atom with a component of velocity v_z parallel to the beams absorbs an amount of energy $\hbar\omega(1 - v_z/c) + \hbar\omega(1 + v_z/c) \sim 2\hbar\omega$. Thus, by this process, resonance is obtained for atoms with all v_z, while the absorption of two photons propagating in the same direction is out of resonance by $2\hbar\omega v_z/c$. On detuning slightly, the width of the Doppler-free resonance is determined by the spontaneous decay rate. The combination of two-photon excitation with counterpropagating beams with ionization measurements should make a simple but powerful tool for Doppler-free spectroscopy.

F. Background effects due to multiphoton ionization

The subject of multiphoton ionization has recently been reviewed by Lambropoulos (1976). A great deal of theory has been done on the subject for the cases of H and the excited states of He. However, most of the experimental work has concentrated on inert gases or alkali metals (Lambropoulos, 1976). Recently a number of calculations have also been directed toward two- and three-photon ionization of alkali metals, and in most of these cases agreement between theory and experiment is good.

Our approach to the subject of multiphoton ionization will sacrifice a great deal in accuracy in order to obtain generality, to save space, and to achieve simplicity. We have already formulated a special case of multiphoton ionization in this section. Equations (3.11) with $|\delta| \gg |u_{11} - u_{00}$ and $|d\eta/dt|$ describe [along with Eq. (3.13)] two-photon ionization when the laser is tuned sufficiently close to resonance between $|0\rangle$ and $|1\rangle$ for $|1\rangle$ to be the dominant virtual state for the process. Thus, using lowest-order perturbation theory to solve for Z_4, we obtain

$$dP_I/dt = 2\Gamma g^2 Z_4 \equiv \mathcal{F}\sigma_I Z_4 = \mathcal{F}\sigma_I \omega_R^2 g^2/(\omega - \omega_1 + \omega_0)^2 . \tag{3.51}$$

Equation (3.51) is equivalent to Eq. (3.34) when $|\delta| \gg |\omega_R|$. Equation (3.51) can also be written $dP_I/dt = \mathcal{F}\sigma_2$, where σ_2 is the power-dependent two-photon ionization cross section. We have $\sigma_2 = \sigma_I \omega_R^2 g^2/\delta^2$. In practice, $|\delta|$ does not have to be very large before the single virtual (or intermediate) state ceases to be dominant. The more general perturbation theory result for the case where $|0\rangle$ is an S state and all P states are included as intermediate states is

$$\frac{dP_I}{dt} = \frac{\pi}{8\hbar^3} g^4 \varepsilon_0^4 \sum_{l=0,2} \left| S_n \frac{\langle 0|\hat{P}_z|n,P\rangle\langle n,P|\hat{P}_z|E_{c0},l\rangle}{\omega_{n,p} - \omega_0 - \omega} \right|^2 . \tag{3.52}$$

In Eq. (3.52) the S_n denotes summation over discrete and integration over continuum states.

When an average $\omega_{n,p}$ is defined and the remainder of a complete set of intermediate states is summed over, Eq. (3.52) becomes

$$\frac{dP_I}{dt} = \frac{\pi}{8\hbar^3} g^4 \varepsilon_0^4 \sum_{l=0,2} \left| \frac{\langle 0|\hat{P}_z^2|E_{c0},l\rangle}{\bar{\omega} - \omega_0 - \omega} \right|^2 \approx \mathcal{F}\bar{\sigma}_I \frac{(ea_B\varepsilon_0/2\hbar)^2 g^2}{(\bar{\omega} - \omega_1 + \omega_0)^2} . \tag{3.53}$$

Similar considerations of n-photon processes, with the same crude approximations, lead to

$$\frac{dP_I}{dt} \approx \frac{\mathcal{F}\bar{\sigma}_I (A ea_B\varepsilon_0/2\hbar)^{2n-2} g^{2n-2}}{\bar{\delta}^{2n-2}} , \tag{3.54}$$

where A is a phenomenological parameter which will be taken to be the same for all n. $\bar{\delta}$ will be taken as ω independent as long as the value of $k\omega$ is no closer than 10^{13}/sec to a k photon resonance ($k \leq n - 1$). Figure 15 shows six-photon ionization of H. This figure gives some encouragement that such a $\bar{\delta}$ can be found, since the valleys between resonances have nearly the same depth within a few orders of magnitude. We take $\bar{\delta} = E_1/\hbar n$, where E_1 is the energy of the first excited state, which is assumed to be greater than $\hbar\omega$. The introduction of E_1 and n roughly scales the results between elements with different ionization potentials. Equation (3.54) is not based on any profound physics, and its

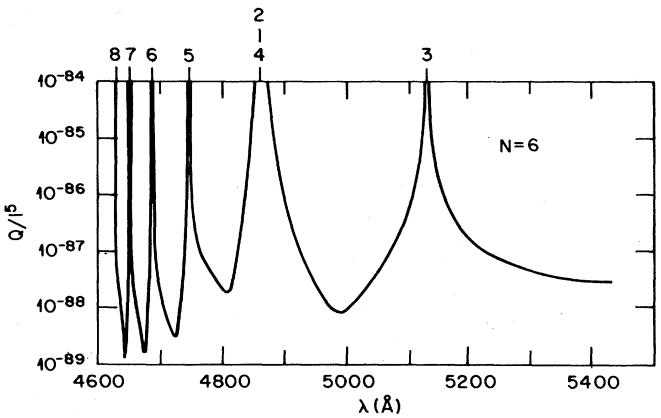

FIG. 15. Power-dependent cross section (in units of cm^{12} sec^5 w^{-5}) for 6-photon ionization of H in the ground state as calculated by Karule (1974). This detailed calculation shows the nearly constant power-dependent cross section in the off-resonance regions of wavelength.

most remarkable property is that is is usually within a few orders of magnitude of more detailed calculations provided ω is well off resonance with all lower excited states and $n < 8$. It is clear that for $n \sim 8$ some of the resonant denominators are small near the atoms' Rydberg levels; but for such high order near resonances, agreement is still reasonable. We note that the photon flux $\mathcal{F}$ in units of $\text{cm}^{-2}\,\text{sec}^{-1}$ is related to the intensity I in W/cm^2 and the laser wavelength in Å by $\mathcal{F} \simeq 5 \times 10^{14} \lambda I$. Taking $A \simeq 5$ and $\bar{\sigma}_I \simeq 3 \times 10^{-18}\ \text{cm}^2$, we obtain

$$\frac{\sigma_n}{\mathcal{F}^{n-1}} \approx 3 \times 10^{-18} \left| \frac{1.5n \times 10^{-14}}{E_1 \sqrt{\lambda}} \right|^{2(n-1)}, \tag{3.55a}$$

$$\frac{\sigma_n}{I^{n-1}} \approx 3 \times 10^{-18} \left| \frac{3n \times 10^{-7}}{E_1} \right|^{2(n-1)}, \tag{3.55b}$$

where E_1 is in eV, λ is in Å, $\mathcal{F}$ is in $\text{cm}^{-2}\,\text{sec}^{-1}$, σ_n is in cm^2, and I is in W/cm^2. Figure 16 shows a graph of (3.55a) as compared with more detailed calculations for the alkali metals.

Consider a laser with pulse length $= 10^{-8}$ sec, $I \simeq 10^8$ W/cm^2, $\lambda \simeq 10^4$ Å, and ionization potential of 6 eV. The probability of ionization well away from any resonance is

$$P_I \simeq \mathcal{F}\tau\sigma_5,$$
$$\simeq 5 \times 10^{18}(10^8)^4 \times 10^{-53} \times 3 \times 10^{-18}$$
$$\simeq 10^{-20}.$$

Thus one would expect that no background would occur even with concentrations $\sim 10^{17}/\text{cm}^3$. The dye lasers present might have $\tau \simeq 10^{-8}$ sec, $I \simeq 10^4\ \text{W/cm}^2$, and $\lambda \simeq 5000$ Å. The probability of ionization is

$$P_I \simeq \mathcal{F}\tau\sigma_3 \simeq 5 \times 10^{14}(10^4)^2 100 \times 10^{-28} \times 3 \times 10^{-18}$$
$$\simeq 10^{-22}.$$

We see that the technique of using several dye lasers with $\tau \simeq 10^{-8}$ sec, $I \simeq 10^4\ \text{W/cm}^2$, $\lambda \gtrsim 4500$ Å, and $\Delta\lambda_L \simeq 10^{-2}$ Å together with a laser having $\tau \simeq 10^{-8}$ sec, $\lambda > 10\,000$ Å, and $I \simeq 10^8\ \text{W/cm}^2$ can be background free with rather high concentrations of a low-ionization-potential impurity. We assume, however, that the pressure is also low so that no pressure-induced resonances occur. Equations (3.55) are obviously only rough approximations. If they predict that there could be a problem or that there are only a few orders of magnitude of margin, a more detailed calculation should be sought or an experiment performed.

The use of multimode lasers for ionization leads to the enhancement of multiphoton ionization over what would be obtained for the same energy per pulse and pulse length with a transform-limited-bandwidth laser (Lambropoulos, 1976). This enhancement can be as large as $n!$ (or perhaps even larger). The reason for the enhancement is that the multimode laser has an **E** made up of several terms in Eq. (3.3). The energy per pulse is the sum of the energy due to each separate term, but for brief time intervals ($\sim 1/\Delta\omega_L$) there can be constructive interference between the various terms so that the instantaneous power is very much larger than would ever be obtained with an extremely narrow-band laser of the same energy per pulse and pulse length. The ionization rate depends on $[I(t)]^n$, so that for large n the enhancement during the brief periods of constructive interference completely dominates the decrease during destructive interference, the net effect being a greatly enhanced ionization probability. In terms of photons, one says that with incoherent light photons arrive in bunches. With multimode lasers, Eqs. (3.55) need to be multiplied on the right-hand side by a factor of the order of $n!$. In the five-photon ionization case considered as an example, the enhancement might be ≈ 100.

The multiphoton ionization of molecules is just beginning to be explored. Again, in order to avoid background problems one should avoid (if possible) having molecules present with low ionization potentials. Any high-power laser should have a long wavelength and should be no more powerful than is neces-

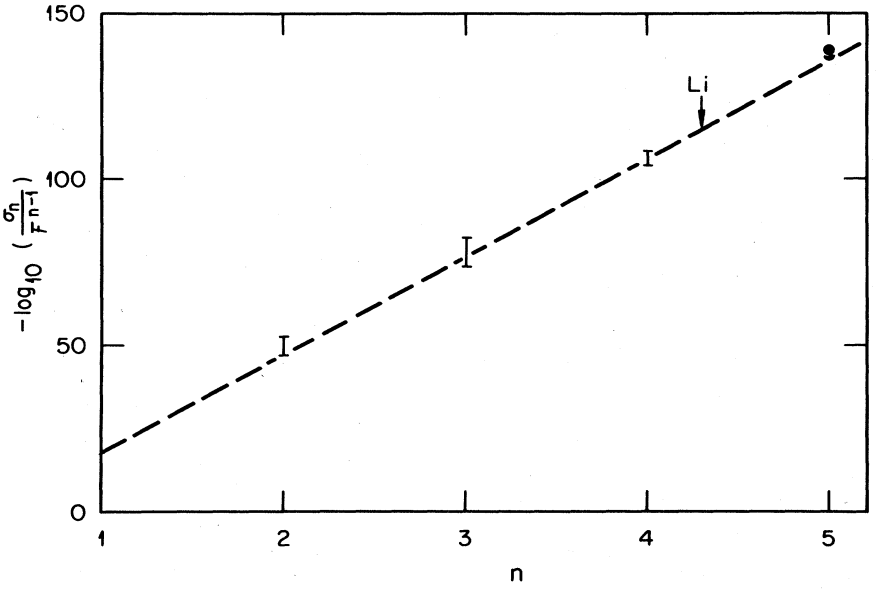

FIG. 16. Simulation of n-photon ionization of the alkali metals. Graph of $-\log_{10}(\sigma_n/\mathcal{F}^{n-1})$ vs n based on Eq. (3.55a) with $E_1 = 5$ eV, $\lambda \simeq 5000$ Å. The data bars represent the range of more detailed calculations on all alkali metals at wavelengths corresponding to the fundamental and various harmonics of the Nd–Yag and ruby lasers. The results of the detailed calculations were taken from the review paper by Lambropoulis (1976).

sary for purposes of saturating ionization. It is very likely that large concentrations ($\sim 10^{18}/cm^3$) of molecules with ionization potentials $\gtrsim 10$ eV and with the lowest electronically excited states lying higher than 6 eV can be tolerated if one observes these general rules. This has already been demonstrated experimentally with methane (Hurst, Nayfeh, and Young, 1977a, 1977b). However, in general the potential for problems is far greater with molecules due to a number of complications. The following are some of these: (1) Even with a molecule in its ground, rotational, and vibrational states, the density of resonant wavelengths is far greater than in atoms. Further, there are usually many rotational states populated at room temperature, with each having a somewhat different set of resonant levels. The potential for having a near resonance is clearly far greater. (2) There are broad bands of frequency over which molecules can be dissociated into neutral fragments, with one fragment being in an electronically excited state which can often be photoionized by a much smaller number of photons. (3) Some molecules can be dissociated into positive and negative ions with further absorption resulting in photodetachment of the electron. Recently a number of experiments have been carried out on multiphoton ionization of molecules (see, for instance, Johnson, Berman, and Zakheim, 1975; Dalby *et al.*, 1977; Zakheim and Johnson, 1978; Feldman, Lengel, and Zare, 1977; Lehmann, Smolarek, and Goodman, 1978). These experiments were carried out for purposes of determining the spectroscopy of higher electronically excited states. But the work can also be used to make crude estimates of the expected background when various molecules are subjected to laser pulses. While this work is excellent in its own right, it is not what we would call molecular RIS. Molecular RIS would involve only discrete–discrete transitions of various orders driven to saturation and followed by saturated ionization. Thus all molecules of a particular type would be ionized or dissociated into neutrals. However, ionization efficiencies can be used to relate the number of ion pairs to the absolute number of molecules in the sample. The implementation of molecular RIS would generally require several simultaneous dye laser pulses at various wavelengths.

IV. A DEMONSTRATION OF ONE-ATOM DETECTION

A. Sensitive detection of ionization

With gas phase ionization detectors, free electrons, negative ions, and positive ions can be detected. The time behavior of the voltage pulse which results from a sudden creation of ions in a parallel-plate ionization chamber can be derived in terms of the drift velocity of the ions as they are separated and ultimately collected with an electric field. Thus the pulse shape can be used to distinguish the electrons from the more

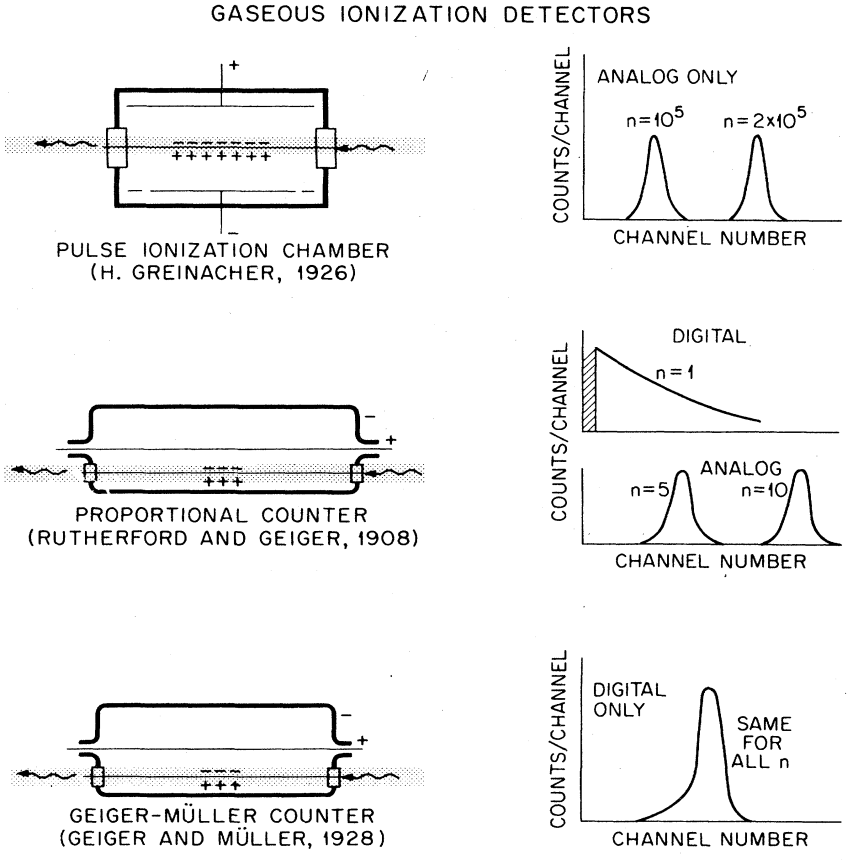

FIG. 17. History of the sensitivity of the ionization chamber, the proportional counter, and the Geiger-Mueller counter.

slowly drifting negative or positive ions. The history of the sensitivity of the ionization chamber is summarized in Fig. 17. Soon after the development of radio, Greinacher (1926) developed a pulse amplifier that could drive both a galvanometer and a loudspeaker to record single alpha particles. Since a 5-MeV alpha particle creates about 2×10^5 ion pairs when it is completely absorbed in a gas, we assign a nominal 10^5 ion pair sensitivity to the method. With modern solid state circuits operating at room temperature, it is now possible to record a few hundred electrons with a pulse ionization chamber. Thus Blalock (1964) has been able to reduce noise to the equivalent of about 200 electrons (rms). The effective use of the ionization chamber (as well as other ionization detectors) requires a good knowledge of the subject of gaseous electronics [see, for example, McDaniel (1964) and Huxley and Crompton (1974)] and the effective use of pulse electronics [see, for example, Nicholson (1974)].

Historically, the proportional counter preceded the pulse ionization chamber. Rutherford and Geiger (1908) invented the proportional counter, a device that amplifies the initial free electrons according to the Townsend method, to record the individual ionization pulses due to alpha particles. With modern proportional counters and modern pulse amplifiers, it is not difficult to record single thermal electrons. Since the height of the pulse from a proportional counter is a linear function of the number of electrons per pulse, it is an analog device; but, as we noted above, it can also be a digital device for the detection of a single electron.

Geiger and Mueller (1928) showed that under certain conditions ionization tubes can be made such that the height of the pulse is independent of the number of initial electrons. Because of very high gas amplification, space charge limits the size of pulses. Hence, these detectors can be used only as digital devices, but they have the often useful characteristic that the pulse initiated by a single electron can have an amplitude of several volts.

Figure 17 summarizes these facts. We note that with the use of laser beams to create ionization inside these detectors, several features are under better control than is usually the case with "ionizing radiation" such as alpha, beta, or gamma radiation. Since the laser beam is parallel to the collector wire, all electrons are at the same distance from the wire; recombination is minimal; and track orientation effects are absent. But perhaps the most useful feature is the time coincidence afforded by triggering the laser at a known time. This feature virtually eliminates background due to all sources that are random in time.

Single electrons and heavy ions can be accelerated in a vacuum system and hence are easily detected as individual particles with detectors such as channel electron multipliers. Therefore RIS can also be used for the detection of atoms that are evaporated from samples placed in a vacuum system.

In summary, ionization detectors are extremely sensitive, quantitative, and reliable. These devices, whose development started with the discovery of x rays, can be used with RIS to make sensitive measurements in a wide variety of circumstances.

B. Experimental demonstration

We shall describe the original one-atom detection experiment in some detail. One-atom detection requires a saturated RIS process and a single-electron detector. Several means for the detection of one electron, such as gas proportional counters (which operate at reasonable gas pressures, e.g., 1–1000 Torr) or electron multipliers (which operate at very low pressures, $<10^{-5}$ Torr), are available. The first demonstration was carried out with a proportional counter to show that a single atom could be picked out in a gas containing an enormously larger number of atoms (or molecules) of another type. The element cesium was chosen for several reasons. It is sufficiently volatile that a wide range of Cs concentrations could be generated. It is very reactive chemically, a fact that would be utilized in ultimately getting to a concentration of one atom in the sampling volume. Lastly, cesium could be photoionized with the $Cs(\omega_1, \omega_1 e^-)Cs^+$ process involving the absorption of two photons of a single energy; thus only one laser was required. In Fig. 18 we show a detailed diagram of spectral wavelengths, transition rates, and lifetimes for the lower levels of the cesium atom. The transitions $6^2S_{1/2}$–$7^2P_{3/2}$ (4555 Å) and $6^2S_{1/2}$–$7^2P_{1/2}$ (4593 Å) fall within the range of flashlamp-pumped dye lasers, and the $7P$ levels can be photoionized by a second photon with reasonable efficiency. The photon fluence (ϕ) required for saturation can be calculated from measured (Zeman, 1974) photoionization cross sections (i.e., 8×10^{-18} cm^2). To make $\sigma\phi = 2.4$ (i.e., 90% ionization) requires 100 mJ cm^{-2}. The light source was a flashlamp-pumped dye laser, having a beam divergence of 1 mrad, a diameter of 3 mm, a linewidth (FWHM) of about 0.7 Å, and a pulse width (FWHM) of 2 μsec. About 1-mJ pulses are obtained at 4555 Å (15 mJ cm^{-2}); therefore, 100 mJ cm^{-2} requires modest focusing of the 3-mm beam.

Considering the pathways shown in Fig. 18, we have a typical situation with respect to spontaneous radiation from the excited state which must be considered in estimating the required laser power level for saturated ionization. If we use a pulsed laser having a width of 1 to 2 μsec, the $7P$–$7S$ transitions are not important because this route leads back to the ground state in less than 1 μsec; therefore, the ground state can be recycled back to the $7P$ level. However, the $7P$ to $5D$ routes are of more concern because the $5D$ level has a lifetime of about 1 μsec, and thus atoms can accumulate here during the laser pulse. But these states will also be photoionized by the laser pulse with very good efficiency since the photoionization process from $5D$ is just above threshold. Whereas radiation processes complicate the measurement of excited-state photoionization cross sections, they are often of less consequence to the saturation of the photoionization.

The apparatus used for the detection of cesium atoms is shown in Fig. 19. With P-10 gas (90% Ar + 10% CH_4) at 100 Torr, the gas amplification was on the order of 10^4 when the wire (0.005 cm in diameter) was at +1000 V. To prevent capture of the free electrons by

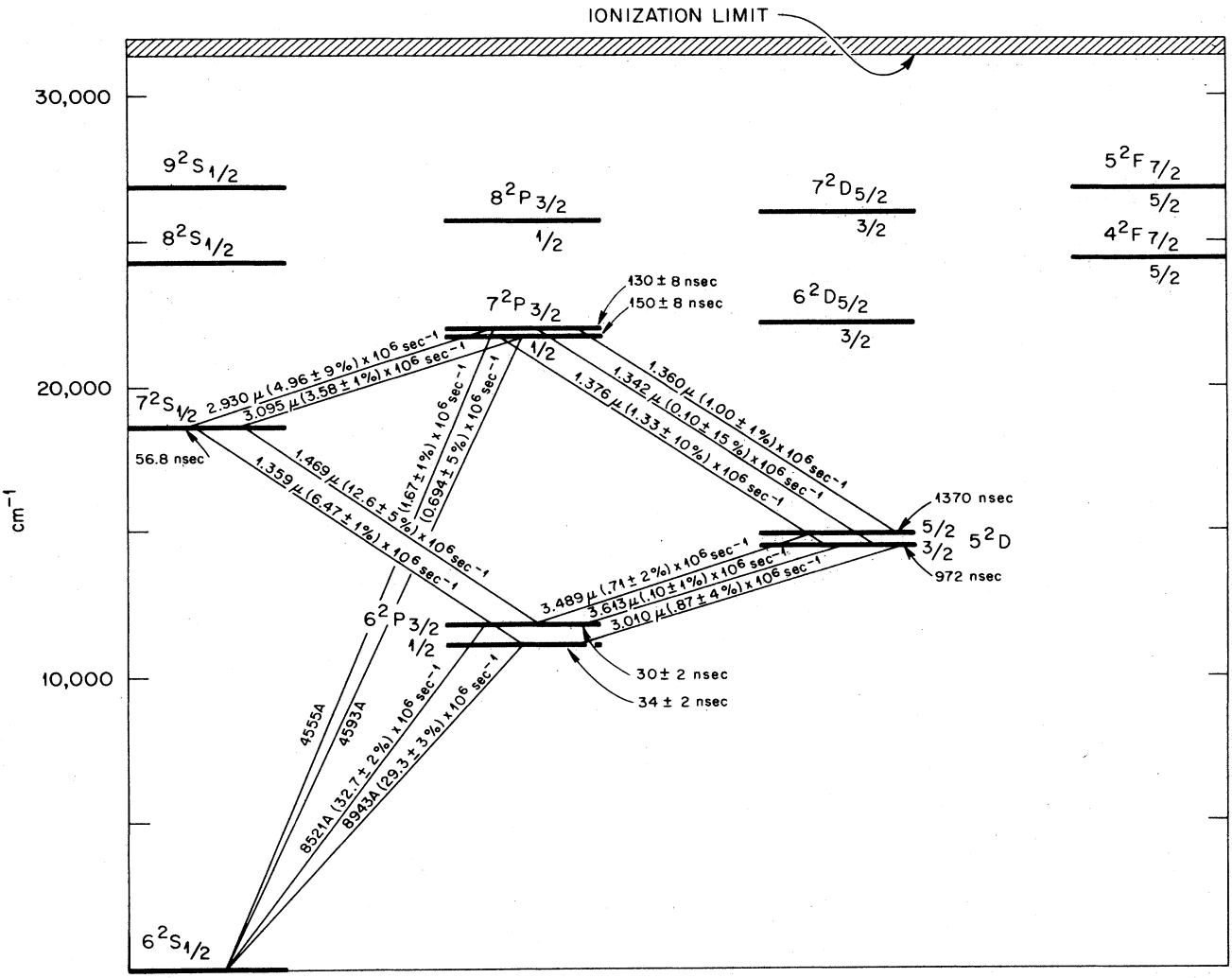

FIG. 18. Spectrum wavelengths, transition rates, and lifetimes for lower levels of the cesium atom. The references for the lifetimes are: $6^2P_{1/2}$: a,b; $6^2P_{3/2}$: b,c,d; 5^2D and 7^2S: b; 7^2P: e. References for all transition rates are b (weight=1) and *f* (weight=2); the "errors" are differences between weighted mean and Ref. f. (a) Gallagher (1967)—Hanle effect. (b) Heavens (1961)—Bates and Damgaard calculations. (c) Altman (1970)—lifetime. (d) Schmeider *et al*. (1970)—Hanle effect. (e) Pace and Atkinson (1975)—laser fluorescence. (f) Fabry and Cussenot (1976)—quantum mechanics; some experimental values for higher levels. Courtesy of Professor Ray Hefferlin of Southern Missionary College.

electronegative molecules such as O_2, the P-10 gas was pumped through the counter. The 3-mm diameter laser beam was focused below the center of the counter wire using a lens of 25-cm focal length. With a 1-mrad divergence, the beam focused to 0.025-cm diameter at the center of the counter and had a 0.10-cm diameter under both ends of the counter wire. The laser beam volume in the active region of the counter was 5×10^{-2} cm^3. Under these conditions and with the field tubes decoupled from the wire to suppress photoelectrons from the quartz windows, there was no measureable photoelectron background. Backgrounds due to external radiations, such as cosmic rays, were eliminated by using electronic time-gating techniques; that is, a coincidence between the detector laser signal D and the proportional counter signal P is required.

The volatility of cesium metal can provide large concentrations of atoms; however, the highly reactive nature of cesium vapor is the dominant factor in establishing a steady-state transport of cesium atoms from source to reaction site. The counter was filled with P-10 counting gas for the demonstration. Although precautions were taken to minimize impurities, there were reactive contaminants such as O_2 present. The concentration $C(r)$ of Cs atoms in the laser beam can be estimated from the equilibrium concentration (C_0) of Cs atoms, the rate of Reaction (β) with impurities in the counting gas, and the diffusion coefficient (D) of Cs atoms in the counting gas. Thus a rough estimate is

$$C(r)=C_0(r_0/r)\exp[-(r-r_0)\sqrt{\beta/D}\,],$$

where r_0 is the radius of the small source. This expression assumes a small spherical source of radius r_0 with an equilibrium concentration near its surface. Wall effects are neglected and the gas and source are

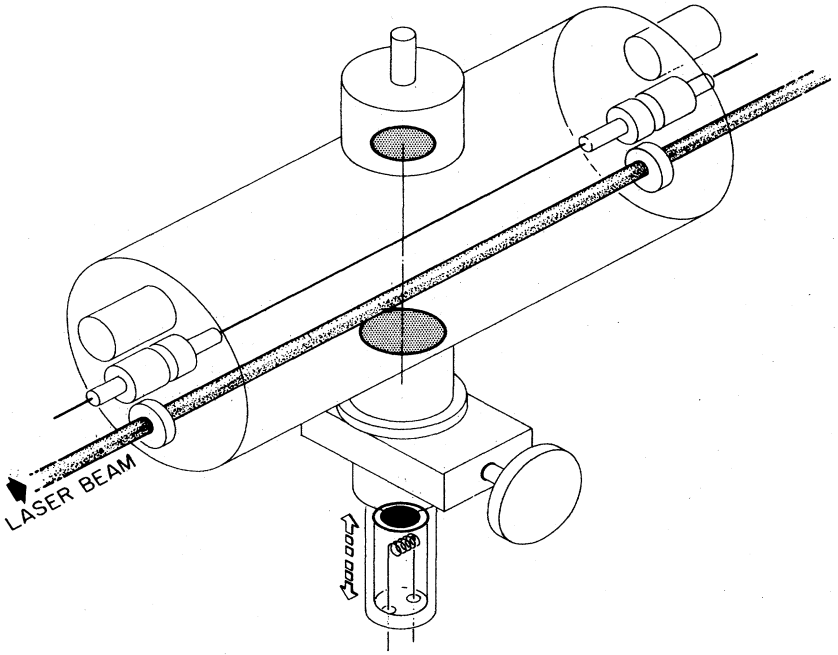

FIG. 19. Schematic of apparatus used for the detection of cesium atoms. A pulsed beam is used to remove from the selected atom one electron which is detected with a proportional counter.

at the same temperature. The quantities (D) and β have both been measured for our particular example; see Sec. V for details. If we use the values for β and D and let $r \simeq 2$ cm, $C_0 \simeq 10^{10}$ cm^{-3}, $r_0 \simeq 0.2$ cm, we find that $C \approx 1$ atom cm^{-3} if $P_{O_2} \simeq 10^{-4}$ Torr when $P_{Ar} = 400$ Torr. Surprisingly, we must keep $P_{O_2}/P_{Ar} \leq 2.5 \times 10^{-7}$ to have even one atom of Cs in a laser beam 2 cm from a small Cs surface held at room temperature. The concentration of cesium vapor in the active laser beam volume could be varied by changing the distance of the cesium source from the laser beam, by controlling the temperature of the cesium source, or by varying the counter gas pressure.

Under separate conditions of saturation, every cesium atom in the laser beam volume was photoionized and detected. In Fig. 20 we plot a pulse-height distribution for a large number of Cs atoms with the condition that the laser always saturated the ionization. From the known fact that each 6.4-keV x ray produces 250 electrons in P-10 gas, we find that the Cs peak in Fig. 20 corresponds to 10^4 Cs atoms. Distributions were measured for populations ranging from 10^2 to 10^6 atoms.

One electron in a proportional counter produces an exponential-like pulse-height distribution [see, for example, Genz (1973)]. Figure 21 was obtained by using a Hg lamp to release single photoelectrons from the inner walls of the counter at a low rate. With the Cs sample in its lowest position and a gas pressure of 200 Torr, a nearly identical distribution due to the ionization of a Cs atom was found. In Fig. 21 the fluctuations in the distribution are due to counting statistics, which do not reflect uncertainty in the total number of atoms counted. By integrating the total number of pulses produced above the normal electronic and laser transient noise, it was found that it is not difficult to count directly 95% of the one-atom pulses. At all population levels, including one atom, it was observed that the signals vanished when the laser was detuned from the Cs transition.

With the demonstration of the detection of a single cesium atom, the validity of the RIS technique for true, unambiguous, single-atom detection is shown. The tremendous potential of the ability to detect single atoms, or small groups of atoms, is presently being pursued in a number of research areas. Some of these applications are summarized later in this paper.

C. Other laser experiments

As pointed out in the Introduction, some laser fluorescence methods applied to certain selected atomic species can be capable of time-resolved single-atom detection. The unique method described by Greenless *et al.* (1977) used photon (fluorescent) bursts emitted by an atom at it was continuously excited during its transit of a laser beam. Time-resolved, single-atom detectability is possible for atoms with the required optical properties. When a laser is tuned to a resonance transition such that the levels are saturated, it is possible to have resonance photons re-emitted at high rates (e.g., 10^8/sec). A schematic of the Greenlees *et al.* system is reproduced in Fig. 22. By collecting photons from only one focal point of the ellipsoid reflecting system and placing a photon counter at the other focus, they obtained an overall counting efficiency of 5.5%. When the intersection of the narrow beam of atoms and the cw laser beam was placed at a focal point, somewhat more than one photon was detected for a single atom crossing the laser beam of 1-mm diameter. As few as 10 atoms/sec have been detected by this technique. This appears to be an extremely useful technique where the atoms, as in an atomic beam, are confined to a small and well defined region of space. By combining this detection scheme with the fast beam technique described by Kaufman

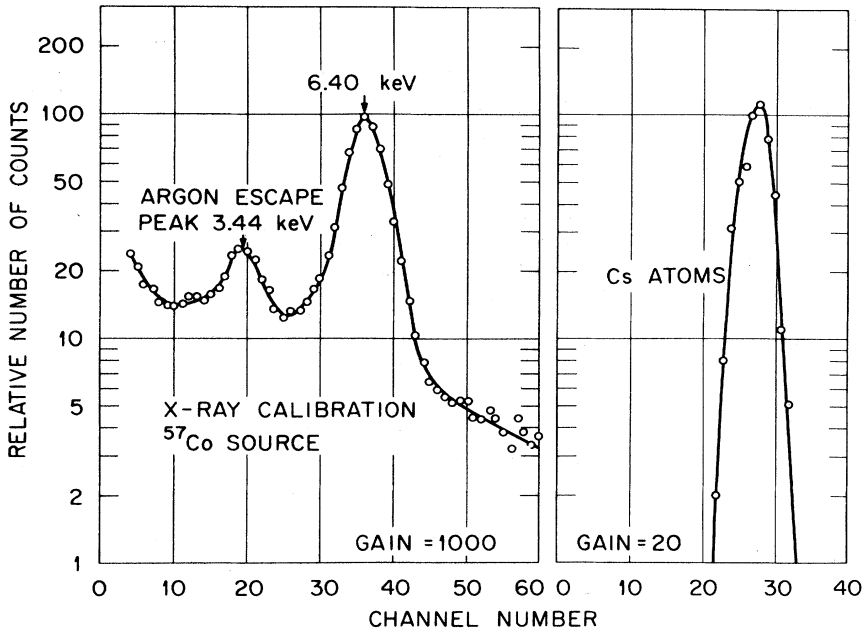

FIG. 20. Pulse-height spectrum due to resonance ionization of Cs atoms. From the gain ratio and the fact that the ^{57}Co x-ray produces 250 electrons, one finds that the most probable number of Cs atoms detected was 10^4.

(1976), it should be possible to do high-resolution spectroscopy at very low atomic beam fluxes. Recently, She, Fairbank, and Billman (1978) proposed a variation of this method using two spatially separated laser beams to measure velocities of individual atoms.

Certainly laser fluorescence is capable of extreme sensitivity for detection of atoms. The original fluorescence technique described by Fairbank, Hänsch, and Schawlow (1975) could detect concentrations of 10 atoms/cm^3 of sodium. In the work of Gelbwachs, Klein, and Wessel (1977) this technique was modified by detecting the nonresonant emission from excited atoms. By shifting the detection to the nonresonant fluorescence, the authors point out, background

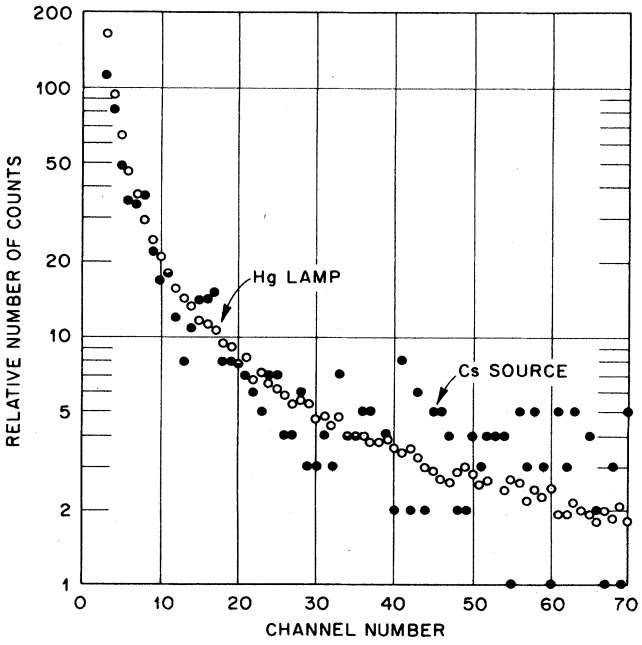

FIG. 21. Pulse-height distribution for the case where one Cs atom was counted per 20 laser pulses, compared with a one-electron distribution produced by an incoherent light source. Sensitive volume was 0.05 cm^3 per laser pulse. With available lasers, the volume per pulse could be greater than 100 cm^3. Background gas was about 10^{19} Ar atoms per cm^3 and 10^{18} CH_4 molecules per cm^3.

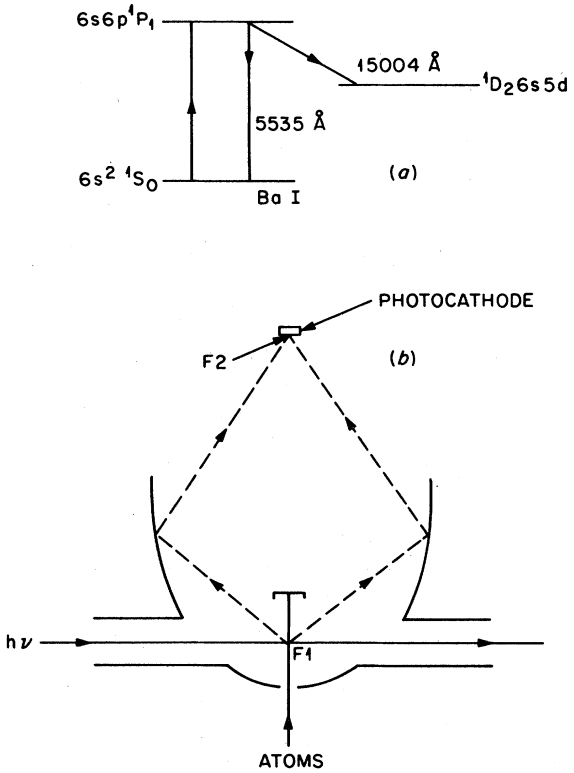

FIG. 22. Illustration of the photon burst spectroscopy developed by Greenlees *et al.* (1977). Part A—barium energy level; Part B—schematic of apparatus.

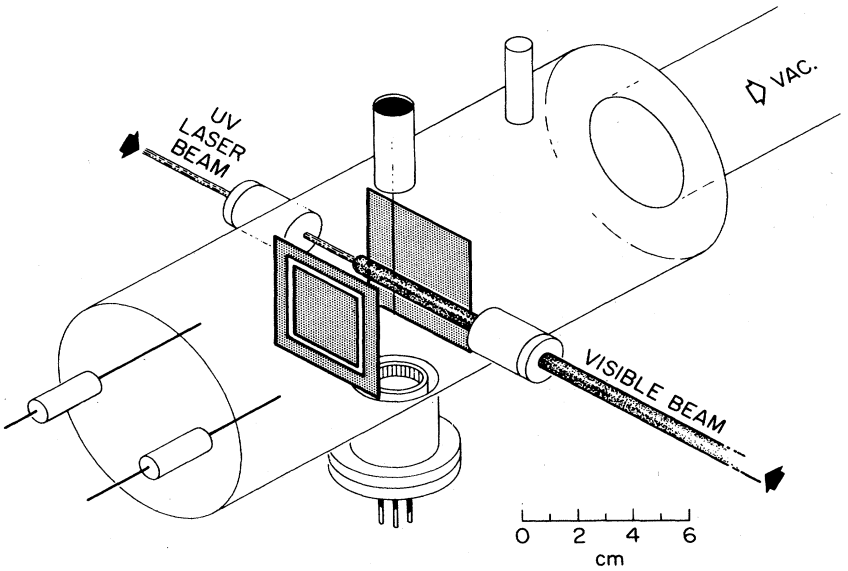

FIG. 23. Experimental arrangement for the study of saturated photodissociation of alkali halide molecules. The pulsed uv laser is used to dissociate CsI molecules at time $t = 0$, and the pulsed visible laser is used to detect Cs atoms at $t > 0$.

scattering effects are eliminated and highly sensitive measurements can be made at atmospheric pressure. Balykin *et al.* (1977) used resonant fluorescence but added the requirement that two independent detectors record the same resonant fluorescence signal so that background effects of scattering, which would only be detected by one photodetector, could be reduced. By this technique, using an atomic beam of sodium, as low as 10 atoms/sec were detected. Other comparisons and comments on RIS methods versus fluorescence methods have been made by Robinson (1978).

V. CLASSICAL APPLICATIONS

Following the demonstrations of one-atom detection it became clear that many of the applications in classical physics and chemistry could best be achieved by the combination of a time-resolved source of atoms and a time-resolved detector of atoms. For example, if atoms can be created at $t = 0$ and detected at arbitrary $t > 0$, then it should be possible to study the diffusion of atoms and the chemical reaction of free atoms in detailed ways which probe both the temporal and the spatial variables of the transport processes. Furthermore, such time-resolved techniques should be ideal for the study of the statistical behavior of atoms and of various fluctuation processes involving free atoms. These considerations led to a series of experiments involving the photodissociation of CsI molecules. Many experiments on various alkali halide molecules remain to be done.

A. Photodissociation of molecules

In an experiment on CsI it was demonstrated that every CsI molecule in a small volume could be photodissociated with a laser pulse; and when combined with the RIS technique for the detection of each Cs atom thus created, the absolute concentration of CsI molecules could be measured. From this information the absolute cross section for photodissociation could be determined without recourse to thermodynamic data on CsI.

The experimental arrangement (Fig. 23) utilizes a parallel-plate ionization chamber mounted inside a vacuum system. Even when the CsI sample is heated to 700 K, the concentration of CsI molecules between the parallel plates is quite low (e.g., 10^7 cm^{-3}); nevertheless, it is more than adequate for the RIS method of detection. A pulsed laser[1] using kiton red dye pumped with a linear flashlamp is frequency doubled and used to dissociate CsI. The narrow beam is about 0.5 mm in diameter when focused and is ideal for defining the initial location of free Cs atoms at time $t = 0$. A second pulsed laser[2] having a much larger beam, about 7 mm in diameter, is coaxial with the first narrow beam. In this way the second pulsed laser can be used to detect those free atoms which were liberated on the axis of the detector beam at time $t = 0$ and which are still contained in the detector cylinder at the arbitrary time $t > 0$. It will be shown below that the photon fluence (ϕ_S) associated with the source beam is large enough to dissociate all of the CsI molecules contained in the volume swept by the source beam, and the photon fluence (ϕ_D) associated with the detector beam is large enough to remove one electron from each of the liberated atoms in the detector volume.

The electronics logic and data acquisition are quite conventional and will not be discussed. Each pulse of the detector laser was fired when a predetermined condition was met—namely, that it be preceded with a pulse from the source laser at a prescribed time. For each event, three quantities were recorded: (1) the relative energy per pulse of the source laser S, (2)

[1]For the dissociation of CsI molecules, we used a linear flashlamp-pumped dye laser, model CMX-4, Chromatix Corp., Sunnyvale, CA 94086.

[2]For the detection of Cs atoms, we used a coaxial lamp dye laser, model 2100C, Phase-R Company, New Durham, NH 03855.

the relative energy per pulse of the detector laser D, and (3) a signal, P, proportional to the amount of ionization (i.e., number of free electrons) produced in the guarded region of the parallel-plate ionization chamber.

In the initial experiments (Grossman *et al.*, 1977b) the wavelength of the source laser was set at 3175 Å near the CsI dissociation peak (Davidovits and Brodhead, 1967). To detect the neutral Cs, the detector laser was set to produce photons at 4593 Å for the process $Cs[\omega_1, \omega_1 e^-]Cs^+$. Carrying out the experiment in a buffer gas such as argon at moderate pressure (e.g., 100 Torr), produced several desirable effects. First, the CsI molecules were in thermal equilibrium near 300 K due to argon collisions. Also, photoionization occurred from all the degenerate magnetic levels. Finally, with a buffer gas, Cs-atom diffusion was of no consequence during the lifetime (FWHM) of the laser pulse (i.e., 1.5 μsec for the source laser and 0.5 μsec for the detector laser). For these reasons, most of the studies were made with a buffer gas. Ionization signals were studied as a function of the detector laser fluence, ϕ_D. As ϕ_D increased, the ionization signal climbed gradually to a saturated value, consistent with earlier work (Hurst *et al.*, 1977) (see Fig. 24).

With sufficient fluence ϕ_D to saturate the ionization (i.e., to detect each free atom in the laser beam), studies were then made of the photodissociation process. Several significant observations were made on the production of neutrals. For instance, there was a gradual decline in the number of free atoms as the time between the source laser and detector laser was increased; but this variation was just what one expected on the basis of calculations of the rate of diffusion of the atoms out of the detection region. Special tests were made with very short time delays between the source and detector lasers; all of the atoms were dissociated in less than 0.5 μsec after the source laser pulse. Berkowitz (1969) observed ionization with a photoionization mass spectrometer only when the photon energy exceeded 7 eV.

Figure 25 shows the ionization signal as a function of the number of photons in a single pulse of the source laser, both for an unfocused beam and for a beam which was focused with a 50-cm focal length lens. The focused beam signals continue to rise gradually because of a nonuniform source beam. To obtain the Cs photoproduction cross section σ, the following analysis was made. Assuming (as found experimentally) a Gaussian beam profile, we write

$$\phi(\rho) = \phi_0 \exp(-\rho^2/R^2), \tag{5.1}$$

where ϕ_0 is the fluence when the radius $\rho = 0$, and R is a constant. Since each atom is detected, the measured signal is proportional to

$$n_l = N \int_0^\infty 2\pi\rho\, d\rho [1 - \exp(-\sigma\phi_0 e^{-\rho 2/R^2})], \tag{5.2}$$

where n_l is the number of atoms dissociated per unit of length and N is number density of the CsI molecules. It can be shown that

$$F(\sigma\phi_0) \equiv n_l/N\pi R^2 = \gamma + \ln\sigma\phi_0 + E_1(\sigma\phi_0), \tag{5.3}$$

where E_1 is the exponential integral

$$\left[E_n(z) = \int_1^\infty e^{-zx} dx/x^n\right]$$

and γ is Euler's constant (0.577...). The ratio of the focused beam signal to the unfocused beam signal (see Fig. 25) is just $F(\sigma\phi_0)/\sigma\phi_0$, since in the limit $\sigma\phi_0 \to 0$, $F(\sigma\phi_0) = \sigma\phi_0$. For a given total number of photons (e.g., 2.5×10^{14}), the $\sigma\phi_0$ which makes $F(\sigma\phi_0)/\sigma\phi_0$ equal to the experimental ratio (0.41) was found. The fluence ϕ_0 was determined experimentally by measuring the energy transmitted through a small aperture with a joule meter. In this way a value of 2.9×10^{-17} cm^2 at 3175 Å was found for the Cs photoproduction cross section.

Figure 26 shows the cross section for the production of Cs neutrals from CsI as a function of wavelength.

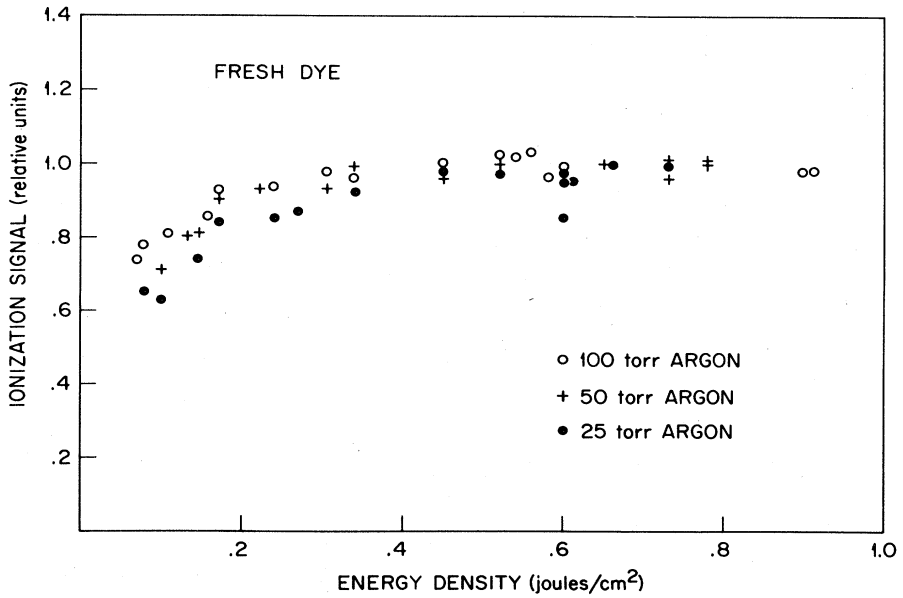

FIG. 24. Measured signals due to Cs atoms as a function of the energy density of the detector laser and at a fixed energy density for the UV laser used to dissociate CsI.

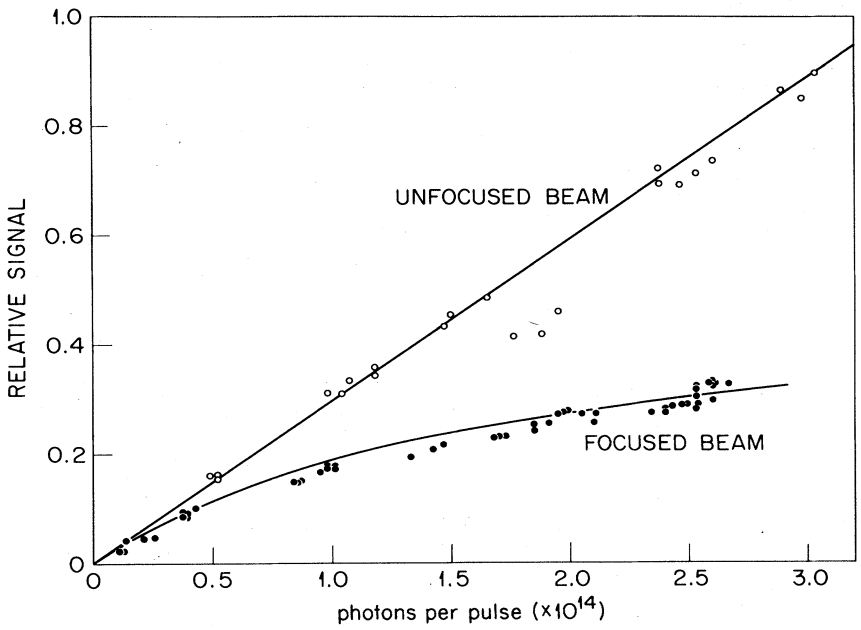

FIG. 25. Signals due to Cs atoms as a function of the number of photons in a single pulse of the source laser. Each atom produced was detected with the RIS process. Data are shown for unfocused and focused beams. The function $F(\sigma\phi_0)$ [Eq. (5.3)] is fitted to the experimental data and is the curve drawn through the focused data points.

These cross sections have a functional form which is similar to that for photoabsorption and at the peak agree to within a few percent with those of Davidovits and Brodhead (1967). The RIS measurements (Grossman *et al.*, 1977b) were made at 320 K, while the photoabsorption data were taken at about 1000 K; the reduction in vibrational populations which results from this temperature difference could account for the difference in widths. A knowledge of the vapor pressure of CsI was not required to obtain the RIS photodissociation cross section. With the RIS technique, the number density of CsI molecules is obtained directly from the saturated curve obtained by plotting the number of Cs atoms per pulse against the laser energy per pulse, or it is obtained through fitting to Eq. (5.3).

Thus it was shown that all CsI molecules in a volume can be dissociated by using a photon fluence exceeding 3×10^{17} cm^{-2} in a single laser pulse of microsecond duration. When this fact is combined with the demonstrated fact that one atom can be detected when using an RIS scheme and a proportional counter (Hurst *et al.*, 1977), the capability for one-molecule detection is obvious.

Some clarifications of the photodissociation process in CsI can be deduced from the present studies. Berry (1957) showed that in the alkali halide molecules one may expect to observe in some cases a band system and in other cases a smooth continuum in the photoabsorption spectrum. Here we observe a smooth continuum in the actual appearance of neutral atoms; furthermore, these neutrals appear in a short time (i.e., in less than 0.5 μsec) after excitation. Presumably, then, the process is one in which photoabsorp-

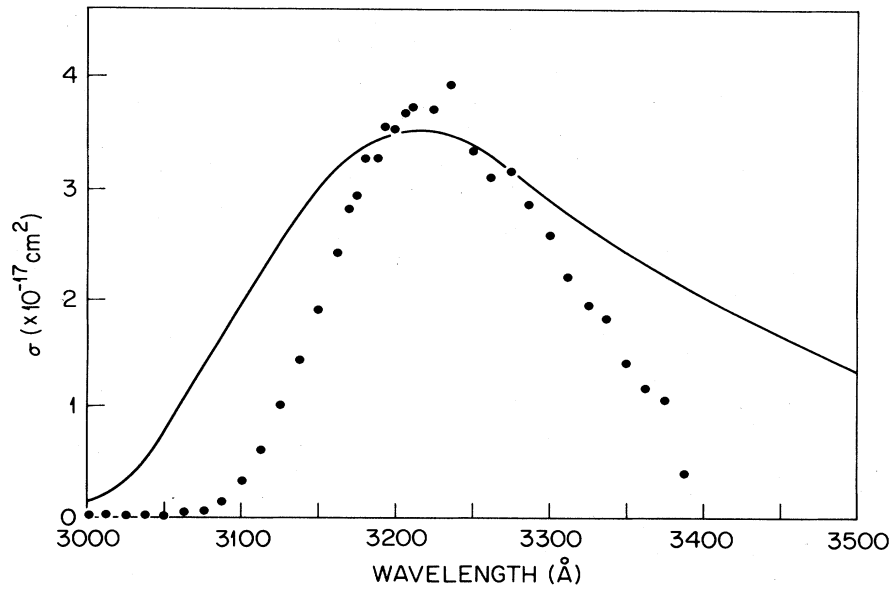

FIG. 26. Cross section for the photoproduction of Cs from CsI as a function of wavelength. Points are those of Grossman *et al.* (1977b) at 320 K; solid curve is data of Davidovits and Brodhead (1967) at 1000 K.

tion occurs from an ionic ground state to a nonionic predissociation state, which dissociates into the neutral continuum state in a short time, perhaps much less than our measured upper limit of 0.5 μsec. Because the predissociation state changes from a nonionic to an ionic state at a rather large internuclear distance (about 20 Å), nuclear motion can no longer be considered adiabatic with respect to electronic motion; hence an otherwise valid noncrossing rule is violated. Direct observations of prompt neutral atoms produced in a smooth photon energy continuum, as well as the observation that no Cs^+ or I^- ions are formed, are consistent with the simple description of the alkali photodissociation process given by Berry (1957), in context with the "harpooning" model of Magee (1940).

B. Mutual diffusion of gases

The measurement of the coefficient for mutual diffusion (Marrero and Mason, 1973) of atoms through other atoms or molecules has always been difficult. Problems arise because it has not been possible to make the measurements in geometries where the diffusion equation can be rigorously solved. Furthermore, if one of the species (such as an alkali atom) is highly reactive with the medium or its impurities, additional problems can be encountered of both experimental and analytical nature. Grossman *et al.* (1977a, 1977b) developed a laser method in which a narrow laser beam produces atoms (by the photodissociation of a trace concentration of a molecule) at time $t=0$ along the axis of an imaginary cylinder which can be swept at $t>0$ with a large-diameter laser beam that detects (by photoionization of the selected type of atom) the atoms which *have not diffused* out of the cylinder.

A much more precise measurement (Hurst *et al.*, 1978b) can be made of mutual diffusion coefficients by using two narrow laser beams which are parallel to each other at a distance ρ. One laser beam pulses at $t=0$, and during a short time Δt, it produces atoms along a narrow line by photodissociation of a trace of a molecular gas. After time t the second laser beam pulses on for another short interval to detect the atoms which *have diffused* into the detector beam at distance ρ from the source beam. It was shown that diffusion processes can be studied in detail and the precision results for $\mathfrak{D}$, the coefficient of mutual diffusion of two gaseous components, can be obtained. The method (Grossman *et al.*, 1977a, 1977b) previously described, however, remains the most straightforward and accurate way of measuring β, the rate at which free atoms react with the medium. In both cases atoms are created and detected in an infinite medium. In the sense that reactive species never reach the walls of the apparatus, containerless chemistry is made possible in the laboratory.

A schematic diagram of a method for precision measurements of the diffusion coefficient is shown in Fig. 27. A source of alkali halide molecules (in the present case, CsI crystals) was heated to about 745 K to produce a concentration of CsI molecules of about 10^9 cm^{-3} in the region of the source laser, SL. This laser (see Footnote 1, this section) produced Cs + I atoms both in their ground states by photodissociation of CsI at a laser wavelength of 3220 Å. A second pulsed laser, DL, detected Cs atoms in a very selective way with the process $Cs[\omega_1, \omega_1 e^-]Cs^+$ with ω_1 corresponding to 4593 Å. Electrons produced in this way can be drifted by means of the ionization drift chamber into the proportional counter for sensitive detection. This method avoids the contamination of the proportional counter surfaces with the CsI products and leads to stability and good reproducibility of the results. Furthermore, in the parallel-beam geometry the distance ρ between the narrow laser beams can be changed over a wide range by using an optical stage equipped with a micrometer screw.

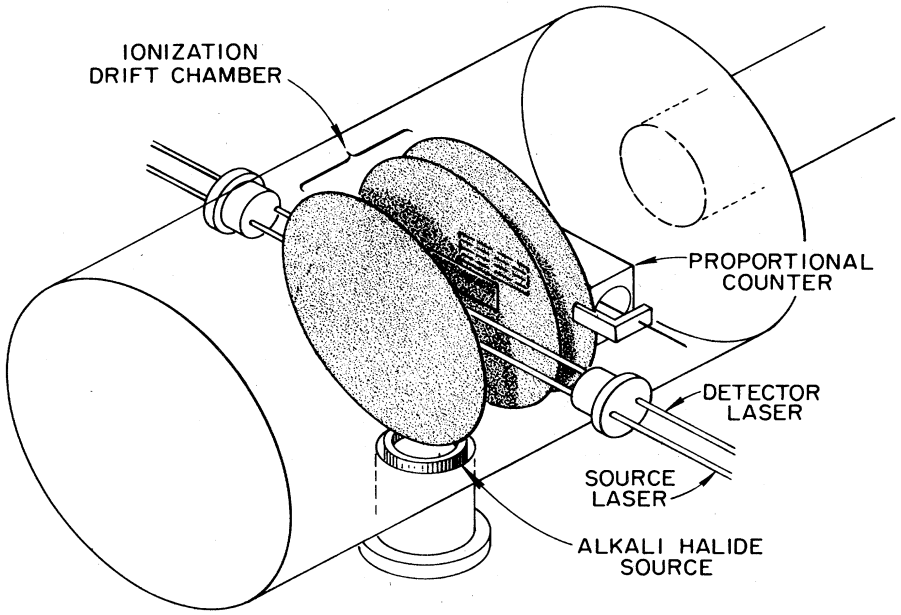

FIG. 27. Schematic of experimental arrangement for studies of the diffusion of alkali atoms through other gases. An alkali halide is first seeded into the gaseous medium, which is then dissociated with a source laser, SL, to produce free alkali atoms, which then diffuse into a detector laser, DL, beam. Electrons created by the RIS process occurring in the DL beam are drifted into a proportional counter for sensitive measurements. By varying the delay between SL and DL and by changing ρ, detailed studies of the diffusion of atoms in an unbounded medium can be made.

With the geometry just described, free atoms are dissociated and detected in a region of space completely decoupled from the walls of the apparatus. Because of the high rate of reaction of the alkali atoms with even trace impurities, it is unlikely that the free atom ever contacts the wall. Under these conditions we can solve the diffusion equation exactly (and trivially). For convenience, we adopt the notation of Marrero and Mason (1973) and define $\mathfrak{D}_1$ as the diffusion coefficient of a tracer in a multicomponent mixture. In the absence of pressure and temperature gradients, but with chemical reaction occurring at a rate β, we seek a solution of

$$\partial n(\rho,t)/\partial t = \mathfrak{D}_1 \nabla^2 n(\rho,t) - \beta n(\rho,t), \tag{5.4}$$

where $n(\rho,t)$ is the number density of free alkali atoms. The solution for Eq. (5.4), where λ is the number of alkali atoms created per unit of length (cm) along the narrow beam, is

$$n(\rho,t) = \frac{\lambda}{4\pi\mathfrak{D}_1 t}\exp\left(-\frac{\rho^2}{4\mathfrak{D}_1 t}\right)e^{-\beta t}. \tag{5.5}$$

In the above, boundary effects have been neglected. In fact, there are no surfaces near either the source of atoms or the detector of atoms.

Since we are stressing here the precision measurement of $\mathfrak{D}_1$, even with large β, it is convenient to note that if measurements are made at two separations $\rho=\rho_1$ and ρ_2, where $\rho_2>\rho_1$, one can write

$$\frac{n(\rho_1,t)}{n(\rho_2,t)} = \exp\left[\frac{(\rho_2^2-\rho_1^2)}{4\mathfrak{D}_1 t}\right]. \tag{5.6}$$

Thus,

$$\ln\left(\frac{n(\rho_1,t)}{n(\rho_2,t)}\right) = \left(\frac{\rho_2^2-\rho_1^2}{4\mathfrak{D}_1}\right)\frac{1}{t}. \tag{5.7}$$

Equation (5.7) expresses the fact that the slope of $\ln(n_1/n_2)$ plotted against $1/t$ is just $(\rho_2^2-\rho_1^2)/4\mathfrak{D}_1$, independent of the chemical reaction rate β. This is the basis of a precision determination of $\mathfrak{D}_1$, since the ρ's can be well defined for parallel-laser-beam geometries.

The data acquisition system schematized in Fig. 28 is consistent with the precision objectives of the above. Sets of signals (S,D,P) are stored in a PDP-11-type computer so that all information on each observation is kept. The signal S is proportional to the source laser energy per pulse, the signal D applies similarly for the detector laser, and P is the pulse height of the proportional counter, giving the number of electrons drifted in and giving accurate information on n. When the data are retrieved, P is normalized in two ways. First, P is divided by S since here the number of atoms produced is a linear function of the laser energy per pulse. Next, (P/S) is divided by F, where $(P/S)=F(D)$ and represents a nonlinear dependence of the number of atoms detected on the energy per pulse of the detector laser. In fact, (P/S) saturates when the energy

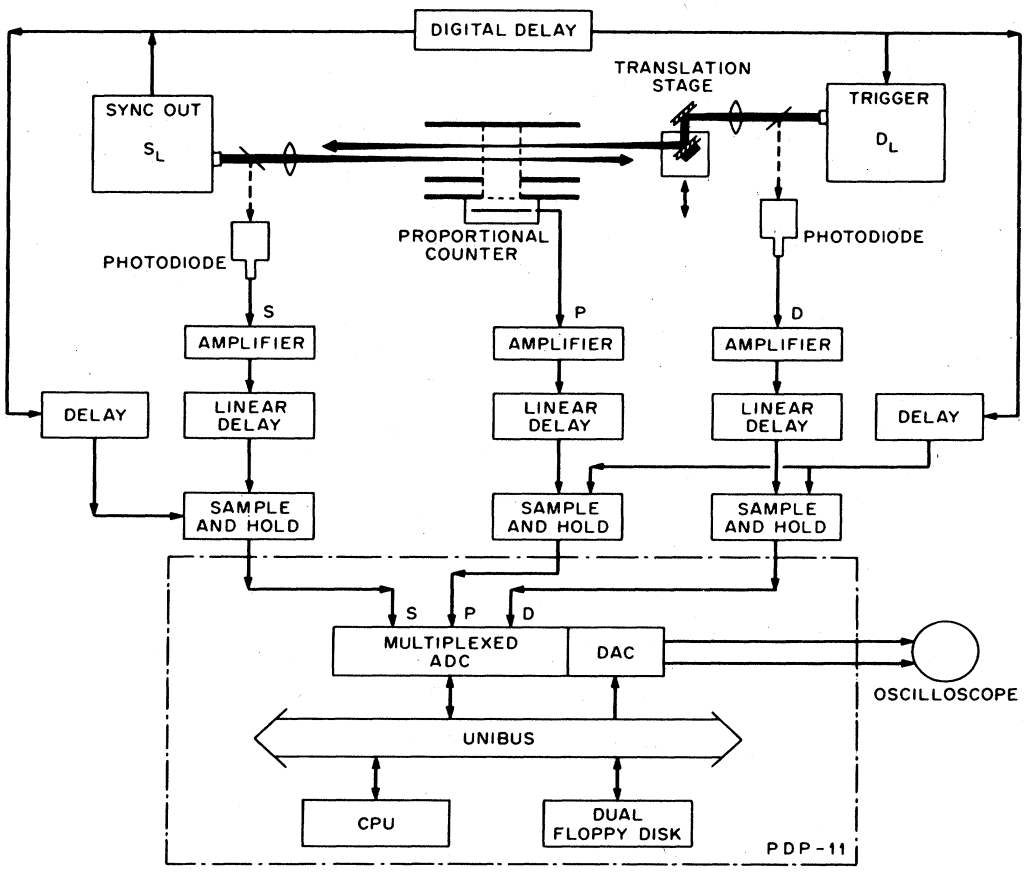

FIG. 28. The signals S, D, and P associated with each observation are listed as sequential sets in a PDP-11 microcomputer. From these data a normalized quantity, $\mathcal{P}$, is generated as described in the text.

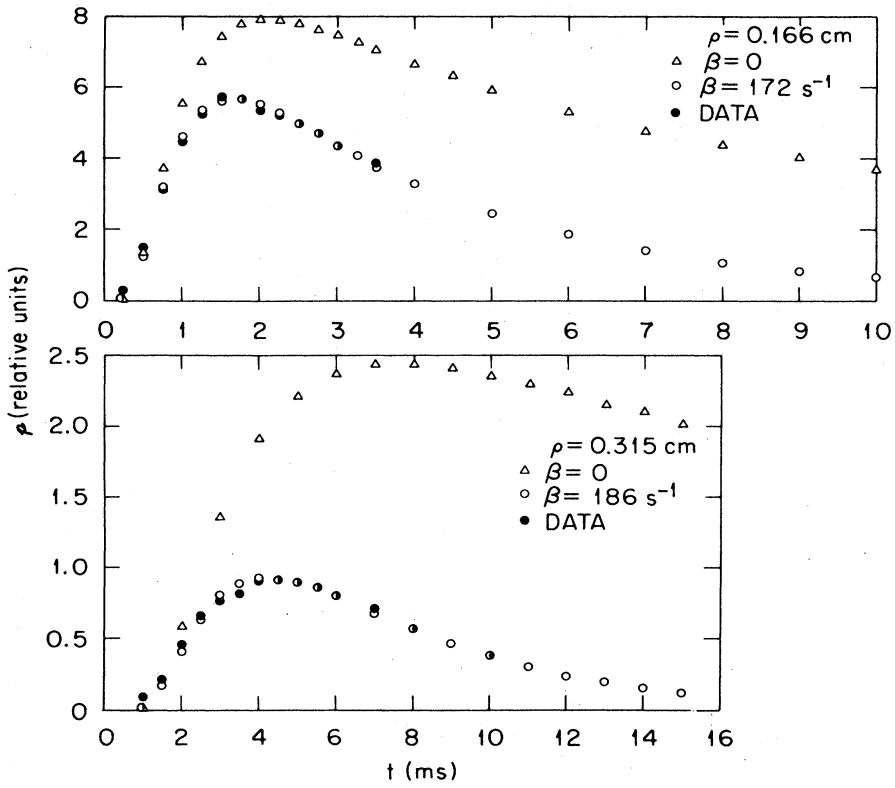

FIG. 29. S,D normalized pulse-height data for two values of ρ are plotted as a function of delay time between SL and DL. Experimental data are compared with calculations using a weighted least-squares fit to the best values of β when using the value of $\mathfrak{D}_1$ as determined from Fig. 30. For additional comparison, the cases where $\beta = 0$ are also plotted.

per pulse per unit of beam area exceeds 100 mJ cm^{-2}. The doubly normalized signals $P_{S,D}$ (i.e., P/SF) are then averaged over many trials to obtain $\bar{P}_{S,D}(\equiv \mathcal{P})$ for many values of t at each ρ. The ratios $\mathcal{P}_1/\mathcal{P}_2$ at $\rho = \rho_1$ and $\rho = \rho_2$ are then computed for each t and used in Eq. (5.7) for the ratios of the n's.

Data are shown in Fig. 29 for the diffusion of traces of Cs in P–10 (90% Ar + 10% CH_4) counting gas at 50 Torr pressure. Plots are shown for $n(\rho_1, t)$ and $n(\rho_2, t)$ for $\rho_1 = 0.166$ cm and $\rho_2 = 0.315$ cm. It was found that Δ (FWHM) = 0.0068 cm for SL, and 0.0075 cm for DL. The points (·) are actual data; we defer until a bit later other comments on Fig. 29. Figure 30 is a plot to test Eq. (5.7). Indeed the agreement is excellent; chemistry completely cancels for the two ρ's if the time factor is kept common. From the slope of Fig. 30, $\mathfrak{D}_1 = 3.30$ cm^2 sec^{-1}; normalized to 760 Torr, it is 0.217 cm^2 sec^{-1} at 55°C. For comparison, a values of 0.25 cm^2 sec^{-1} was reported (Franzen, 1959) for Rb in Ar. The consistency between the value for $\mathfrak{D}_1$ and the β derived from Fig. 29 was tested. Using the above $\mathfrak{D}_1$ and a simple least-squares fitting procedure in which data was weighted by the square of its amplitude, it was found that $\beta(\rho = \rho_1) = 186$ sec^{-1} and $\beta(\rho = \rho_2) = 172$

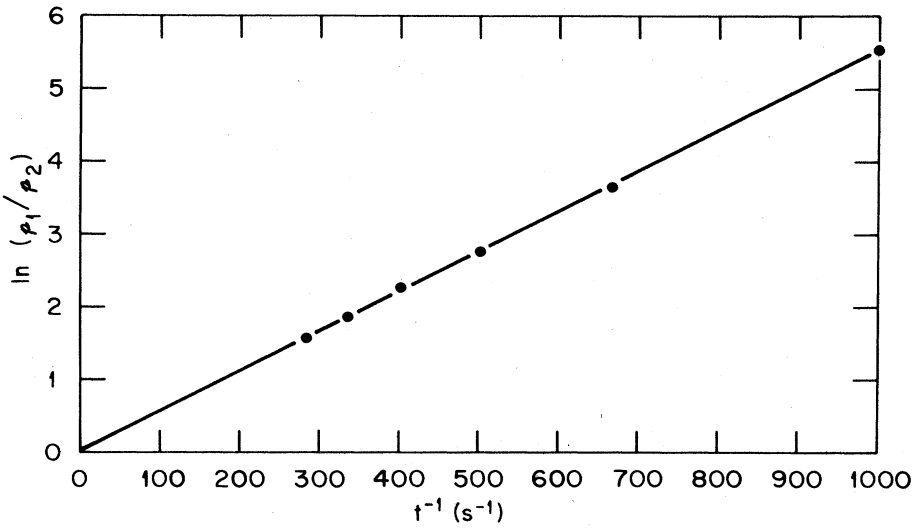

FIG. 30. Plot of $\ln(p_1/p_2)$ against t^{-1}. The excellent agreement with Eq. (5.7) implies that the diffusion coefficient can be accurately determined even when the atoms are diffusing in a highly reactive medium.

sec^{-1}—in remarkable agreement. Plotted in Fig. 29 are the fits to the complete data for these β's, and also for comparison what would be expected for both ρ's when $\beta = 0$. The value of β derived above is consistent with the presence of about 10 ppm of O_2 in the apparatus. This was a steady-state balance between a small rate of leakage of O_2 into a static system and O_2 reaction with a cesium getter sealed into the system. It is gratifying to see such agreement even when the medium is so reactive that severe distortion of the data is found at a given ρ; nevertheless, the technique involving the ratio $n(\rho_1, t)/n(\rho_2, t)$ gives accurate results for $\mathfrak{D}$.

Grossman *et al.* (1977a) had shown earlier that the coaxial geometry could also be used for the measurement of the diffusion coefficient. From Eq. (5.8) we see that the fraction $\gamma(t)$ of the number of atoms contained in a cylinder of radius R is

$$\gamma(t) = \lambda^{-1} \int_0^R 2\pi\rho\, d\rho n(\rho_1 t) = [1 - \exp(-R^2/4\mathfrak{D}_1 t)] e^{-\beta t} . \tag{5.8}$$

In Eq. (5.8) $\gamma(t)$ is a slowly declining function of t only if β is small. The success of fitting to $\gamma(t)$ to obtain $\mathfrak{D}_1$ depends, therefore, on a small β (i.e., a nonreactive medium). Furthermore, to obtain an accurate $\mathfrak{D}_1$, the detector laser must have a well defined beam of uniform quality so that R can be precisely known.

The parallel-beam geometry is a precision method for the measurement of the diffusion of atoms. Moreover, the diffusion equation has been tested rather completely in both its spatial and temporal domains. Uncertainties in the absolute values of $\mathfrak{D}_1$ here are about ±5% due to uncertainty in the ρ's. With smaller β, the ρ's. With smaller β, the ρ's could be made large enough to reduce uncertainties in the absolute values to ±1%.

C. Chemical reaction of free atoms

The coaxial-beam geometry is an excellent method for determining the rate of chemical reaction of a free atom with its environment. This point is illustrated in Fig. 31 for Cs interactions with O_2 in the presence of Ar. For 100-Torr Ar, the $\gamma(t)$ [see Eq. (5.8)] is slow but goes over into a rapidly decaying function that is exponential in time when traces of O_2 are added. From the slopes of these semilog plots, one can easily deduce β. It was found for the region $0 \leq P_{O_2} \leq 0.02$ Torr and $25 \leq P_{Ar} \leq 1200$ Torr,

$$\beta = 7000 P_{Ar} P_{O_2} , \tag{5.9}$$

where β has units of sec^{-1} when the pressure units are in Torr at 300 K. For $P_{O_2} > 0.5$ Torr, Eq. (5.9) overestimates the observed rate, suggesting a somewhat complex reaction scheme. Basically, however, the following mechanism appears to reproduce the results:

$$Cs + O_2 \overset{k}{\rightleftarrows} (Cs\,O_2)^{**} , \tag{5.10a}$$

$$(Cs\,O_2)^{**} + A \overset{k_1}{\rightarrow} (Cs\,O_2)^{*} + A , \tag{5.10b}$$

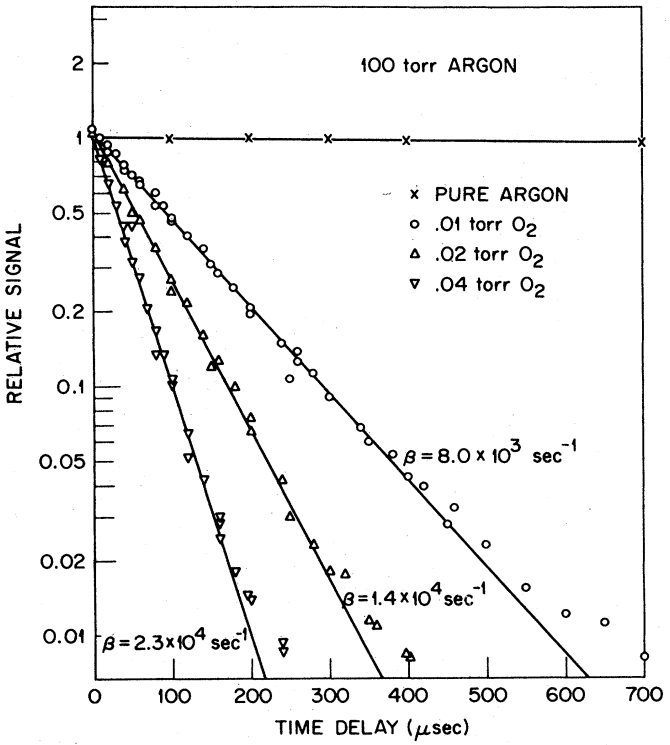

FIG. 31. Relative number of Cs atoms surviving a function of time for various partial pressures of O_2 in 100 Torr of Ar.

$$(CsO_2)^{*} + O_2 \overset{k_2}{\rightarrow} Cs + O_4 , \tag{5.10c}$$

$$(CsO_2)^{*} + A \overset{k_3}{\rightarrow} Cs\,O_2 + A . \tag{5.10d}$$

In these, $(CsO_2)^{**}$ is a highly excited vibrational state of the cesium superoxide molecule which will reverse to $Cs + O_2$ unless an atom A (=Ar) removes some energy to make $(CsO_2)^{*}$. However, Cs can be released (i.e., a back reaction can occur) due to collisions of $(CsO_2)^{*}$ with O_2 creating the O_4 molecule. Further relaxation of $(CsO_2)^{*}$ with the inert atom A makes a stable (CsO_2) molecule. The O_4 molecule has been known for a long time (Herzberg, 1950) both as an atmospheric and a laboratory species. Furthermore, the CsO_4 molecule has been observed (Andrews, Hsang, and Trindle, 1973) in solid matrix samples at low temperatures.

The example above shows how the rate of reaction of free atoms with their chemical environment can be determined in a rather direct way, even when the free atoms are so reactive that normal chemistry studies are not feasible. Here we do not have to be concerned about corrosive reactions on the walls, because only a small number of free atoms are formed at a given time and these react before they find the wall.

D. Statistical mechanics and atomic fluctuations

One-atom detection makes it possible to examine some basic questions in statistical mechanics. One of these is the statistics obeyed by free atoms diffusing in a gas. The history of this subject shows that this problem has never been put to direct test. We must remind ourselves that randomness is frequently assumed (proof is more elusive), and we are led to the binomial dis-

tribution for which the Poisson distribution is a special case. Smoluchowski (1908) derived an expression for the frequency distribution of the number of atoms found at a given time in a small volume surrounded by an infinite medium. Similarly, Rutherford and Bateman (Bateman, 1911) showed that the number of alpha particles emitted from the nucleus in a fixed interval of time can be described by a formula which is exactly the same as the Poisson equation. Many other examples in statistical physics start with a prescribed physical situation and end with the Poisson distribution. These are all done independently of the work of Poisson (1837), who derived purely mathematical expressions and applied them to civil and criminal questions such as the optimum size of a jury!

Another basic question which can be tackled is that of the ergodic hypothesis. Einstein (1956), while analyzing the diffusion problem in the context of the Brownian motion studies of Perrin, suggested a "Gedanken" experiment to test the assumption of an ergodic system. He visualized a time-resolved diffusion experiment in which the diffusion equation could be tested both by "time summation" and "space summation." Such an experiment is now feasible with atoms. It is convenient that a proportional counter can be used as both a digital detector for measuring the probability that an atom is in a volume and as an analog detector to measure the number of atoms in the volume in a given trial. The ergodic hypothesis takes on a very modern context in connection with the use of short-duration laser pulses for the photodissociation of complex molecules; see, for example, Bloembergen and Yablonovitch (1978).

With the availability of a detector of single atoms, it is now possible to record atomic fluctuation phenomena with electronic methods. Previously direct observation of density fluctuations had to be made on particles which could be seen under a microscope. Apart from these studies of the Brownian motion of particles, information on density fluctuations was deduced from such indirect sources as the Smoluchowski (1908) and Einstein (1910) theories of the blue of the sky. According to these theories, scattering can only occur from an inhomogeneous medium; it is, therefore, argued that concentration fluctuations of particles in the atmosphere are responsible for the observed spectrum of scattered light, and this is consistent with Poisson (1837) statistics. Just prior to the development of the methods described here, it was not possible to record even as low as 10^6 atoms in a time-resolved measurement. Thus $\sqrt{\bar{N}}/\bar{N}$ was too small for accurate measurement of fluctuations. Now, however, with $\bar{N}$ as small as 100 (or much less, if desired) $\sqrt{\bar{N}}/\bar{N}$ can be made quite large. A wide range of these fluctuation experiments are, in fact, rather straightforward. The list includes:

(1) The direct measurement of the density fluctuation of free atoms,

(2) The fluctuation of the number of interactions of a given (large) number of photons with a given (large) number of atoms,

(3) The fluctuation of the collision frequency of pairs of atoms accounting for collisional line broadening,

(4) The fluctuation of the total number of ion pairs produced by absorption of a fixed amount of energy from a swift charged particle,

(5) The fluctuation of the gas amplification of a proportional counter.

We conclude this section with a review of some preliminary observations on (1) above and a more detailed study of (4) and (5) to obtain the Fano factor associated with ionization fluctuations.

E. Measurement of the Fano factor

Previously (Curran, Cockroft, and Angus, 1949; Campbell and Ledingham, 1966; Alkhazov, Komar, and Voreb'ev, 1967; Charles and Cooke, 1968; Alkhazov, 1970; Genz, 1973; Breyer, 1973; Sipila, 1976) radiation sources such as low-energy x rays or other sources of swift charged particles were used to study both the magnitude and the fluctuation of the amplification of gas proportional counters. In contrast to this, the RIS method involves the production of free thermal electrons in a spatially well defined laser beam at a known time. Furthermore, the mean number of electrons produced in the proportional counter can be "dialed in" electronically, and the statistical fluctuation about the arbitrarily chosen mean number is described by the known Poisson function, which involves no Fano factor.

In the proportional counter literature, use is made of the following equation, which describes the standard deviation δP of the mean pulse height $\bar{P}$,

$$\left(\frac{\delta P}{\bar{P}}\right)^2 = \left(\frac{\delta N}{\bar{N}}\right)^2 + \frac{[\delta A/\bar{A}]^2}{\bar{N}}, \tag{5.11}$$

where $\bar{N}$ and δN are, respectively, the mean and the standard deviation of the number of free electrons before gas amplification, and $\bar{A}$ is the mean gas amplification whose standard deviation is δA. When the free electrons are produced by charged particles (e.g., swift electrons created by photoelectron ejection from an atom due to an x-ray interaction), the standard deviation δN of the number N is smaller than that for a purely random source (Fano, 1947). The term $(\delta N/\bar{N})^2$ can be replaced with $F/\bar{N}$, where F is now known as the Fano factor. An F value less than 1 has its origin in the fact that the total energy of the charged particle is exact, and the process in which this energy is dissipated to produce ion pairs and excited states in a gas cannot be purely random, owing to a definite pattern of oscillator strengths for given kinds of atoms and molecules (the counting gas). By studying $(\delta P/\bar{P})$ as a function of $\bar{N}$ by laser ionization of atoms which are subject to density fluctuations, one can be reasonably assured that the ionization process is random and, therefore, $F=1$. We shall be thus in a unique position to determine the relative standard deviation $\delta A/\bar{A}$ of the amplification process and, by incorporating studies using x-ray sources, we can also obtain F in a new (and hopefully more accurate) way.

The concept of the experimental method is shown in Fig. 32. Two laser beams at separation ρ and parallel

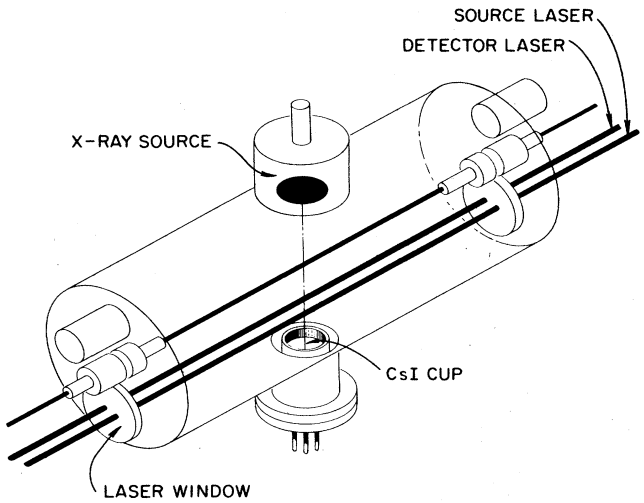

FIG. 32. Schematic of the proportional counter fluctuation experiment. A pulsed laser in the ultraviolet can be used to dissociate an alkali halide (e.g., CsI) molecular vapor to provide a time-resolved source of atoms which diffuse into a detector beam. A pulsed laser (detector laser) in the visible can be used to ionize Cs atoms in the resonance, two-step process $Cs[\omega_1, \omega_1 e^-]Cs^+$. The electrons thus created are detected with a proportional counter.

to the counter wire are pulsed into the proportional counter with an aribitrary time delay τ set between the lasers. With CsI crystals in the small furnace, a very low vapor pressure of CsI (e.g., 10^8 molecules/cm^3) can be created in the proportional counter otherwise filled with P-10 gas at a few hundred Torr. Thus the source laser set at 3220 Å dissociates (Grossman *et al.*, 1977b) CsI into Cs + I and the detector laser ionizes Cs according to the RIS process $Cs[\omega_1, \omega_1 e^-]Cs^+$ with ω_1 corresponding to 4555 Å or to 4593 Å. Several parameters are available to control the number of electrons created (i.e., the CsI concentration, laser energies per pulse, the distance ρ, and finally, for fine control, the delay time τ). In this way the average number $\bar{N}$ of electrons per pulse is under excellent control, and the various fluctuations associated with the counter can be measured as a function of $\bar{N}$. This experimental arrangement is suitable for a number of other studies such as the fluctuation of the density of atoms, collisional fluctuations, and photon-atom interaction fluctuations.

Both lasers are linear flashlamp-pumped dye lasers which produce about 1 mJ of photons tunable over a wide spectral range in the visible. A time delay can be set between the source laser (SL) and the detector laser (DL) by using a digital delay generator. The SL is monitored with a photodiode via a beam splitter; and with kiton red dye (frequency-doubled to give 3220-Å photons), it is stable enough so that a narrow (4% FWHM) window could be set on a single-channel analyzer without rejecting more than 50% of the laser shots. However, with the coumarin-2 dye, the DL is so unstable that control with a narrow window is not feasible. The general data acquisition shown in Fig. 28 is, therefore, very appropriate.

As previously mentioned, the resonance ionization process provides good control over the location, the statistical fluctuation, and the average number of electrons created in the proportional counter. For a CsI temperature = 585 K for $\rho = 0.5$ cm and for $\tau = 10$ msec, $\bar{N} = 1 \times 10^3$ when the SL provides 0.15 mJ per pulse and the DL provides 0.5 mJ. The unfocused beam diameters for both SL and DL are about 0.3 cm; therefore lenses of 50-cm focal length were placed 50 cm from the wire center for focusing the beams. Thus both lasers were focused to about 0.050-cm diameter waist at the center of the counter and were about 0.10-cm diameter at the ends of the wire defined by the field tubes. Under these conditions, the number of Cs atoms dissociated from CsI molecules is nonlinear with the energy per pulse S of the source laser. The number of detected atoms (electrons) also begins to saturate for the larger values of the energy per pulse D of the detector laser.

Several pulse-height spectra (i.e., plots giving the relative probability of observing various pulse heights) corresponding to various $\bar{N}$ in the range of 4 to 20 are shown in Fig. 33. Since the values of D were large enough to partially saturate the RIS process, one sees that the RIS signals fluctuate due to fluctuation of atoms combined with the fluctuation of photon-atom interactions.

It is convenient to have somewhat larger values of $\bar{N}$ (i.e., $\bar{N} > 25$) so that the data can be represented with Gaussian functions. Several of these are plotted in Fig. 34 and compared to x-ray spectra with $\bar{N} = 100$ and $\bar{N} = 227$. At comparable values of $\bar{N}$, the spectra due to the laser interactions are clearly wider than those associated with the x-ray sources. This presentation vividly shows that the Fano process is operative. Without data analysis of any sort, one sees there is a Fano factor less than unity.

To analyze the RIS data and to compare them with the x-ray data requires only the following extension of Eq. (5.11):

$$\left(\frac{\delta P}{\bar{P}}\right)_L^2 = \left(\frac{\delta N}{\bar{N}}\right)_L^2 + \frac{[\delta A/\bar{A}]^2}{\bar{N}} + (\delta l)^2 , \tag{5.12}$$

where the term $(\delta N/\bar{N})_L^2$ will be just $1/\bar{N}$, assuming Poisson statistics for the fluctuation of the RIS signals, and the term $(\delta l)^2$ represents any fluctuation which is independent of $\bar{N}$. For instance, fluctuation of the energy per pulse of the source laser can give rise to a term which is independent of $\bar{N}$. The term $(\delta A/\bar{A})^2$ is related to the single-electron pulse-height spectrum as follows:

$$(\delta A/\bar{A})^2 = [\bar{\varepsilon}^2 - (\bar{\varepsilon})^2]/(\bar{\varepsilon})^2 , \tag{5.13a}$$

where

$$\bar{\varepsilon}^m = \int_0^\infty P(\varepsilon)\varepsilon^m d\varepsilon , \tag{5.13b}$$

and $P(\varepsilon)$ is the probability density function for pulse height ε due to a single electron. For x-ray sources, we have, from Eq. (5.12)

$$\left(\frac{\delta P}{\bar{P}}\right)_x^2 = \frac{[F - 1 + \varepsilon^2/(\bar{\varepsilon})^2]}{\bar{N}} , \tag{5.14a}$$

while for the RIS process,

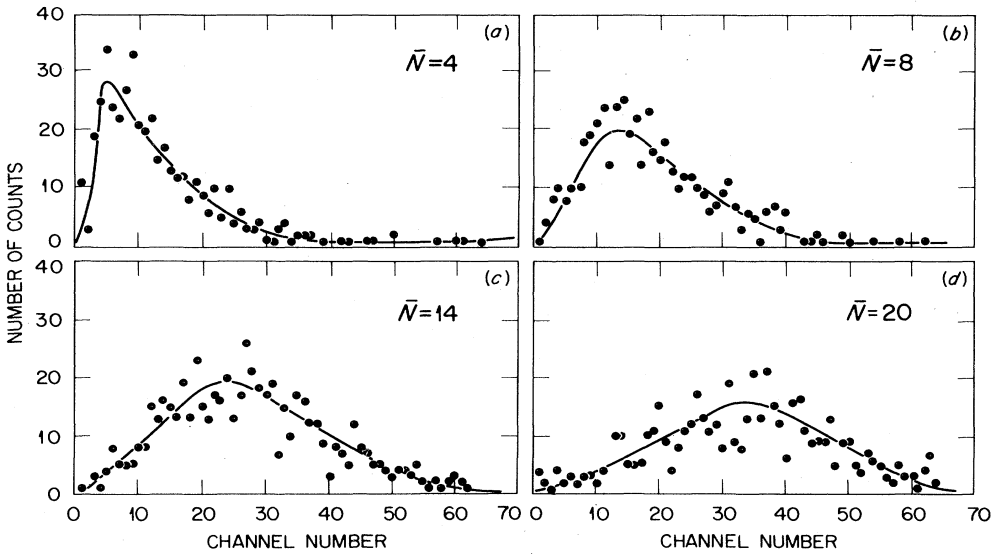

FIG. 33. Pulse-height spectra for a small number of electrons created by the laser in an RIS process. The mean numbers of electrons, $\bar{N}$, are approximately 4, 8, 14, and 20, respectively. Note the definite trend from a Gaussian to a Poisson distribution as $\bar{N}$ decreases. Solid lines drawn through data serve as a visual aid only.

$$\left(\frac{\delta P}{\bar{P}}\right)^2_L = (\delta l)^2 + \frac{[\bar{\varepsilon}^2/(\bar{\varepsilon})^2]}{\bar{N}}. \qquad (5.14b)$$

When the RIS data of Fig. 34 are plotted to fit Eq. (5.14b), the results in Fig. 35 are obtained. From the figure, $(\delta l)^2 = 0.015$ and $\bar{\varepsilon}^2/(\bar{\varepsilon})^2 = 2.31$. From Eq. (5.14a), $F = 0.31$ and 0.21 for the ^{37}Ar and ^{55}Fe x-ray lines, respectively.

Previously the Fano factor was determined experimentally by measuring the pulse-height fluctuation due to the complete absorption of ^{224}Ra alpha particles in a pulsed ionization chamber. In this case the relative fluctuation was small due to the fact that $\bar{N}$ is on the order of 2×10^5 and it is difficult to separate the small fluctuation of ionization from other fluctuations associated with the measurements. However, by using this method, Alkhazov, Komar, and Voreb'ev (1967) were able to avoid the fluctuations associated with the gas amplification process that are encountered when a proportional counter is used. Prior to the RIS method there was no satisfactory way to independently measure the fluctuation of gas amplification. The above values for F for the two x-ray sources, compared with the value measured by Alkhazov, Komar, and Voreb'ev (1967) for alpha particles, are shown in Table II. Also listed is the mean number $\bar{N}$ of electrons produced in a single pulse for each of the sources, where $\bar{N}$ was calculated by dividing the energy in electron volts by the W value (Melton, Hurst, and Bortner, 1954) for P-10 gas (i.e., $W = 26$ eV). Fano factors can depend on the energy of the swift particle producing the ionization. Therefore, in principle, the value for the 2.6-keV photoelectrons could be larger than the value for the 5.9-keV photoelectrons. The method reported here gives a Fano factor for each source independently.

Finally, we stress that the technique for studying the fluctuation of proportional counters by using the RIS process allows one to determine the fluctuation of gas amplification under conditions where $\bar{N}$ can be arbitrarily selected and where the fluctuation about $\bar{N}$ can be assumed to be that of Poisson statistics. With this independent determination of $(\delta A/\bar{A})$, one can more accurately determine the Fano factor which enters into the statistics of the ionization of gases by fast charged particles.

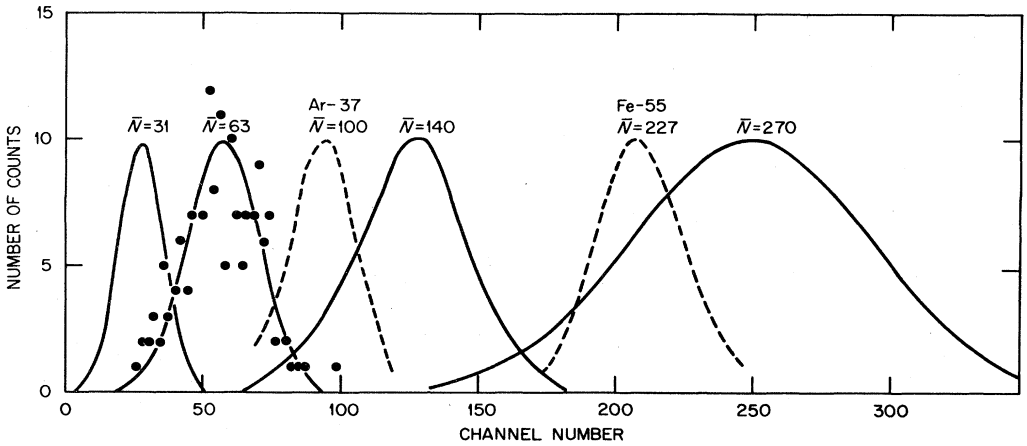

FIG. 34. Pulse-height spectra for the indicated $\bar{N}$ produced by laser ionization in the RIS process. When the RIS distributions are compared with the narrower x-ray distributions, the existence of a Fano factor is immediately apparent.

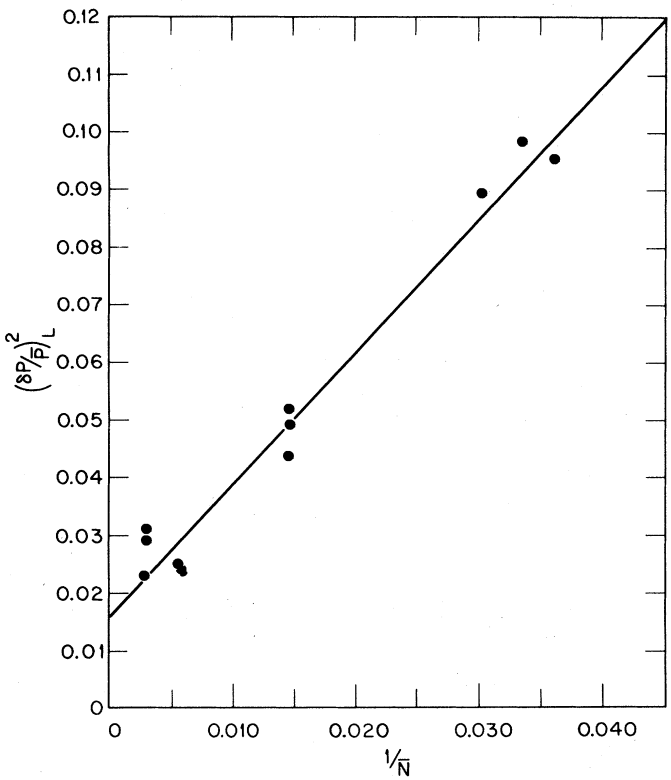

FIG. 35. The quantity $(\delta P/\overline{P})^2_L$ (i.e., the square of the standard deviation of the relative pulse height when electrons are produced with laser pulses) plotted against the reciprocal of the average number of electrons in a pulse.

VI. PHOTOPHYSICS APPLICATIONS

A. Previous use of RIS for study of excited states

The use of saturated RIS for the purpose of making time-resolved measurements of the absolute number of atoms in an excited state began at Oak Ridge National Laboratory in 1975 (Hurst *et al.*, 1975; Payne *et al.*, 1975). However, the use of RIS for isotope separation and for studies in photophysics began earlier (see Sec. I). A number of applications of RIS to the study of excited-state populations are described here.

Some of the earliest and most beautiful work involving the use of RIS for the study of excited-state populations was carried out by the group of R. F. Stebbings at Rice University. In the Stebbings experiments (Stebbings, Dunning, and Rundel, 1974) a sophisticated beam apparatus (Riola *et al.*, 1974) (see Fig. 36) was used in order to obtain populations of rare gas metastable atoms. The beam of metastable atoms is crossed with a pulsed dye laser beam which could be used to promote them to higher excited states or to ionize them in one- or two-step processes. The number density of metastable rare gas atoms is measured independently of the ionization so that saturated RIS is not required for purposes of determining accurate cross sections for photoionization of the metastable atoms. Stebbings' group has measured accurate photoionization cross sections for He(2^1S) and He(2^3S) by one-photon ionization (Stebbings *et al.*, 1973). They also saturated the transition from He($2^{1,3}S$) to higher P state, He($n^{1,3}P$), where $n=3, 4$, and observed ionization out of these states (Dunning and Stebbings, 1974). Results of these photoionization studies are given in Fig. 37 and Table III. In other studies (Rundel *et al.*, 1975) Xe metastable atoms were excited to autoionizing resonance, and they showed that the ionization signal gives the line shape for the autoionizing level. More recently the Rice group has introduced a few μ Torr of target gas into the cell and studied collisional ionization of Xe atoms which are laser excited to high Rydberg states. West *et al.* (1976) concerned themselves with collisions with SF_6 for $25 \leq n \leq 40$, and Foltz *et al.* (1977) studied collisions of the $|nF\rangle$ levels with CCl_4, CCl_3F, and SF_6. Absolute rate constants for Xe^+ production were reported; values up to 10^{-7} cm^3/sec were found for $25 \leq n \leq 40$.

Photoionization of excited states has also been studied in cell experiments by a number of groups. In 1975 the Oak Ridge group confirmed a cross section for the photoionization of He(3^1P) at 5015 Å of $\sim 1 \times 10^{-17}$ cm^2 by a study of the saturation curve for the two-step ionization of proton-excited He(2^1S) (Hurst *et al.*, 1975). A bit later, Ambartsumyan *et al.* (1976) reported a similar cell experiment on the 6^2P state of Rb. This group found $\sigma_I(6^2P)$ on the order of 1.7×10^{-17} cm^2 at the fundamental of the ruby laser and 1.9×10^{-18} at the first harmonic. A saturation curve from this study is shown in Fig. 38. Photoionization cross sections for Cs($5D$) at 4593 Å and Cs($7P$), also at 4593 Å, have been reported by Nayfeh *et al.* (1977). The latter study also made use of the saturation curve for two-step ionization of ground-state Cs atoms with Cs($7P_{1/2}$) as an intermediate. The Cs($5D$) state was populated by spontaneous emission from the Cs($7P$) levels.

Nayfeh *et al.* (1977) also demonstrated the feasibility of using the laser ionization technique in order to study far wing line broadening. The basic idea in these measurements is that each time far wing absorption occurs the atom is ionized. Thus, by making sensitive measurements of the ionization, it is possible to make

TABLE II. Measured values of the Fano factor, F, for ^{37}Ar and ^{55}Fe x-ray sources in P-10 gas. Comparison is made with a measurement made for α particles in a mixture of Ar and CH_4.

Source	$\overline{N}$	Observer	F
^{37}Ar (2.6 keV, x-ray)	100	Hurst *et al.* (1978a)	0.31 ± 0.10
^{55}Fe (5.9 keV, x-ray)	227	Hurst *et al.* (1978a)	0.21 ± 0.10
^{224}Ra (3.68 MeV, α particle)	2.2×10^5	Alkhazov, Komar, and Voreb'ev (1967)	0.19

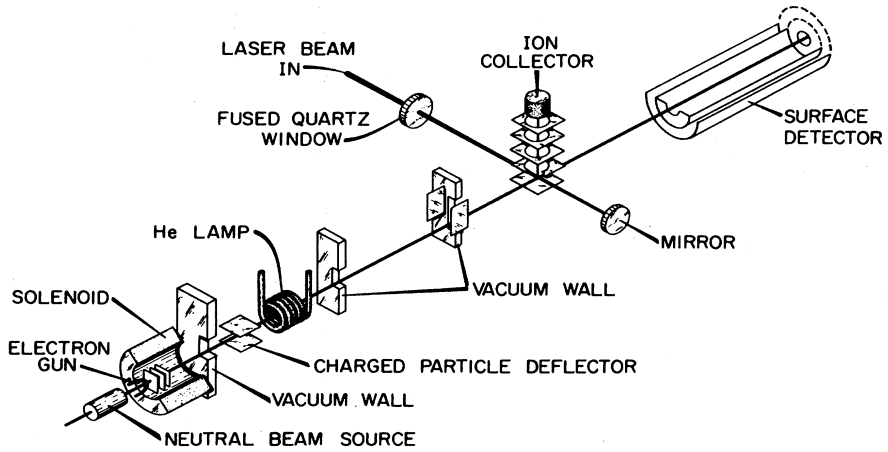

FIG. 36. Schematic of the Rice University group's beam apparatus. Metastable atoms are generated by the incidence of an electron beam on a rare gas. Charged particles are deflected out of a resulting collimated beam leaving a ground state and a metastable beam. A dye laser beam is crossed with the particle beam between the plates of a detector which measures ion production. The metastable beam intensity is measured by a surface detector farther downstream, and the velocity distribution can be measured by pulsing the metastable source.

absolute measurements of absorption as far from line center as 100 Å while keeping the gas pressure as low as 50 Torr. The Oak Ridge group has also made absolute measurements of cross sections for the photodissociation of diatomic molecules by using standard RIS as a tool (Grossman *et al.*, 1977b). This work is described in detail in Sec. V.

It is suggested in Sec. III that the observation of ionization would also be an excellent tool in laser spectroscopy. In fact, Niemax and Weber (1978) have recently used the ionization signal in carrying out Doppler-free, two-photon spectroscopy on Rydberg states in Rb. They suggest many advantages over the more conventional technique of observing fluorescence from the excited level. In the case of Doppler-free, two-photon excitation the excited state often lies high enough so that another photon can ionize it, and the power levels are sufficiently high so that there is an appreciable probability of ionization. Thus, given the high sensitivity of electron detection (with channel electron multipliers) in the presence of a concentration $\approx 10^{11}/\text{cm}^3$ of an atomic vapor, there should be a proliferation of this technique.

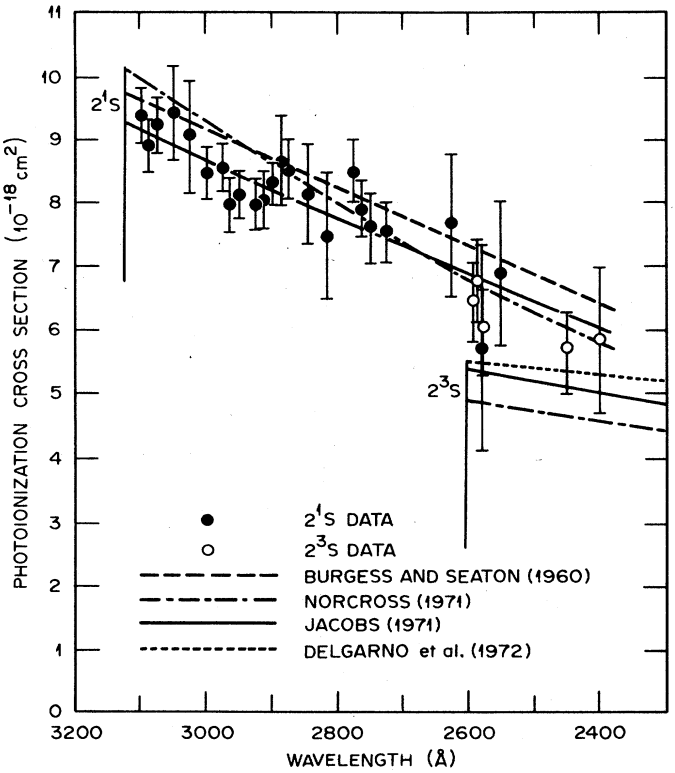

FIG. 37. The photoionization cross section of He(2^1S) as a function of wavelength. The data points are the measurements of Stebbings *et al.* (1973).

B. Photophysics experiments with coaxial beams

It is clear from the previous discussions that the sensitivity and time resolution inherent in RIS make possible a large number of accurate, but relatively easy, measurements in atomic physics. In the next subsection measurement techniques are described for the following:

(1) Photoionization cross sections for excited states,
(2) Far wing line broadening,
(3) Thermal rate constants for quenching or collisional redistribution among states,
(4) Imprisonment of resonance radiation.

In most of this section it is assumed that the atoms to be studied have been produced along a narrow line in space at $t=0$ by the pulsed dissociation of molecules and that the free atoms are detected in a second beam of larger diameter concentric with the source beam and pulsed at some $t>0$. This geometry has already been illustrated in Fig. 23. Dissociation of molecules into free atoms can be brought about either by a short laser pulse or by a pulse of heavy charged particles. The advantage of producing the atoms in this way is that in the presence of a buffer gas the atoms will remain for about 10^{-3} sec in a region very near their original

TABLE III. Summary of results for helium.[a]

n	Excitation wavelength Å	Lifetime μ sec	Oscillator strength for He 2^3S-n^3P transition	*Triplet system* Present experiment	Cross section-cm^2 quantum defect calculation	Close coupling calculation length approx[2]	Close coupling calculation velocity approx[2]
3	3888.6	0.105	6.7×10^{-2}	8.7 ± 2.0 10^{-18}	7.9×10^{-18}	7.5×10^{-18}	
4	3187.7	0.198	2.3×10^{-2}	2.1 ± 0.4 10^{-18}	2.1×10^{-18}	1.8×10^{-18}	2.1×10^{-18}
5	2945.1	0.341	1.14×10^{-2}	8.6 ± 1.8 10^{-19}	8.8×10^{-19}		
n	Excitation wavelength Å	Lifetime nsec	Oscillator strength for He 2^1S-n^1P transition	*Singlet system* Present experiment	Cross section-cm^2 quantum defect calculation	Close coupling calculation length approx[2]	Close coupling calculation velocity approx[2]
3	5015.6	1.6	1.5×10^{-1}	1.0 ± 0.2 10^{-17}	1.1×10^{-17}		
4	3964.7	4.1	5.07×10^{-2}	2.2 ± 0.4 10^{-18}	2.4×10^{-18}	2.4×10^{-18}	2.5×10^{-18}
5	3613.6	7.8	2.21×10^{-2}	8.8 ± 1.8 10^{-19}	9.7×10^{-19}		

[a] This table is from Stebbings, Dunning, and Rundel (1974).

position and there will be none of the selected atoms elsewhere. Further, this technique enables one to use a nonreactive compound as a source of reactive atoms so that concentration is relatively insensitive to small concentrations of impurities up until the time the atoms are desired. With this method it is easy to reproduce the generation of 10^5 to 10^8 atoms along a line.

With reactive atoms, such as the alkali metals, it is difficult to obtain 10^5 to 10^8 atoms/cm^3 in a reproducible way by working with the vapor of the element. The density is too low for the system to be self-cleaning, with the result that the actual density varies in a complicated way with position and is extremely sensitive to small concentrations of impurities. If the cell is heated to a higher temperature, the vapor concentration eventually becomes high enough to react with all impurity molecules and a clean system results. However, the density is now high enough so that saturated ionization leads to extremely large space-charge effects (space-charge effects become important for plasma density $> 10^8$/cm^3).

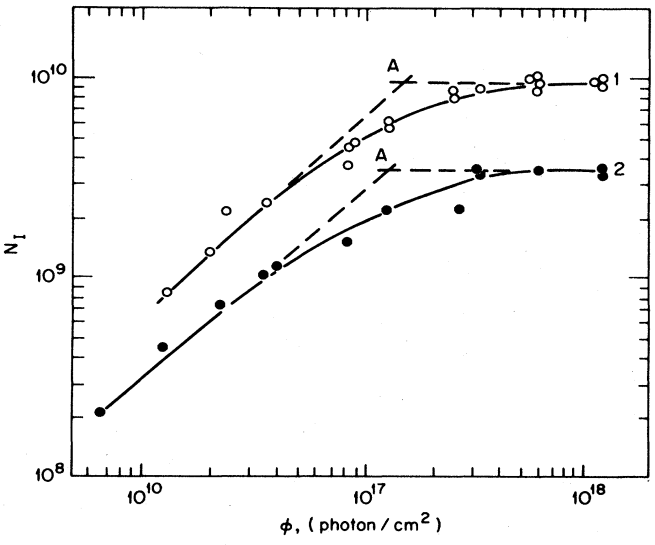

FIG. 38. Saturation curve obtained by Ambartsumyan *et al.* (1976) for the two-step ionization of Rb.

Apart from the practical chemical reactivity question discussed above, the coaxial-beam arrangement has another major advantage—namely, the data are extremely simple to interpret. This simplicity is due to the fact that all atoms see the same peak power density; while in a situation where the atoms are everywhere, some atoms see high peak power and others low, so that the shape of the saturation curve depends on the detailed radial intensity distribution of the laser beam.

C. New methods for measuring photoionization cross sections

As an example, suppose that one wants to measure the photoionization cross section for the $7P_{1/2}$ level of Cs. The chamber is filled with 20 Torr of Ar in the presence of a CsI sample heated to ~700 K. A laser pulse at about 3200 Å is reduced to a beam radius of 0.01 cm and produces ~10^7/cm^{3}Cs atoms at $t = 0$. After a delay time of a few microseconds, the RIS scheme Cs$[\omega_1, \omega e^-]$Cs$^+$ is used to ionize Cs. The laser at ω_1 has $\lambda \simeq 4593$ Å, $I \simeq 10^6$ W/cm^2, and $\Delta\lambda_L \simeq 0.01$ Å and is plane polarized, while the laser at ω has $I > 10^7$ W/cm^2, $\Delta\lambda_L < 1$ Å, and its wavelength is to be varied from ionization threshold to well into the ionization continuum. Both of the detector lasers have beam radii ≈ 0.5 cm and are concentric with the line of atoms. The following rate equations describe the process:

$$\begin{aligned} dN_0/dt &= -\bar{\sigma}\,\mathcal{F}_1(N_0 - N_1)\,, \\ dN_1/dt &= \bar{\sigma}\,\mathcal{F}_1(N_0 - N_1) - \sigma_I(\omega)\mathcal{F}(\omega)N_1\,, \\ dN_I/dt &= \sigma_I(\omega)\mathcal{F}(\omega)N_1\,, \end{aligned} \tag{6.1}$$

where $\bar{\sigma}$ is the mean cross section for absorption or stimulated emission, $\mathcal{F}_1$ is the photon flux for the laser at ω_1, $\sigma_I(\omega)$ is the photoionization cross section for the $7P_{1/2}$ level at frequency ω, N_0 is the population of the $6S_{1/2}$ level, $\mathcal{F}(\omega)$ is the photon flux for the laser with frequency ω, N_1 is the population of the $7P_{1/2}$ level, and N_I is the number of ions. One has $\bar{\sigma}\,\mathcal{F} \simeq 10^{10}$/sec, which is typically much larger than $\sigma_I(\omega)\mathcal{F}(\omega)$. Neglecting $\sigma_I(\omega)\mathcal{F}(\omega)$ at early times and solving for N_0 and N_1, one finds that in a time ~10^{-10} sec, $N_0 \simeq N_1$. Thus for most of the pulse time the two populations stay in equilibri-

um. Let $N_T = N_0 + N_1$; thus, except very early in the pulse, $N_T = 2N_1$. By adding the equations, one obtains

$$dN_T/dt = -\sigma_I(\omega)\mathcal{F}(\omega)N_1 ,$$

or

$$dN_1/dt = -\tfrac{1}{2}\sigma_I(\omega)\mathcal{F}(\omega)N_1 .$$

Thus,

$$N_I = \int_{-\infty}^{\infty} \sigma_I(\omega)\mathcal{F}(\omega)dt \frac{N_0(0)}{2} \exp\left(-\frac{1}{2}\int_{-\infty}^{t} \sigma_I(\omega)\mathcal{F}(\omega)dt'\right) ,$$

$$= N_0\left[1 - \exp\left(-\frac{1}{2}\int_{-\infty}^{\infty} \sigma_I(\omega)\mathcal{F}(\omega)dt\right)\right] ,$$

$$= N_0[1 - \exp(-\tfrac{1}{2}\sigma_I(\omega)\phi(\omega))] , \qquad (6.2)$$

where $\phi(\omega)$ is the fluence due to the ionizing laser as seen by an atom at beam center. The fluence on the axis of the beam can be monitored by defining the beam with an aperture of known radius and using a beam splitter and photodiode to monitor the transmitted signal for each pulse. These signals are calibrated by using a joule meter on a known number of the transmitted pulses and correlating with the mean of the same number of photodiode signals.

The data analysis is easy if $\sigma_I(\omega)\phi(\omega) \gg 1$ at some value of $\phi(\omega)$, since $N_I = N_0(0)$. The ionization does not have to be saturated for all ω; in fact, when $\sigma_I(\omega)\phi(\omega) \ll 1$, a graph of N_I vs $\phi(\omega)$ is a straight line with slope $N_0\sigma_I(\omega)/2$.

By using three dye lasers one could study the ionization of excited S and D levels of Cs (or any other alkali). However, in this case the photoionization cross section of the intermediate P level must be measured in detail. In cases where excited levels are involved with $J > \frac{1}{2}$, the dependence on the pressure of the buffer gas enables one to determine not only the photoionization cross sections but also the rate of collisional mixing of the magnetic substates.

D. Method for measurement of far wing line broadening

The concept is again illustrated by considering a specific example. Generalizations on the concepts of such experiments are obvious. Suppose we want to determine the cross section for absorption on the red wing of the 4593 Å line of Cs. The same laser system and configuration are used as described in determining photoionization cross sections for excited states. In this study the laser at ω_1 will be tuned away from line center and the laser at ω will be tuned to a wavelength where $\sigma_I(\omega)\mathcal{F}(\omega) \gg 1$ can be achieved. The rate equations for the process are

$$\begin{aligned} dN_0/dt &= -\sigma(\omega_1)\mathcal{F}(\omega_1)(N_0 - N_1) , \\ dN_1/dt &= \sigma(\omega_1)\mathcal{F}(\omega_1)(N_0 - N_1) - \sigma_I(\omega)\mathcal{F}(\omega)N_1 , \\ dN_I/dt &= \sigma_I(\omega)\mathcal{F}(\omega)N_1 , \end{aligned} \qquad (6.3)$$

where the laser has been assumed to be sufficiently monochromatic so that the cross section, $\sigma(\omega_1)$, is nearly constant for all photons in the pulse and ω is assumed to be very far from line center. Above, $\mathcal{F}(\omega_1)$ is the photon flux due to the laser tuned to the line wing and $\mathcal{F}(\omega)$ is the photon flux of the ionizing laser. Equation (6.3) is appropriate to relatively low pressures where collisional mixing of the fine-structure levels can be neglected. Also, absorption by other levels (such as $7P_{3/2}$) has been neglected but is not valid on the far wing.

The laser does not have to be tuned very far onto the wing before $\sigma_I(\omega)\mathcal{F}(\omega) \gg \sigma(\omega_1)\mathcal{F}(\omega_1)$; therefore,

$$N_I = N_0\{1 - \exp[-\sigma(\omega_1)\phi(\omega_1)]\} , \qquad (6.4)$$

where N_0 is determined by doing saturated ionization at line center. Thus $\sigma(\omega_1) = -[\ln(1 - N_I/N_0)]/\phi(\omega_1)$. The cross section of interest, $\sigma(\omega_1)$, is best determined by plotting $-\ln[1 - N_I/N_0]$ vs $\phi(\omega_1)$ for each ω in question. The slope of the resulting straight line is $\sigma(\omega_1)$. This technique is extremely sensitive since every excited atom gets ionized and $\sigma(\omega_1)$ can be made quite large. In a less refined version of this method (Nayfeh *et al.*, 1977) absorption was easily studied 100 Å from line center. This high sensitivity permits absolute measurements to be made on the very far wing even at rather low pressures.

Obviously, higher excited states which do not have dipole-allowed transitions to the ground state can also be studied by using a laser to saturate a transition between the ground state and a state which is optically connected to the state of interest. A second laser is tuned to the wing of the transition between the saturated excited state (having population $N_0/2$ at early times) and the state of interest. If the state of interest lies higher than the other populated excited state, it can be selectively ionized with $\sigma_I(\omega)\mathcal{F}(\omega) \gg 1$, yielding

$$N_I = N_0\{1 - \exp\{-[\sigma(\omega_1)/2]\phi(\omega_1)\}\} , \qquad (6.5)$$

where $\sigma(\omega_1)$ is the absorption cross section for the off-resonance transition.

Again, the localization of the atoms along a line, together with the use of more than one laser having a short pulse length, results in a high degree of simplicity in the data analysis. To appreciate this, one need only compare the present concept with our earlier study where cascading and nonuniformity of the laser intensity had to be accounted for in detail (Nayfeh *et al.*, 1977).

E. Studies of quenching phenomena

The selected atoms are again produced along a line at $t = 0$ by dissociating molecules with the narrow beam of a pulsed laser. However, in this case a laser with only slightly more power than is required to saturate a discrete-discrete transition is fired almost immediately after dissociation. After this laser pulse, $N_0/2$ ground-state atoms and $N_0/2$ excited atoms are located along the line. Obviously, RIS can be used to selectively ionize any excited state after various delay times. This is a situation where a single state is initially excited with a known population and all excited states can be monitored on an absolute basis as a function of time after excitation. A total rate of destruction of the initial excited state can be measured, as can the subsequent population of other states. Quenching and collisional redistribution processes can be studied in de-

tail over a wide range of partial pressures and temperatures.

F. Studies of imprisonment of resonance radiation

When an atomic gas or vapor is present at concentration $\gtrsim 10^{14}/cm^3$, photons emitted in transition to the ground state are absorbed resonantly by other ground-state atoms. At concentrations $>10^{15}/cm^3$ and with system dimensions >1 cm, a single excited atom may emit a photon which will be absorbed and re-emitted hundreds (or even thousands) of times before it reaches a wall of the container. This phenomenon is usually referred to as radiation trapping or resonance radiation imprisonment. One of the practical consequences of radiation trapping is that atomic states with very short natural lifetimes may, at some gas pressure, have population lifetimes a thousand times longer. Thus, like other long-lived excited-state populations, resonant states play an important role in kinetic studies of excited-state populations. Up to the present time almost all studies of radiation trapping have been based on observing the escape of trapped radiation through a window in the cell or on observing fluorescence from a short-lived population which was excited by discrete-discrete energy transfer from the resonance-state population (Payne *et al.*, 1974).

The theory of radiation trapping (Holstein, 1947; Holstein, 1951; Biberman, 1949; Payne and Cook, 1970; Payne *et al.*, 1974) predicts not only the rate of escape of radiation to the walls but also the detailed distribution of excited atoms in space as a function of the time after excitation. A description of how the spatial distribution can be measured as a function of time is now given. Again, the trick is to produce a line of the species to be detected at $t = 0$. If, for example, one wants to study the 1048-Å resonance radiation in Ar, a line of excited Ar atoms can be produced by a short pulse of heavy charged particles. Once the line of excited atoms is made at $t = 0$, the spatial distribution of resonance atoms is measured by firing the detecting lasers parallel and at a distance ρ from the initial line after various delay times. In this way, one measures $N(\rho, t)$, the number of excited atoms per unit volume at ρ at a time t following the generation of λ excited atoms per unit length at $\rho = 0$ and $t = 0$. The situation appears similar to the diffusion studies described in Sec. V; however, the transport process being studied here can never be described as a diffusion process.

VII. MODERN APPLICATIONS

A. One-atom detection in fission tracks

Many modern applications of one-atom detection require both time and spatial resolution of a single atom of a specified type. The most general demonstration of one-atom detection is a digital experiment in which a signal is generated if and only if a single atom is in a specified volume at a specified time. These requirements are necessary if a certain class of "rare-event" experiments is to be undertaken.

To demonstrate the detection of a single atom that is in a volume v during a time interval $\Delta\tau$, it is first necessary to develop a method for producing a single atom at a known location in space and time. One technique which has been used (Kramer *et al.*, 1978) depends on the spontaneous fission of ^{252}Cf. It is well known that this isotope undergoes binary asymmetric fission. This means that in the fission process the nucleus splits into two fragments of unequal masses (and unequal energies) and that these particles will recoil in exactly opposite directions. The kinetic energy and mass distributions of the two fragments are the well known double-peaked functions.

The ^{252}Cf nuclei were ion-implanted in a thin Ni foil. The foil was mounted in front of an apertured surface-barrier detector which sensed a fission fragment to signal that the complementary fragment had been injected into the sample chamber. About one fission fragment per second was emitted through the aperture. By performing energy discrimination on the complementary fragment in the surface-barrier detector and by using a recent parametrization (Erten and Aras, 1978) of the nuclear charge distribution in fission, it was estimated that 15% of the time when the surface-barrier detector senses the fragment of highest energy a Cs fission fragment will be injected into the sampling region. Since the complementary fragments are created simultaneously, the surface-barrier detector signal serves to indicate that a fragment is recoiling in the direction of the laser beam; with pulse-height selection, the surface-barrier detector signal can indicate that a heavy or a light fragment is directed toward the laser beam.

The heavy fragment was stopped at a known position in 317 Torr of P-10 gas (90% Ar, 10% CH_4). At this pressure, 65% of the signaled heavy-mass fragments stopped in the laser probe volume of about 1 cm^3. Direct ionization of the buffer gas due to the dissipation of the fission fragment energy (about 50 MeV in the gas) resulted in the production of more than 10^6 free electrons in the ionization track. All of these electrons had to be cleared before the laser could be fired at the single atom. This criterion dictated the experimental design shown in Fig. 39 in which the fission fragment is stopped in a region between two plates that are physically separated from the proportional counter. With the collector plate held at a positive potential with respect to a parallel field plate, electrons produced in the fission track are swept onto a collector plate and away from the proportional counter. It was necessary to allow 40 μsec for collecting all the free electrons. Grossman *et al.* (1977a) showed that in this time scale neither diffusion nor chemical reactions will remove Cs from the probe volume. At a time of 40 μsec following a fission event and 10 μsec prior to probing the chamber with the laser, the collector plate was pulsed negative with respect to the field plate. Single electrons created by photoionization of a single atom drifted through an aperture in the field plate and into the proportional counter where they were detected.

The wavelength of the laser could be tuned to ionize selectively the neutralized fission fragment of interest. In the case of Cs, the laser was tuned to either 4555 Å or 4593 Å in order to excite either the $7P_{3/2}$ or the

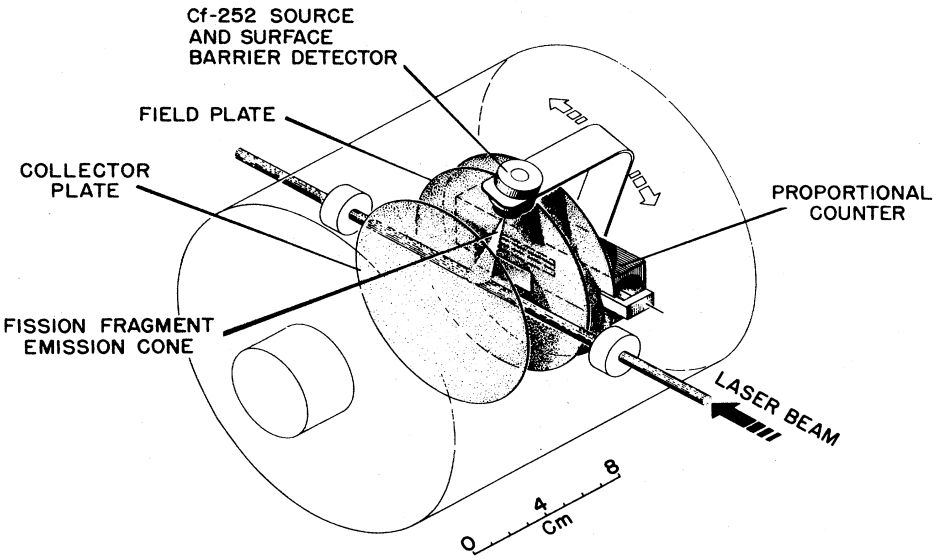

FIG. 39. Schematic of apparatus used to detect a single atom formed in spontaneous fission. A signal generated in the surface-barrier detector indicates the occurrence of a single fission of ^{252}Cf. After the initial ionization has been swept onto the collector plate, a tunable laser pulse is used to photoionize the selected single atom. The liberated photoelectron then drifts into a proportional counter and is detected as a single event.

$7P_{1/2}$ level, respectively, in the scheme $Cs[\omega_1, \omega_1 e^-]Cs^+$. With a laser linewidth of only 4 Å (which was somewhat greater than the pressure-broadened Cs lines at 317 Torr) with a fluence of 0.3 J/cm^2, saturation was easily achieved (Grossman *et al.*, 1977b). Therefore one free photoelectron was created each time a Cs atom was injected into the laser beam.

Pulse-height discrimination of the proportional counter signal was required to eliminate electrical transients associated with the laser. At the discrimination level used, only 80% of the pulses due to single-electron events could be counted. Combining this counting fraction with the 65% geometrical factor described above, the expected Cs resonant signal is about 7% of N_1, where N_1 is the number of triggered fission fragments observed in the surface-barrier detector.

In order to establish a tuning curve for the expected Cs RIS effect, eight wavelengths in the interval 4500 Å to 4620 Å were studied. The results, after correcting for a wavelength-dependent background, are shown in Fig. 40. Both neutral Cs resonant line peaks at 4555 Å and 4593 Å stand out dramatically at a level exceeding two standard deviations above the background. At these two peaks, the average net effect is (8.5± 2.2)%, which compares with the 7% effect expected if all the Cs ions are neutralized. Since we detected neutral Cs atoms directly, the results show quite conclusively that an appreciable fraction, if not all, of the Cs fragments thermalize as neutral atoms in P-10 gas.

This evidence for complete neutralization deserves some comment. Since the neutral detection technique had not been available prior to this work, we can make no direct comparisons with other experimental observations. Extensive studies (Bohr, 1941; Betz, 1972) have been carried out on the charge state of energetic ions, and the tendency for them to become neutral as they are reduced to low energy has been noted. However, when an ion is completely stopped (thermalized) in a gas, its final charge state is uncertain because the studies have not been extended below 1 keV. But it was shown with a method in which the neutral atom is detected directly that the positive ion of Cs born from the spontaneous fission decay of ^{252}Cf forms, with high probability, a neutral Cs atom when the ion is thermalized in P-10 gas. In this case the ionization potential of the projectile, Cs, is less than that of the buffer gas constituents, Ar and CH_4.

Kramer *et al.* (1978) proposed a new model to explain the observation of a high neutral yield for this case where the ionization potential of the neutralized particle is much less than that of the buffer gas. As an energetic positive ion loses its energy in a gas, its charge state is governed by dynamical processes involving primarily electron capture and electron loss since recombination of Cs^+ with free electrons is negligible. At high energies, where the particle makes many collisions before losing a significant fraction of its energy, a rate equation formulation based on electron capture

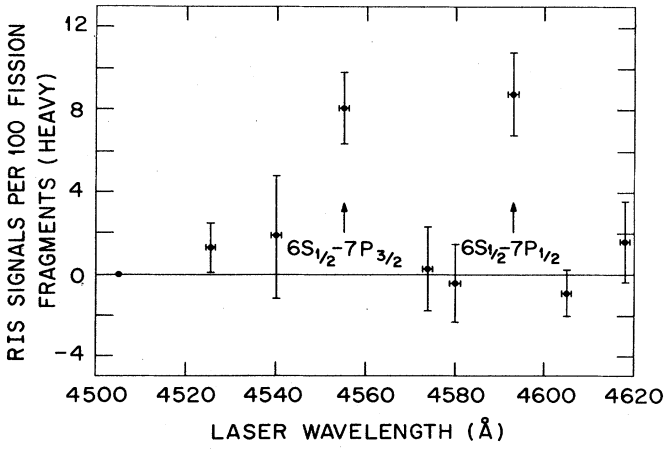

FIG. 40. Summary of results obtained by Kramer *et al.* (1978). The data points at the indicated wavelengths represent the number of photoelectron events per 100 heavy-mass fission fragments. The data points at wavelengths of 4555 Å and 4593 Å show clearly a Cs resonant ionization effect at the known $7P$ resonant levels indicated by the arrows.

and loss cross sections $\sigma_c(E)$ and $\sigma_l(E)$, respectively, is valid for determining the average charge state. For the simple case where the particle can only be in a 0 or +1 charge state, the fraction of neutrals at energy E is $f_N(E)=\sigma_c(E)/[\sigma_c(E)+\sigma_l(E)]$. If the quasiequilibrium solution to the rate equations held at all energies, it would not be possible to account for Cs due to Cs^+ thermalization in Ar or CH_4 for the following reason. Since, as shown in Fig. 41, conservation of energy requires $\sigma_c=0$ for $E<E_2$ while $\sigma_l>0$ for $E>E_1$, there is a narrow range of particle energy, $E_1<E<E_2$, where conservation of energy requires that $\sigma_c=0$, while σ_l can be finite. The quasiequilibrium approximation for a solution to the rate equations predicts $f_N=0$ for all particles that pass through the gap.

However, for E less than about 100 eV, only a few collisions are required for a particle to lose a large fraction of its energy; thus the quasiequilibrium approximation is no longer valid. In fact, if the cross section for total energy loss $\sigma_T(E)\gg\sigma_l(E)$, it is likely that the particle will cross the ionization gap without charge exchange. We note, in particular, that when a neutral particle at energy $E\geq E_2$ suffers a charge-conserving collision that reduces E below E_1, it must thermalize as a neutral; that is, the ionization gap is crossed and the charge state has been fixed. In the "charge fixation model" the final charge state at thermal energy is then determined by $\sigma_c(E)$ and $\sigma_l(E)$ at E *above* the gap.

For the case of identical atoms (symmetric charge transfer), it is generally believed (Rapp and Francis, 1962) that $\sigma_c(E)$ becomes larger than $\sigma_l(E)$ for energies just above the ionization gap; thus we expect a large neutral fraction at thermal energies. In the case of unlike projectile and target (the asymmetric case), the behavior of $\sigma_c(E)$ and $\sigma_l(E)$ is more complex. Even here (Rapp and Francis, 1962), however, an accidental energy degeneracy between the projectile in a +1 charge state and an electronically excited state of the target gas can lead to a large $\sigma_c(E)$ compared to $\sigma_l(E)$ at low energies. A near degeneracy of this type in the case of Cs^+ moving through Ar does exist with an electronically excited state in Ar, and quite likely with many possible levels in the electronic–vibrational quasicontinuum in CH_4. In view of the mechanism reported here, it should be possible to choose an appropriate buffer gas to ensure a high probability of ion neutralization; thus one-atom detection is possible for particles initially produced as energetic ions.

Direct extensions of the above technique in a number of directions is possible. For example, simply by using lasers at other appropriate wavelengths the ionization tracks due to $^{252}_{98}$Cf fission could be scanned for other neutral species. It is even conceivable that fission sources could provide atoms which are otherwise difficult to produce in the gas phase, so that chemical reactions of these atoms with other species could be studied at room temperature. Recently other possible applications of the technique in which single atoms are detected in dense ionization tracks were pointed out at a track structure conference (Hurst *et al.*, 1978c). These include the detection of single negative ions and the production of single excited atoms due to the absorption of nearly 80 MeV of energy in an individual ionization track.

B. Detection of single daughter atoms

The fission daughter atom experiment is an example of a more general possibility—the detection of daughter atoms in time coincidence with the decay of radioactive parent atoms. Alpha particles, beta rays, positrons, gamma rays, and fission recoils can all be used as a signal that a daughter atom has been created. The applications of such a capability are many; a few examples are listed to show the variety:

(1) Exotic light nuclei (Cerny and Poskanzer, 1978) and other unstable nuclei created by accelerated particles could be identified.

(2) The chemical reaction of heavy elements could be studied at room temperature even though their vapor pressure is very low.

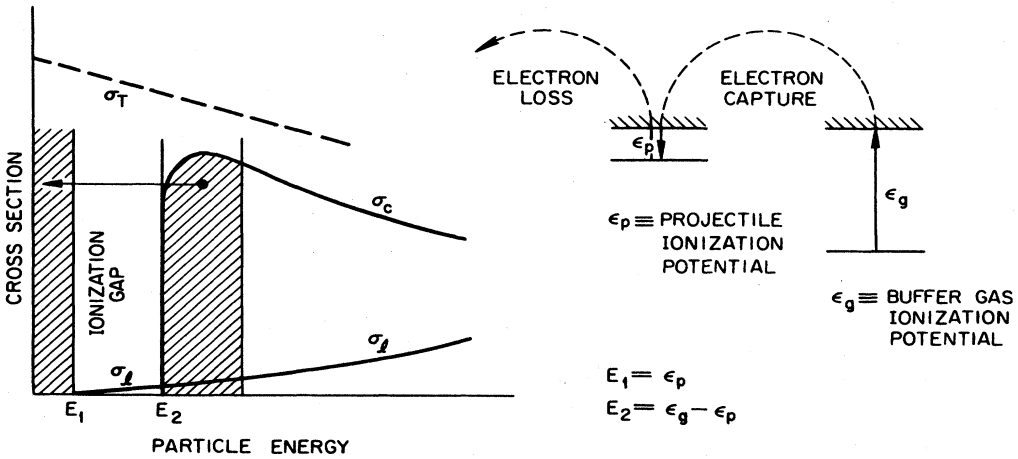

FIG. 41. Schematic of the charge fixation model. Electron loss, but not capture, is energetically possible in the ionization gap. However, if $\sigma_T\gg\sigma_l$, electron loss is unlikely in the gap; thus a neutral particle passes through the gap without electron loss. (σ_c, σ_l, and σ_T are cross sections for electron capture, electron loss, and total energy loss, respectively.)

(3) The detection of lower concentrations of isotopes such as ^{39}Ar would provide better information on environmental transport processes occurring in the atmosphere, the oceans, and the soil (Geiss, Oeschger, and Schwarz, 1963).

(4) The determination of the flux of solar neutrinos on the earth could be improved by making available a wider range of neutrino detectors (Bahcall, 1978).

(5) Cosmochronology would benefit from the ability to detect lower concentrations of certain radionuclides (Kirsten, 1978).

This abbreviated list already includes a variety of disciplines: nuclear physics, chemistry, environmental research, and solar research. In this subsection we point out some general considerations which are common to all of these areas, while the next subsection discusses the solar neutrino application in much greater detail. Essentially, the basic idea is that the detection of a daughter atom in time coincidence with the decay of the parent makes it possible to reduce backgrounds by orders of magnitude, opening up the possibility of analyses at extremely low levels. For a more extensive review of the applications of low-level counting, see Oeschger and Wahlen (1975).

The common considerations are as follows:

(1) A laser scheme is needed for each daughter atom; see the Periodic Table in Sec. II.

(2) A signal that the parent has decayed is needed.

(3) In many cases the daughter product is a positive ion that must be neutralized to create a free atom.

The last two requirements depend critically on the type of decay—whether α, β^-, β^+, EC, γ, or spontaneous fission. For all of the decay modes, except γ, a charged particle is emitted and can be detected with nearly unit efficiency in a proportional counter. Therefore it is expedient to have an arrangement in which the daughter atom is stopped in a counting gas which can be swept with a laser pulse after some short delay time, as in Fig. 42. Thus we require that the initial signal corresponding to the decay of a single parent be in delayed coincidence with the electron removed from the daughter atom in the selective RIS process. In the case of α decay the radiation signature could already be reasonably good, while in the case of β^- and β^+ it would be poorer. This difference is, of course, due to the fact that α decay is characterized by a distinct energy, while there is a wide possible energy range for the charged particles in β^- and β^+ decay. However, if the daughter atom is required to be a given type, these radiation signatures are of little significance except as a starting signal.

Electron capture, EC, offers several interesting possibilities. In some cases good characteristic radiation signatures are available through x rays or Auger electrons, while in other cases only very low-energy Auger electrons are emitted. With EC it should be generally possible to require spatial (as well as time) coincidence, since the range of the low-energy Auger electrons is very short; thus the initiating electrons and the final

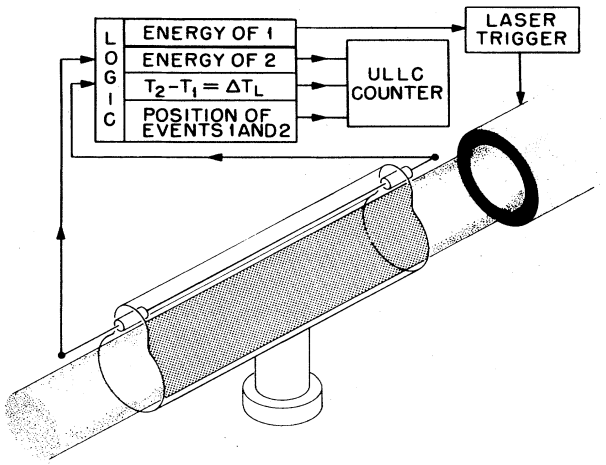

FIG. 42. Proportional counter designed for RIS detection of single daughter atoms. Displaced wire permits sweeping of a large fraction of the counter volume with a laser beam. R. E. Zedler, ORNL Instrumentation and Controls Division, designed and tested the proportional counter. Ray Davis, Jr. of Brookhaven National Laboratory contributed to the design of the counter for its use in solar neutrino detection.

RIS electron are created at the same place in the detector. Position determination can be done rather simply by using a one-dimensional, position-sensitive proportional counter (Borkowski and Kopp, 1968) which has a resolution of about 1 mm. More elaborate position-sensitive proportional counters and drift chambers have been reviewed in a recent article (Charpak, 1978).

The charge state of the daughter product also depends critically on the type of decay process. For α decay the recoil ion may have enough energy to ensure neutralization via the charge fixation model discussed above, even if the ion has an ionization potential less than those of the counting gas constituents. However, for β^- or EC the positive ion could have only a few electron volts of energy and may not be automatically neutralized in the counting gas. In these cases, neutralization via charge exchange from some suitable donor will be necessary. The simplest approach is to add a gas species M which has an ionization potential IP less than that of the daughter atom A i.e.,

$$A^+ + M \rightarrow A^0 + M^+ .$$

Some of the lowest IP's known are for tetrakis-(dimethylamino)-ethylene, and 1, 1′, 3, 3′-tetramethyl-$\Delta^{2,2'}$-bi(imidazolidine). These all have adiabatic ionization potentials of about 5.4 eV (Nakato *et al.*, 1971). With one of these the above process would neutralize every daughter atom except Li, Na, K, Rb, Cs, Fr, Ra, and Ac. However, these are important exceptions. In addition, as discussed in Sec. III, the addition of low-ionization molecules to the sample could adversely affect the signal background. A possible neutralization method which avoids this difficulty is the scheme

$$A^+ + M + B \rightarrow (AM)^+ + B ,$$

$$h\nu + (AM)^+ \rightarrow A + M^+ .$$

In this method an ion molecule is formed by a three-body process where B is a buffer gas atom. The complex (AM^+) is then photodissociated with a suitable laser pulse. Candidates for M will depend on the particular choice of A and the laser available. For the case of Cs and letting $\lambda = 4000$ Å, M can have an ionization potential of up to 7 eV. The rate of the clustering process of 10^{-30} cm^6 sec^{-1} is typical. Thus, with 300 Torr of Ar and 3 Torr of M, the ion molecule association occurs in about 10^{-6} sec.

The effort to achieve charge neutralization of daughter ions led to the concept of resonance ionization spectroscopy with amplification (RISA) (Hurst et al., 1979b). Amplification of the ionization signal could come about due to repeated electron transfer occurring in various collisional processes (as illustrated above). Thus RISA offers the advantage of signal gain along with the sought for charge neutralization. Viewed in another way, RISA cycles can be started equally well in the ionization continuum or the ground state of an atom.

It will often be necessary to incorporate the parent nucleus into a compound (e.g., when the parent is chemically very reactive or when it has a very low vapor pressure). In the previous discussion it was assumed that upon decay a daughter atom or ion would be separated completely from the carrier molecule. Some general rules can be used to evaluate the chance that neutrals are ejected in nuclear decay processes (Snell, 1965; Wexler, 1965). Those nuclear processes which result in large recoil energies, such as often occur in alpha decay, will produce free daughter neutrals. In addition, those events which cause deep electron vacancy formation and extensive electron cascading and Auger electron emission, such as internal conversion and electron capture, will virtually always produce a free daughter atom or ion. For example, in studies of $CH_3{}^{125}I$ and $C_2H_5{}^{125}I$, where ^{125}I undergoes electron capture to give ^{125}Te, it was found (Carlson and White, 1963) that the ^{125}Te remained bound to the carrier molecule in only 1% of the decays. Similarly, in the internal conversion of ^{80m}Br incorporated in gaseous HBr (Luebbe and Willard, 1958), CH_3Br (Hamill and Young, 1952), and C_2H_5Br and CCl_3Br (Gordus and Willard, 1957), molecular disruption occurred in no less than 93% of the decays.

In contrast, those decay mechanisms such as gamma-ray emission which do not affect the electronic shells will, in the absence of sufficient recoil energy, leave the molecule intact. The case of β^- and β^+ decay is somewhat more complicated. Although these decays also do not to first order affect the number of binding electrons, they do result in a change of nuclear charge between the parent and daughter nuclei. A change of Z can free the daughter nucleus, but is not a necessary consequence. For example, the parent and daughter nuclei may be chemically similar and bond breakage fail to occur; hence a molecular ion is formed. This mechanism has been seen (Edwards and Coryell, 1948) in ^{144}Ce-acetylacetonate, where ^{144}Ce undergoes β^- decay to ^{144}Pr. In a more subtle mechanism the carrier molecule may dissociate, but the daughter molecule may remain bound to one of the molecular fragments. In some cases the molecule may remain bound even if the chemical properties of the parent and daughter are quite different. For example, it was found (Wolfgang, Anderson, and Dodson, 1956) that in 47% of the β^- decays of ^{14}C to ^{14}N in $^{14}CH_3CH_3$ the final product of CH_3NH_2 was formed.

C. Solar neutrino measurements

Although electron capture processes have already been discussed as a time-resolved source of atoms for one-atom detection, there is one application which deserves special mention—the detection of atoms produced by neutrino interactions. Neutrinos are the only particles that are able to escape from the center of the sun where thermonuclear processes occur. They thus serve as the only direct means of testing the standard theory (Bahcall and Sears, 1972) of solar fusion processes.

Recent measurements (Davis and Evans, 1973) of the neutrino flux indicate that it is less than one-third of that expected from standard models. This discrepancy can apparently only be resolved by rather drastic changes in the solar model or in weak-interaction theory (Bahcall, 1978). Due to the large discrepancy between the only available measurements and theory, it is highly desirable to perform other experiments.

Neutrino experiments are difficult due to the fact that typically 10 000 kg of matter are needed to generate one neutrino event per day. For example, in the only experiment done to date (Davis and Evans, 1973), which depended on the reaction $\nu + {}^{37}Cl \rightarrow {}^{37}Ar + e^-$, only about 50 ^{37}Ar atoms were created in 400 000 liters of C_2Cl_4 after an exposure of several months. The ^{37}Ar was detected by counting the 2.8-keV Auger electrons produced in the inverse electron capture reaction in a shielded proportional counter. It was found necessary, in order to discriminate against background counts, to monitor both the peak height and the rise time of the counter pulses (Bahcall and Davis, 1976; Rowley *et al.*, 1977).

Two new radiochemical neutrino detection schemes have been proposed. One (Bahcall *et al.*, 1978) makes use of the reaction $\nu + {}^{71}Ga \rightarrow e^- + {}^{71}Ge$, while the other (Bahcall, 1969) uses $\nu \rightarrow {}^{7}Li \rightarrow e^- + {}^{7}Be$. Both the ^{71}Ge and ^{7}Be then decay back by electron capture to ^{71}Ga and ^{7}Li, respectively, causing the emission of an Auger electron. Figures 43 and 44 show the decay schemes in more detail. It is important to note that the Auger electron in the ^{7}Li example has only 50 eV of energy. This low energy makes the pulse-height analysis technique that was used in the ^{37}Ar experiment inadequate to differentiate between an actual ^{7}Be decay and background pulses. Furthermore, even though the ^{71}Ge decay yields Auger electrons of higher energy, it would be extremely useful to have a way of testing for an actual ^{71}Ge decay that did not depend on pulse-height analysis. The one-atom detection scheme can provide this additional test. As shown in Figs. 45 and 46, there exist several possible energy level sequences which could be used to saturate the photoionization process in ^{7}Li and ^{71}Ga. A particularly advantageous sequence for ^{7}Li is shown in Fig. 45(b). Besides using wavelengths which can be easily generated, the cross sections for the

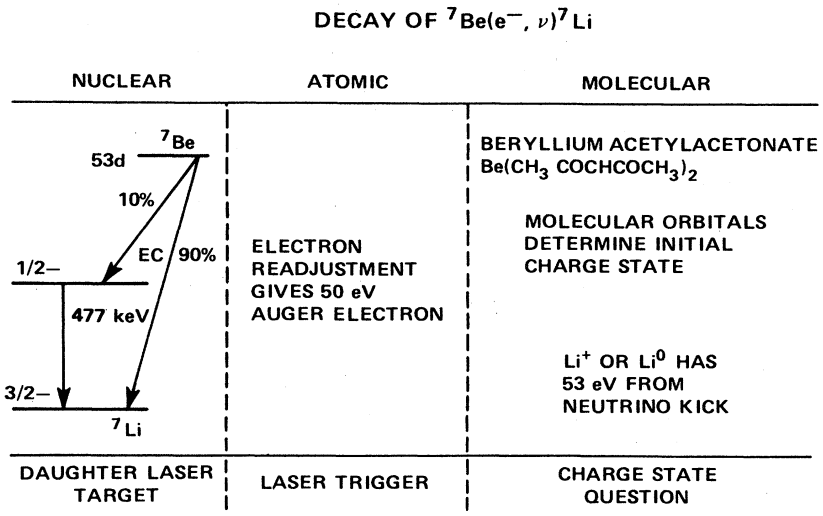

FIG. 43. Decay of $^{7}Be(e^{-}, \nu)^{7}Li$.

discrete-discrete transitions are known to be large, with lifetimes of about 15×10^{-9} sec (Weiss, Smith, and Glennon, 1966), while the final transitions from the $3D$ states to the continuum have been calculated to be about 10^{-17} cm^2 (Gezalov and Ioanova, 1968; Bhatia, Temkin, and Silver, 1975; Manson, 1978). This means that for a laser pulse, fluence of only a few hundred millijoules per cm^2 is necessary for saturation of photoionization. Recent experimental results (Kramer *et al.*, 1978) confirm this estimate. This combination of relatively long wavelengths and low power fluxes will also decrease the possibility of unwanted multiphoton ionization processes in other species present in the sample.

The technique for detecting the ^{7}Be decay is outlined in Fig. 43. Using standard chemical techniques, all of the neutrino-created ^{7}Be (approximately 100 atoms) would be incorporated into the compound beryllium acetylacetonate. This compound, which has a high enough vapor pressure so that the complete sample will be vaporized at 150 °C, will be placed into a heated position-sensitive proportional counter. In the decay process $e^{-} + {}^{7}Be \rightarrow {}^{7}Li + \bar{\nu}$, a 50-eV Auger electron is produced as well as a 53-eV ^{7}Li recoil nucleus. As these particles are brought to rest, they will produce a small amount of ionization which will trigger the proportional counter (see Fig. 42). A few microseconds after the initial pulse, the lasers tuned to the ^{7}Li resonance levels will be fired. If neutral ^{7}Li is indeed present, the electron produced in the photoionization process will trigger the counter. This pulse will be pulse-height analyzed to confirm that it is truly a one-electron event, and its position in the counter will be determined. Within the position resolution of the counter (~0.2 mm), the original Auger electron and the laser-induced photoelectron will be produced at the same position. The large number of checks inherent in a multicoincidence experiment of this type should eliminate essentially all background effects.

The main assumption that is made in this scenario is that the ^{7}Li has become a neutral atom by the time the laser is fired. There is no *a priori* reason to suppose that this is true (Perlman and Miskel, 1953), although

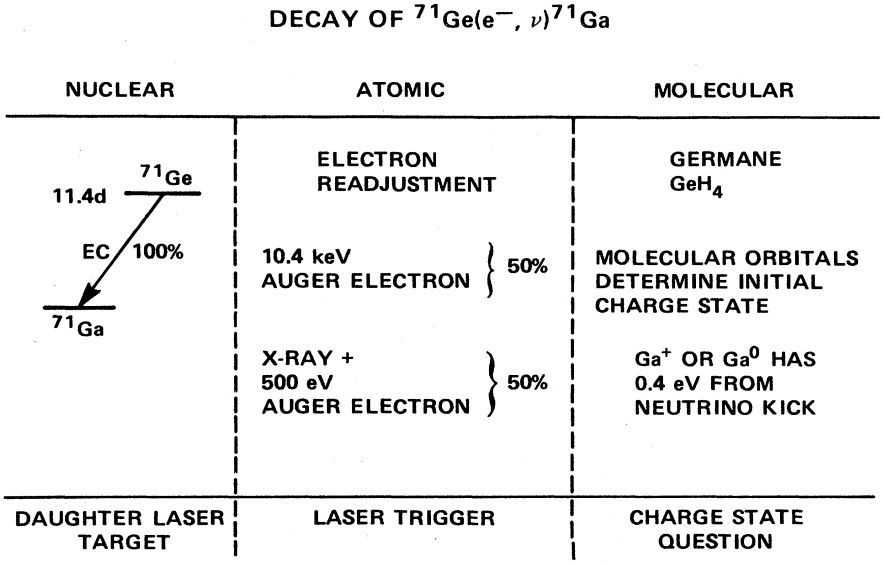

FIG. 44. Decay of $^{71}Ge(e^{-}, \nu)^{71}Ga$.

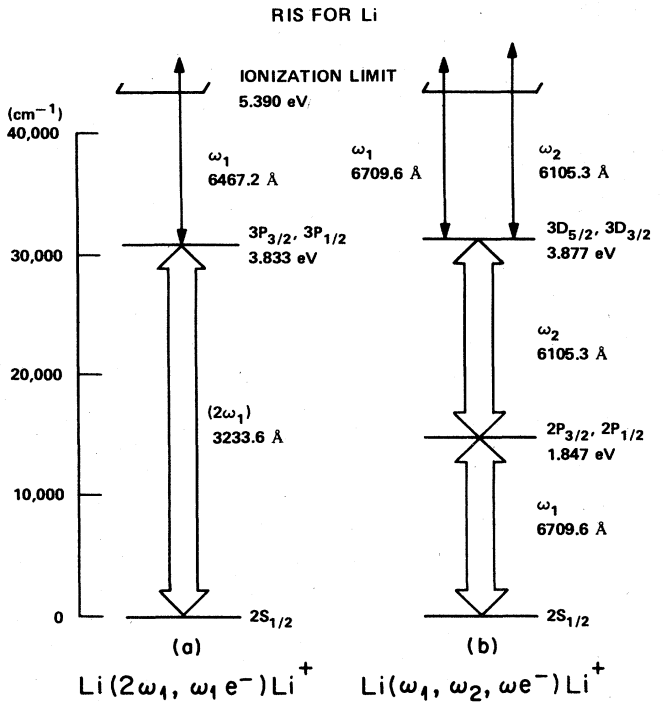

FIG. 45. Resonance ionization spectroscopy for Li.

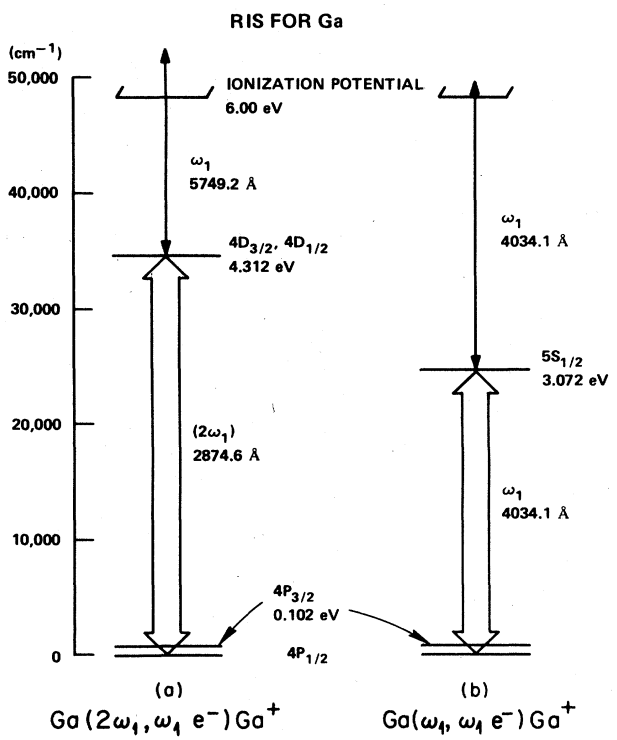

FIG. 46. Resonance ionization spectroscopy for Ga.

the ^{7}Li nucleus has enough energy initially to start above the ionization gap. Lithium has a relatively low ionization potential of 5.39 eV, as does Ga, which has an ionization potential of 6.00 eV. Therefore it should be possible to neutralize Li^+ by a collisional charge transfer between the ion and a neutral species with an ionization below 5.39 eV. As discussed previously, photodissociation of a positive ion cluster might also produce neutral cesium. In any case, the neutralization agent should have a reasonable vapor pressure (~1 Torr) at 150 °C and it should not be electronegative. In addition, it should be stable and nonreactive over the approximately three-month period of the experiment.

D. Detection of exotic atoms

It is not our purpose to speculate on a large number of applications of one-atom detection to the detection of "exotic" atoms, even though they are of considerable interest. Because the spectroscopy of most of the "normal" atoms is known, we know where to tune a laser to look for them. However, the spectroscopy of many kinds of exotic atoms is not known.

Bemis (1977) proposed to use one-atom detection in a search for fission isomers. For example, ^{240}Am has an isomeric state that lives a few milliseconds before its highly distorted nucleus decays by fission. Bemis proposed to produce the nuclear isomer of ^{240}Am by bombardment of a ^{238}U target with pulses of ^{6}Li, so that the accelerator itself furnishes the laser trigger signals. With the Oak Ridge Isochronous Cyclotron, isomers can be created at a rate of about one per minute. To detect the isomer and to distinguish it from ^{240}Am requires tuning the laser wavelength to a perturbed resonance level (i.e., an electronic level that is shifted due to the distorted nucleus).

Another exotic atom to receive attention is the quarked atom. For a review of various efforts to detect quarks, see Jones (1977); and for a recent report of evidence for fractional charge using the levitation method, see LaRue, Fairbank, and Hebard (1977). Fairbank, Hänsch, and Schawlow (1975) proposed a spectroscopic method in which a laser is tuned to a quark-perturbed electronic transition to look at fluorescence from quarked atoms. Obviously, one-atom detection using RIS offers another spectroscopy method. The addition of a quark to the nucleus of an atom can perturb electronic levels appreciably because of the change in the effective nuclear charge seen by the outer electrons. Several methods have been used to calculate the shifted energy levels, but perhaps the simplest is the fitting of spectral lines to isoelectronic series (Skutnik, 1970; Rau, 1978).

The exotic atom is of most recent vintage and is not to be confused with the lone atom, a concept used by Lucretius, ca. 60 B.C. (Winspear, 1956).

> But many wander through unending space
> And have no chance
> To meet and link themselves with other forms,
> Or unify their moves with theirs.
> Of these lone atoms, just as I've said ....

The objective of ultralow-level counting is to find small numbers of perfectly normal atoms. Finding the few lone atoms produced by prolonged exposure of a large sample on earth to solar neutrinos is currently one of the challenges in science.

VIII. CONCLUSION

This paper has reviewed the emergence of a new measurement principle that makes possible a wide range of new experimental studies which include one-atom detection. Thus the process in which a single electron can be removed from each atom of a selected type brings together the selectivity long utilized in spectroscopy with the ultrasensitivity which was developed for the measurement of ionizing radiation soon after its discovery by Roentgen in 1895. Modern laser technology makes it possible to carry out the RIS process in nearly all of the elements; on the other hand, the technology of single-electron and single-ion detection makes it possible to utilize the process in a wide variety of physical configurations.

The practice of measuring just one atom of nearly any selected type while discriminating against the background atoms (whose abundance is many order of magnitude greater) is rapidly emerging. Some of the remaining problems are practical matters such as the availability of reliable lasers to carry out saturated RIS in each case of interest. Other problems are more fundamental and require research for their solution. For example, the use of one-atom detection to detect single daughter atoms in time coincidence with the decay of the parent atom is only possible in those cases where neutral daughters can be produced. In a few cases (e.g., BaII and CaII) RIS can be applied to the direct detection of positive ions. Likewise, the work with surfaces is just underway. Here we need to learn how to cause surfaces to emit their atoms; and if focused laser beams are used for this purpose, we need to learn how to cope with the concomitant plasma before the atoms themselves are detected.

The practical utilization of RIS and OAD have been demonstrated. We have discussed in this paper their applications in a wide variety of classical as well as modern phenomena. We note here that the solar neutrino problem is just one example of a wider class of applications which we could label ultralow counting. The methods of resonance ionization spectroscopy and of one-atom detection are also beginning to find their places in process control and environmental applications previously belonging to conventional analytical chemistry. For instance, at the National Bureau of Standards, Santos Mayo and Thomas Lucatorto are using the technique to detect minute quantities of impurities such as sodium in semiconducting materials, while Andrzej Miziolek at the Scripps Institution of Oceanography is using RIS to measure the vapor pressure of nonvolatile elements at ambient temperature to determine the sources of heavy metals that are known to be present in the atmosphere (Robinson, 1978). While it is true that the most pressing applications are those such as the solar neutrino problem which *require* one-atom sensitivity, it is significant that the more traditional areas of analytical chemistry are also finding the technique competitive.

The above discussion has concentrated on the use of a proportional counter for the detection of single electrons. Indeed that is appropriate because it illustrates the solution of the most difficult problems in one-atom detection—the detection of one atom with extremely high rejection of the background gas atoms. However, another class of applications involves the release of atoms from a surface into an evacuated region of space. In these applications the single electrons or the ions created by the saturated RIS process can be detected with a channel electron multiplier or with similar devices.

Our discussion has also concentrated on the detection of the cesium atom; this allowed us to show a wide variety of applications of the method of RIS, even for only one kind of atom. Recently at this laboratory and elsewhere a much wider variety of atoms has been studied with the resonance ionization process. Therefore we predict with confidence that the techniques which have been discussed here will be extended into applications involving nearly all of the atoms in a very wide spectrum of circumstances.

In principle, RIS and the techniques used for the detection of single atoms can be extended to the detection of single ions, single molecules, or free radicals. In a few cases, as already noted, positive ions can be further ionized with RIS; in other cases they must be neutralized as a first step in the detection process. Negative ions can also be detected with great sensitivity by photodetachment of electrons followed, for specificity, by delayed coincidence detection of the RIS electron ejected from the neutral species. Molecules (and free radicals) can be detected either by first photodissociating atoms or by using the RIS process directly on the molecule. In the latter case, one electron may not correspond to one molecule of the selected type, even when the RIS process is saturated, because photoabsorption at a given wavelength can cause both ionization and neutral fragmentation. However, ionization efficiencies are known for many molecules; hence calibrations are straightforward. Detection of single atoms in quantum-selected states with spatial and time resolution is important enough to ensure the future of RIS; extension to other species could add exciting new dimensions to that future.

Alkhazov, G. D., 1968, Ioffe Institute of Physics and Technology Report No. FTI-108 (unpublished). (Translation: Scientific Translation Service, STS Order No. 7926).
Alkhazov, G. D., 1970, Nucl. Instrum. Methods 89, 155.
Alkhazov, G. D., A. P. Komar, and A. A. Voreb'ev, 1967, Nucl. Instrum. Methods 48, 1.
Altman, E. L., 1970, Opt. Spectrosc. (USSR) 28, 556.
Ambartsumyan, R. V., A. M. Apatin, V. S. Letokhov, A. A. Makarov, V. I. Mishin, A. A. Puretskii, and N. P. Furzikov, 1976, Sov. Phys. JETP 43, 866.
Ambartsumyan, R. V., V. N. Kalinin, and V. S. Letokhov, 1971, Zh. Eksp. Teor. Fiz. Pis'ma Red. 13(6), 305.
Ambartsumyan, R. V., and V. S. Letokhov, 1972, Appl. Opt. 11(2), 354.
Andrews, Lester, Jenn-Tai Hsang, and Carl Trindle, 1973, J. Phys. Chem. 77, 1065.
Aymar, M., E. Luc-Koenig, and F. Combet Farnoux, 1976, J. Phys. B 9, 1279.
Bahcall, J. N., 1969, Phys. Rev. Lett. 23, 251.
Bahcall, J. N., 1978, Rev. Mod. Phys. 50, 881.
Bahcall, J. N., B. T. Cleveland, R. Davis, Jr., I. Dostrovsky,

J. C. Evans, Jr., W. Frati, G. Friedlander, K. Lande, J. K. Rowley, R. W. Stoenner, and J. Weneser, 1978, Phys. Rev. Lett. **40**, 1351.
Bahcall, J. N., and R. Davis, Jr., 1976, Science **191**, 264.
Bahcall, J. N., and R. L. Sears, 1972, Annu. Rev. Astron. Astrophys. **10**, 25.
Balykin, V. I., V. S. Letokhov, V. I. Mishin, and V. A. Semchishen, 1977, JETP Lett. **26**, 357.
Bartell, D. M., G. S. Hurst, and E. B. Wagner, 1973, Phys. Rev. A **7**, 1068.
Bateman, H., 1911, Philos. Mag. **21**, 745.
Bekov, G. I., V. S. Letokhov, O. I. Matveev, and V. I. Mishin, 1978, Opt. Lett. **3**, 159.
Bekov, G. I., V. S. Letokhov, and V. I. Mishin, 1978, Sov. Phys. JETP **21**, 52.
Bemis, C. E., 1977, private communication.
Berkowitz, J., 1969, J. Chem. Phys. **50**, 3503.
Berry, R. S., 1957, J. Chem. Phys. **27**, 1288.
Betz, H. D., 1972, Rev. Mod. Phys. **44**, 465.
Bhatia, A. K., A. Temkin, and A. Silver, 1975, Phys. Rev. A **12**, 2044.
Biberman, L. M., 1949, Zh. Eksp. Teor. Fiz. **17**, 584.
Bjorklund, G. C., C. P. Ausschnitt, R. R. Freeman, and R. H. Storz, 1978, Appl. Phys. Lett. **33**, 54.
Blalock, T. V., 1964, IEEE Trans. Nucl. Sci. NS–**11**(3), 361.
Bloembergen, N., and E. Yablonovitch, May 1978, Phys. Today, p. 23.
Bohr, N., 1915, Philos. Mag. **30**, 581.
Bohr, N., 1941, Phys. Rev. **59**, 270.
Borkowski, C. J., and M. K. Kopp, 1968, Rev. Sci. Instrum. **39**, 1515.
Bortner, T. E., G. S. Hurst, and W. G. Stone, 1957, Rev. Sci. Instrum. **28**, 103.
Bradley, D. J., P. Ewart, J. V. Nicholas, J. R. D. Shaw, and D. G. Thompson, 1973, Phys. Rev. Lett. **31**, 263.
Breyer, B., 1973, Nucl. Instrum. Methods **112**, 91.
Brinkmann, U., W. Hartig, H. Telle, and H. Walther, 1974, Appl. Phys. **5**, 109.
Burgess, A., and M. J. Seaton, 1960, Mon. Not. R. Astron. Soc. **120**, 121.
Bushaw, B. A., and T. J. Whitaker, 1976, in *Proceedings of 20th Annual Technical Symposium of the Society of Photo-Optical Instrumentation Engineers (San Diego, August, 1976)* (SPIE Publications, Bellingham, Washington), Vol. 82, pp. 92–94.
Calcott, T. A., D. Beekman, S. D. Kramer, E. T. Arakawa, and G. S. Hurst, 1979, to be published.
Campbell, J. L., and K. W. D. Ledingham, 1966, Br. J. Appl. Phys. **17**, 769.
Carlson, L. R., J. A. Paisner, E. F. Worden, S. A. Johnson, C. A. May, and R. W. Solarz, 1976, J. Opt. Soc. Am. **66**, 846.
Carlson, T. A., and R. M. White, 1963, J. Chem. Phys. **38**, 2930.
Carmichael, H. J., and D. F. Walls, 1975, J. Phys. B **8**, L77.
Cerny, Joseph, and Arthur M. Poskanzer, 1978, Sci. Am. **238**(6), 60.
Charles, M. W., and B. A. Cooke, 1968, Nucl. Instrum. Methods **161**, 31.
Charpak, Georges, October 1978, Phys. Today, p. 23.
Choi, C. W., and M. G. Payne, 1977, Oak Ridge National Laboratory Report No. ORNL/TM-5754 (unpublished).
Chen, C. H., J. P. Judish, and M. G. Payne, 1978, J. Phys. B **11**, 2189.
Conway, John G., Earl F. Worden, Jean Blaise, Pierre Camus, and Jean Verges, 1977, Spectrochim. Acta, Part B **32**, 101.
Curran, S. C., A. L. Cockroft, and J. Angus, 1949, Philos. Mag. **40**, 929.
Dalby, F. W., G. Petty-Sil, M. H. L. Pryce, and C. Tai, 1977, Can. J. Phys. **55**, 1033.
Dalgarno, A., H. Doyle, and M. Oppenheimer, 1972, Phys. Rev. Lett. **29**, 1051.
Davidovits, P., and D. C. Brodhead, 1967, J. Chem. Phys. **46**, 2968.
Davis, R., Jr., and J. M. Evans, 1973, in *Proceedings 13th International Cosmic Radiation Conference*, Vol. 3, p. 2001.
deMeijere, J. L. F., and J. H. Eberly, 1978, Phys. Rev. A **17**, 1416.
Dunning, F. B., and R. F. Stebbings, 1974, Phys. Rev. Lett. **32**, 1286.
Eberly, J. H., 1976, Phys. Rev. Lett. **37**, 1387.
Edwards, R. R., and C. P. Coryell, 1948, U.S. Atomic Energy Commission Report 50.
Einstein, A., 1910, Ann. Phys. (Leipzig) **33**, 1275.
Einstein, A., 1956, *Investigations on the Theory of the Brownian Movement*, edited by R. Fürth (Dover, New York).
Erten, H. N., and N. K. Aras, 1978, to be published.
Fabry, M., and J. R. Cussenot, 1976, Can. J. Phys. **54**, 836; J. Quant. Spectrosc. Radiat. Transfer **16**, 127.
Fairbank, W. M. Jr., T. W. Hänsch, and A. L. Schawlow, 1975, J. Opt. Soc. Am. **65**, 199.
Fano, U., 1947, Phys. Rev. **72**, 26.
Farrar, R. L. Jr., and D. F. Smith, 1968 (Rev. 1972), Oak Ridge Gaseous Diffusion Plant Report K–L–3054.
Feldman, D. L., R. K. Lengel, and R. N. Zare, 1977, Chem. Phys. Lett. **52**, 413.
Foltz, G. W., C. J. Latimer, G. F. Hildebrandt, F. G. Kellert, K. A. Smith, W. P. West, F. B. Dunning, and R. F. Stebbings, 1977, J. Chem. Phys. **67**, 1352.
Franzen, W. F., 1959, Phys. Rev. **115**, 850.
Fred, M., and F. S. Tomkins, 1957, J. Opt. Soc. Am. **47**, 1076.
Fred, M., F. S. Tomkins, J. E. Blaise, P. Camus, and J. Verges, 1977, J. Opt. Soc. Am. **67**, 7.
Gallagher, A., 1967, Phys. Rev. **157**, 68.
Geiger, H., and W. Mueller, 1928, Phys. Z. **29**, 839.
Geiss, J., H. Oeschger, and U. Schwarz, 1963, "Cosmic Rays, Solar Particles and Space Research," in *Proceedings of the International School of Physics "Enrico Fermi,"* Course XIX, edited by B. Peters (Academic, New York).
Gelbwachs, J. A., C. F. Klein, and J. E. Wessel, 1977, Appl. Phys. Lett. **30**, 489.
Genz, Harald, 1973, Nucl. Instrum. Methods **112**, 83.
Gezalov, B., and A. V. Ioanova, 1968, High Temp. **6**, 400.
Glauber, Roy J., 1963, Phys. Rev. **130**, 2529.
Gordus, A. A., and J. E. Willard, 1957, J. Am. Chem. Soc. **79**, 4609.
Greenlees, G. W., D. L. Clark, S. L. Kaufman, D. A. Lewis, J. F. Tonn, and J. H. Broadhurst, 1977, Opt. Commun. **23**, 236.
Greinacher, H., 1926, Z. Phys. **36**, 364.
Grossman, L. W., G. S. Hurst, S. D. Kramer, M. G. Payne, and J. P. Young, 1977a, Chem. Phys. Lett. **50**, 207.
Grossman, L. W., G. S. Hurst, M. G. Payne, and S. L. Allman, 1977b, Chem. Phys. Lett. **50**, 70.
Hagan, P. B., S. J. Smith, A. T. Georges, and P. Lambropoulos, 1978, Phys. Rev. Lett. **41**, 229.
Hamill, W. H., and J. A. Young, 1952, J. Chem. Phys. **20**, 888.
Heavens, O. S., 1961, J. Opt. Soc. Am. **51**, 1058.
Hertel, G. R., 1967, J. Chem. Phys. **47**, 335.
Herzberg, Gerhard, 1950, *Molecular Spectra and Molecular Structure. I. Spectra of Diatomic Molecules* (Van Nostrand, Princeton), 2nd edition.
Hindmarsh, W. R., 1974, in *Atoms, Molecules, and Lasers* (International Atomic Energy Agency, Vienna), pp. 133–173.
Holstein, T., 1947, Phys. Rev. **72**, 1212.
Holstein, T., 1951, Phys. Rev. **83**, 1159.
Hurst, G. S., June 1978, Laser Focus, 8.
Hurst, G. S., S. L. Allman, M. G. Payne, K. A. Marshall, and K. L. SooHoo, 1978a, Nucl. Instrum. Methods **155**, 203.
Hurst, G. S., S. L. Allman, M. G. Payne, and T. J. Whitaker, 1978b, Chem. Phys. Lett. **60**(1), 150.
Hurst, G. S., J. P. Judish, M. H. Nayfeh, J. E. Parks, M. G.

Payne, and E. B. Wagner, 1974, in *Proceedings Third Conference on Application of Small Accelerators*, edited by J. L. Duggan and I. L. Morgan (National Technical Information Service, Springfield, Va.), Vol. I, pp. 97–119.
Hurst, G. S., S. D. Kramer, C. E. Bemis, Jr., and J. P. Young, 1978c, in *Proceedings Sixth Symposium on Microdosimetry*, edited by J. Booz and H. G. Ebert (Harwood, London), Vol. 1, pp. 321–330.
Hurst, G. S., S. D. Kramer, M. G. Payne, and J. P. Young, 1979a, IEEE Trans. Nucl. Sci. NS-26, 133.
Hurst, G. S., M. G. Payne, S. D. Kramer, and J. P. Young, 1979b, Chem. Phys. Lett. **63**, 1.
Hurst, G. S., M. H. Nayfeh, and J. P. Young, 1977a, Appl. Phys. Lett. **30**, 229.
Hurst, G. S., M. H. Nayfeh, and J. P. Young, 1977b, Phys. Rev. A **15**, 2283.
Hurst, G. S., M. H. Nayfeh, J. P. Young, M. G. Payne, and L. W. Grossman, 1977, in *Laser Spectroscopy III*, Springer Series in Optical Sciences, edited by J. L. Hall and J. L. Carlsten (Springer, Berlin), Vol. 7, pp. 44–55.
Hurst, G. S., M. G. Payne, M. H. Nayfeh, J. P. Judish, and E. B. Wagner, 1975, Phys. Rev. Lett. **35**, 82.
Hurst, G. S., M. G. Payne, and E. B. Wagner, 1976, United States Patent No. 3,987,302, "Resonance Ionization for Analytical Spectroscopy," Filed 1975.
Huxley, L. G. H., and R. W. Crompton, 1974, *The Diffusion and Drift of Electrons in Gases* (Wiley, New York).
International Commission on Radiation Units and Measurements, 1978, ICRU Report No. 31 (in preparation).
Jacobs, V., 1971, Phys. Rev. A **4**, 939.
Jesse, W. P., and J. Sadauskis, 1955, Phys. Rev. **100**, 1755.
Johnson, P. M., M. R. Berman, and D. Zakheim, 1975, J. Chem. Phys. **62**, 2500.
Jones, L. W., 1977, Rev. Mod. Phys. **49**, 717.
Karule, E., 1974, *Atomic Processes*, Report of the Latvian Academy of Sciences, Paper No. YΔK 539.188, pp. 5–24.
Kaufman, S. L., 1976, Opt. Commun. **17**, 309.
Keto, J. W., R. E. Gleason, and G. K. Walters, 1974, Phys. Rev. Lett. **33**, 1365.
Kimble, H. J., and L. Mandel, 1977, Phys. Rev. A **15**, 689.
Kirsten, T., 1978, in *Origin of the Solar System*, edited by S. F. Dermott (Wiley, Chichester/New York), pp. 267–346.
Kramer, S. D., C. E. Bemis, Jr., J. P. Young, and G. S. Hurst, 1978, Opt. Lett. **3**, 16.
Kramer, S. D., J. P. Young, G. S. Hurst, and M. G. Payne, 1979, Opt. Comm. (in press).
Lambropoulos, P., 1976, Adv. At. Mol. Phys. **12**, 87.
LaRue, G. S., W. M. Fairbank, and A. F. Hebard, 1977, Phys. Rev. Lett. **38**, 1011.
Lawrence Livermore Laboratory, 1977, Chemistry Division Quarterly Report, July to October, 1977, LLL Report No. UCID 15644–77–3.
Lehmann, K. K., J. Smolarek, and L. Goodman, 1978, J. Chem. Phys. **69**, 1569.
Leichner, P. K., 1973, Phys. Rev. A **8**, 815.
Leichner, P. K., J. D. Cook, and S. Luerman, 1975, Phys. Rev. A **12**, 2501.
Leichner, P. K., K. F. Palmer, J. D. Cook, and M. Thieneman, 1976, Phys. Rev. A **13**, 1787.
Levy, Richard H., and George Sargent Janes, 1973, United States Patent No. 3,772,519, "Method of and Apparatus for the Separation of Isotopes."
Loudon, R., 1973, *The Quantum Theory of Light* (Clarendon, Oxford), Chapter 5.
Luebbe, R. H., and J. E. Willard, 1958, J. Chem. Phys. 29, 124.
Magee, John L., 1940, J. Chem. Phys. **3**, 687.
Mallow, B. R., 1975, Phys. Rev. A **12**, 1919.
Manson, S. T., 1978, private communication.
Marrero, T. R., and E. A. Mason, 1973, AIChE J. (Am. Inst. Chem. Eng.) **19**, 498.
Martin, W. C., R. Zalubas, and L. Hagen, 1978, *Atomic Energy Levels—The Rare-Earth Elements*, NSRDS-NBS 60 (U.S. GPO, Washington, D.C.).
Mayo, Santos, and Thomas Lucatorto, 1978, private communication.
McDaniel, Earl. W., 1964, *Collision Phenomena in Ionized Gases* (Wiley, New York), pp. 731–735.
Melton, C. E., G. S. Hurst, and T. E. Bortner, 1954, Phys. Rev. **96**, 643.
Mohler, F. L., 1933, J. Res. Natl. Bur. Stand. (U.S.) **10**, 771.
Moody, S. E., and M. Lambropoulos, 1977, Phys. Rev. A **15**, 1497.
Moore, C. E., 1948, *Atomic Energy Levels*, USNBS Circular 467, Vols. 1, 2, and 3 (U.S. GPO, Washington, D.C.).
Msegane, A., and S. T. Manson, 1975, Phys. Rev. Lett. **35**, 374.
Nakato, Y., M. Ozaki, A. Egawa, and H. Tsubomura, 1971, Chem. Phys. Lett. **9**, 615.
Nayfeh, M. H., G. S. Hurst, M. G. Payne, and J. P. Young, 1977, Phys. Rev. Lett. **39**, 604.
Nebenzahl, Isaiah, and Manahm Leven, 1973 Patent Disclosure 2 312 194, German Patent Office (W. J. Grimes and Co., Custom Technical Translation), "A Process for Isotope Separation."
Nicholson, P. W., 1974, *Nuclear Electronics* (Wiley, London/New York).
Niemax, K., and K. H. Weber, 1978, J. Phys. B **11**, L267.
Norcross, D. W., 1971, J. Phys. B **4**, 652.
Nygaard, K. J., 1975, Phys. Rev. A **12**, 1440.
Oeschger, H., and M. Whalen, 1975, Annu. Rev. Nucl. Sci. **25**, 423.
Pace, P. W., and J. B. Atkinson, 1975, Can. J. Phys. **53**, 937.
Payne, M. G., and J. D. Cook, 1970, Phys. Rev. A **2**, 1238.
Payne, M. G., G. S. Hurst, M. H. Nayfeh, J. P. Judish, C. H. Chen, E. B. Wagner, and J. P. Young, 1975, Phys. Rev. Lett. **35**, 1154.
Payne, M. G., C. E. Klots, and G. S. Hurst, 1975, J. Chem. Phys. **63**, 1422.
Payne, M. G., J. E. Talmage, G. S. Hurst, and E. B. Wagner, 1974, Phys. Rev. A **9**, 1050.
Perlman, M. L., and J. A. Miskel, 1953, Phys. Rev. **91**, 899.
Phelps, A. V., 1955, Phys. Rev. **99**, 1307.
Poisson, S. D., 1837, "Récherches sur la Probabilité des Jugements en Matière Criminelle et en Matière Civile, Précédés des Règles Générales du Calcul des Probabilités" (Bachelier, Paris).
Power, E. A., and S. Zinau, 1959, Philos. Trans. R. Soc. Lond. **A251**, 927.
Rapp, D., and W. E. Francis, 1962, J. Chem. Phys. **37**, 2631.
Rau, A. R. P., 1978, to be published.
Richards, E. W. T., and A. Ridgeley, 1965, Spectrochim. Acta **21**, 1449.
Riola, J. P., J. S. Howard, R. D. Rundel, and R. F. Stebbings, 1974, J. Phys. B **7**, 376.
Robieux, J., and J. M. Auclair, 1965, French Patent No. 1,391,738 (Compagnie Général d'Electricité).
Robinson, A. L., 1978, Science **199**, 1191.
Rothe, D. E., 1969, J. Quant. Spectrosc. Radiat. Transfer **9**, 49.
Rothe, D. E., 1971, J. Quant. Spectrosc. Radiat. Transfer **11**, 355.
Rowley, J. K., B. G. Cleveland, R. Davis, Jr., and J. C. Evans, 1977, Brookhaven National Laboratory Report No. BNL-23418.
Rundel, R. D., F. B. Dunning, H. C. Goldwire, Jr., and R. F. Stebbings, 1975, J. Opt. Soc. Am. **65**, 628.
Rutherford, E., and H. Geiger, 1908, Proc. R. Soc. Lond. A **81**, 141.
Schmeider, R. W., A. Lurio, W. Happer, and A. Khadjavi, 1970, Phys. Rev. A **2**, 1216.
She, C. Y., W. M. Fairbank, Jr., and K. W. Billman, 1978, Opt. Lett. **2**, 30.
Sipilä, Heikki, 1976, Nucl. Instrum. Methods **133**, 251.

Skutnik, B. J., 1970, Phys. Rev. D 2, 635.
Smirnov, B. M., 1977, Sov. Phys.-Usp. 20, 119.
Smith, D. F., "Abstracts of Recent Work on Laser Isotope Separation, 1971–1973," 1974, Oak Ridge Gaseous Diffusion Plant Report No. UCC–ND–266, Rev. 1.
Smith, D. H., 1971, J. Chem. Phys. 54, 1424.
Smith, D. H., and G. R. Hertel, 1969, J. Chem. Phys. 51, 3105.
Smoluchowski, M. V., 1908, Ann. Phys. (Leipzig) 25, 205.
Snell, Arthur H., 1965, in *Alpha-, Beta-, and Gamma-Ray Spectroscopy*, edited by Kai Siegbahn (North-Holland, Amsterdam), Vol. 2, pp. 1545–1555.
Stebbings, R. F., and F. B. Dunning, 1973, Phys. Rev. A 8, 665.
Stebbings, R. F., F. B. Dunning, and R. D. Rundel, 1974, in *Proceedings Fourth International Conference on Atomic Physics, Heidelberg*.
Stebbings, R. F., F. B. Dunning, F. K. Tittel, and R. D. Rundel, 1973, Phys. Rev. Lett. 30, 815.
Sugar, J., 1974, J. Chem. Phys. 60, 4103.
Taylor, T. S., 1913, Philos. Mag. 26, 402.
Thonnard, N., and G. S. Hurst, 1972, Phys. Rev. A 5, 1110.
van Kampen, N. G., 1975, in *Proceedings International Summer School in Wageningen, Netherlands*, edited by E. G. D. Cohen (North-Holland, Amsterdam).
Weisheit, J. C., 1972, J. Quant. Spectrosc. Radiat. Transfer 12, 1241.
Weiss, L. W., M. W. Smith, and B. M. Glennon, 1966, *Atomic Transition Probabilities* (Natl. Bur. Stand., Washington, D.C.), Vol. I, p. 16.
Wellenstein, H. F., and W. W. Robertson, 1972a, J. Chem. Phys. 56, 1072.
Wellenstein, H. F., and W. W. Robertson, 1972b, J. Chem. Phys. 56, 1077.
West, W. P., G. W. Foltz, F. B. Dunning, C. J. Latimer, and R. F. Stebbings, 1976, Phys. Rev. Lett. 36, 854.
Wexler, S., 1965, in *Actions Chimiques et Biologiques des Radiations*, edited by M. Haissinsky (Masson, Paris), pp. 105–215.
Winspear, Alban Dewes, 1956, *The Roman Poet of Science, Lucretius (Titus Lucretius Carus, ca. 99–55BC): De Rerum Natura* (S. A. Russell · The Harbor Press, New York).
Wolfgang, R. L., R. C. Anderson, and R. W. Dodson, 1956, J. Chem. Phys. 24, 16.
Worden, E. F., and J. G. Conway, 1976, J. Opt. Soc. Am. 66, 109.
Worden, E. F., R. W. Lougheed, R. G. Gutmacher, and J. G. Conway, 1974, J. Opt. Soc. Am. 64, 77.
Zakheim, D., and P. Johnson, 1978, J. Chem. Phys. 68, 3644.
Zeman, H. D., 1974, in *International Symposium on Electron and Photon Interactions with Atoms*, edited by H. Kleinpoppen and M. R. C. McDowell (Plenum, New York), pp. 591–594.